# 國立交通大學

電子物理研究所

博士論文

# 半導體雷射激發光纖雷射系統之物理與技術

# Physics and technology of diode-pumped fiber laser systems

研 究 生： 黃哲彥

指導教授： 陳永富 教授

中華民國九十八年七月

# 半導體雷射激發光纖雷射系統之物理與技術

# Physics and technology of diode-pumped fiber laser systems

研 究 生：黃哲彥　　Student：Je-Yen Huang

指導教授：陳永富　　Advisor：Yung-Fu Chen

國立交通大學

電子物理研究所

博士論文

A Thesis

Submitted to Department of Electrophysics

College of Science

National Chiao Tung University

in partial Fulfillment of the Requirements

for the Degree of Doctor of Philosophy of science in Electrophysics

June 2009
Hsinchu, Taiwan, Republic of China

中華民國九十八年七月

# 半導體雷射激發光纖雷射系統之物理與技術

學生: 黃哲彥　　　　　　　　　　　　指導老師:陳永富

國立交通大學電子物理學系博士班

## 摘要

本文主要使用雙包層之摻鐿及鉺鐿共摻之大模態光纖(摻鐿光纖之纖核直徑:30μm，鉺鐿共摻光纖之纖核直徑:25μm)作為研究雷射二極體激發之高功率光纖雷射的特性。首先我們使用窄頻寬的薄膜濾光片作為控制雷射縱模之元件，完成了波長可調且窄波段的的光纖雷射;之後則建立了被動式及被動式的Q開關光纖雷射。在被動式Q開關中，首先是使用摻鐿之光纖作為增益介質。我們分別使用Cr:YAG晶體以及半導體材料AlGaInAs作為飽和吸收體。在以$Cr^{4+}$:YAG晶體作為飽和吸收體的實驗中可得到脈衝能量為350 μJ;在以半導體作為飽和吸收體的實驗中，實驗結果其可操作在5~30 kHz且脈衝能量約為 450 μJ。另外在使用鉺鐿共摻光纖作為增益介質的實驗中，我們亦利用同樣材料的半導體但比例不同而使其吸收波段在1.5 μm來作為飽和吸收體。結果在13.5 W的激發功率之下可得到平均功率為1.26 W，脈衝能量為100μJ及重覆率為12 kHz輸出。主動式Q開關光纖雷射中我們採用聲光晶體來產生腔內的損耗，我們測試了幾種不同的方法來增加聲光晶體的調變損耗以提升脈衝波能量。實驗結果可得到600 μJ的脈衝能量及42ns的脈衝寬度。

# Physics and technology of diode-pumped fiber laser system

Student: Je-Yen Huang
Advisor: Prof. Yung-Fu Chen

Institute and Department of Electrophysics
National Chiao-Tung University

## Abstract

An Yb doped large-mode-area (LMA) fiber with a core diameter of 30 μm and an inner cladding diameter of 250 μm, and an Er/Yb codoped fiber with a core diameter of 25 μm and an inner cladding diameter of 300 μm have been used for researching in development of high power fiber lasers. Firstly we demonstrated tunable and narrow linewidth Yb and Er/Yb fiber lasers by use of thin film narrowband filters. Afterwards we have demonstrated passively and actively Q-switched fiber lasers. By use of Yb doped fiber as the gain medium, we have obtained passively Q-switched fiber lasers by employing a $Cr^{4+}$:YAG crystal and an AlGaInAs semiconductor material as saturable absorbers respectively. The results revealed that with a Cr:YAG as a saturable absorber in a diode-pumped Yb fiber laser, the laser could generate a pulse energy of 350 μJ at a repetition rate of 38 kHz. For the use of AlGaInAs based saturable absorber experiment, we have realized a pulsed laser with 450-μJ pulse energy and can be operated at pulse repetition rate of 5~30

kHz. The pulse train is very stable of ~10% fluctuation. Besides, we also obtained a passively Q-switched Er/Yb codoped fiber by means of another AlGaInAs semiconductor saturable absorber. Greater than 0.1 mJ of pulse energy at a repetition rate of 12 kHz was generated. Finally in the actively Q-switched fiber lasers, by enhancing the loss modulation of the active Q-switch (acoustic-optical modulator), we have obtained pulse of 600-μJ pulse energy and 42-ns pulse width.

# 誌謝

五年的光景轉眼即逝，在交大的研究生生活也即將劃下句點。這五年是我人生中重要的精華，不僅學到了許多研究方法，也認識了許多好友。首先感謝陳永富老師在這五年來的不懈指導，讓我得已在此學習許多實驗的方法，更重要的是讓我了解做研究的精神以及研究的本質；陳永富老師對實驗總是有令人驚豔的想法，分析問題的能力給予我對於研究內容有更深入的了解。此外陳老師總是以身作則、嚴己寬人，做人處事的態度是我學習的目標。同時也非常感謝黃凱風老師對我的幫助，除了提供實驗所需的半導體材料外，您對物理的直覺與實驗的想法，也讓我在短時間內就能夠了解問題的所在並釐清錯誤的觀念。在這個實驗室我看到了用熱忱打造出的研究殿堂，兩位老師對於研究的態度是我學習到最重要的事情。

在研究的生活裡還要感謝有許多同學及學長姐和學弟妹的陪伴，你們是我在實驗室時的良師益友。感謝老大總是不厭其煩地解決我在實驗上及學識上的大量問題；感謝以前的學長姐歐大戶、古寶妹、廖羽嵐及蔡玲意，你們都是非常好相處的人，讓我剛進這個實驗室很快地就能融入這個環境。另外很高興能認識同梯的亭樺、偉立與仕璋以及學弟妹：興弛、建誠、依萍、雅婷、彥廷、毅帆、威哲、家禎、還有大學部三個可愛的學弟妹。另外也要感謝阿龍學長跟文正，雖然認識你們的時間不長，但跟你們的討論總能使我得到更多的想法；另外感謝文正兄分享的各地美食，希望你也儘快找到另一半。另外也要感謝工研院的耀文、健銘、信嘉等人，在我人生地不熟的時候陪我在下班後一起運動跟吃飯。

最後我要感謝我的女朋友雅璿與我的家人；你們總是在我有困難時幫助我，有你們的支持與鼓勵我才能順利完成我的學業。

## *Chapter 2 Continuous-wave tunable Yb doped and Er/Yb codoped fiber lasers* 19

## *Chapter 3 Fiber lasers passively Q-switched by Cr$^{4+}$:YAG crystals* 43

## *Chapter 6 Summary and Future works* 119

# List of Figures

# List of Tables

# *Chapter 1 Introduction*

## 1.1 Overview of fiber lasers

### 1.1.1 Progress of fiber lasers

The first fiber laser was proposed and invented by Snitzer [1,2] at 1961, one year after the birth of the first laser. The 1st fiber laser used a neodymium doped fiber and was pumped by a flashtube. However the pump scheme possessed low efficiency and was improved a decade later by Burrus and Stone who employed a laser diode as a pump source at 1973 [3]. Another important milestone is the technique of modified chemical vapor deposition (MCVD) by Poole et al., allowing the fabrication of low-loss rare-earth doped silica fibers [4]. Two years later Payne et al. also demonstrated the first erbium doped fiber amplifier [5].

EDFAs induced widespread interest due to the gain region of erbium ions match the wavelength of optical communication, i.e. 1.5 μm. Afterward tremendous researches and developments in EDFAs made long haul optical communication inexpensive and reliable and thus push ahead the development of telecommunication systems. Besides, the development of EDFAs also promoted the growth of novel laser diodes and fiber components. In addition to the telecommunication, power-scaling fiber lasers have also been developed and fabricated well owing to the invention of double clad fiber [6] and rapid progress in high power laser diodes. Since then many high power fiber lasers were developed, mostly with Neodymium and Yb doped fibers. $Nd^{3+}$ ions have the advantage of a 4-level pumping system resulting in a low lasing threshold and have been utilized as an active ion in bulk solid state lasers [7-9]. The first Yb doped fiber laser was demonstrated by Etzel et al. [10], however they attracted less attention then cause of the pumping scheme of an $Yb^{3+}$ ion is a 3 or quasi 3 systems, which demands higher threshold than a four one. Nevertheless thanks to their simple electric energy level and lower quench effect [11], Yb doped fiber lasers provide higher power conversion efficiencies in heavily doped scale and thus emit larger output powers. Therefore Yb doped fibers have been employed as the gain medium in many high power fiber lasers and high power amplifiers. Recently many high power fiber lasers of hundred watts and even kW-level with excellent beam quality were reported [12-14]. High brightness lasers provide more extensive applications such as wielding, cutting, and scanning. The progress of fiber lasers and fiber amplifiers are fast and steady and many commercial products are available now.

### 1.1.2 Double-clad fibers

In the 1980 single-mode fibers could only be pumped by the single-mode pump sources such as Ti:sapphire solid-state lasers and single-mode laser diodes. The low output powers of the pump sources restrain the power-scaling of fiber lasers. The solutions to the challenge are to develop single-mode pump sources of higher power or fabricate a single-mode fiber allowing pumped by multi-mode sources. A breakthrough was done by Elias Snitzer's describing the cladding-pumped lasers in 1988 [6]. As shown in Fig. 1.1, he invented a double clad fiber which constrains the pump light by the refractive index difference of 1st cladding and 2nd cladding instead of that of core and cladding in single-clad fibers. The numerical aperture of the 1st clad could be designed to as large as >0.46 to support low-bright but high-power pump source. At the same time the core is still single-mode and the output radiation possesses high brightness. Therefore double clad fiber (DCF) is an excellent brightness converter which not only allows the use of high-power pump sources such as multi-mode diode arrays, but also radiates single-mode output. The outer cladding and the core are usually made of silica while the outer cladding is composed of low refractive index polymer. DCFs are easily fabricated and are commercially available for very high power scale.

However, as the ratio of the diameter of clad to core gets larger, the mode overlapping efficiency as well as the pump absorption gets worse. Consequently a longer or heavily-doped fiber is needed to achieve an efficient fiber laser. The doping concentration is about hundred to thousand ppm restrained by the quench effect of dopants and the length of fiber is restrained by the background loss and nonlinearity. Besides, ingenious clad-design could increase the interaction between the pump light and the doped core to enhance the absorption. There is a variety of designs of double-clad fibers. The design criterion is to reduce symmetry of inner-cladding to eliminate whisper-galley mode. For example, Fig. 1.2 shows the common design of DCFs. Fig. Fig.1.2 (a) shows a skew or whisper-galley mode formed in circular cladding while (b) to (e) shows the elliptic, square, D-shaped, off-centered cladding. The modes are high-order Bessel functions and less occurring at the center. One improvement to enhance the absorption is to bend the fiber to mix up the modes. The symmetry-broken core would induce the interaction of clad mode with the core directly due to the chaotic-like trajectory of wave. The properties of beam confinement combined with excellent heat dissipation make double-clad fiber lasers superior to conventional bulk solid-state lasers with regard to high-power applications in continuous-wave as well as in Q-switched operation.

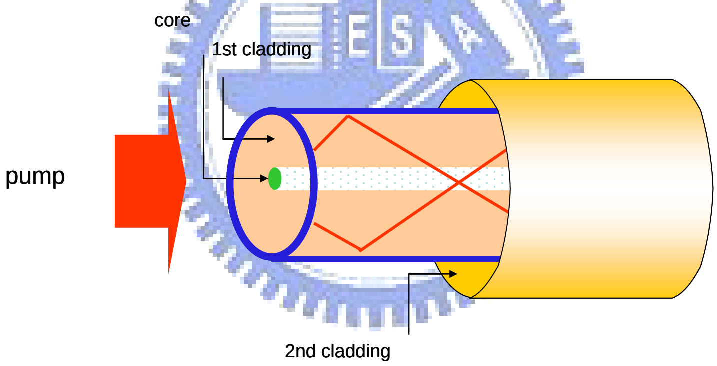

Fig. 1.1. Double-clad fiber structure. Pump light is injected into the 1st cladding and confined between 1st and 2nd cladding while signal propagates in the core.

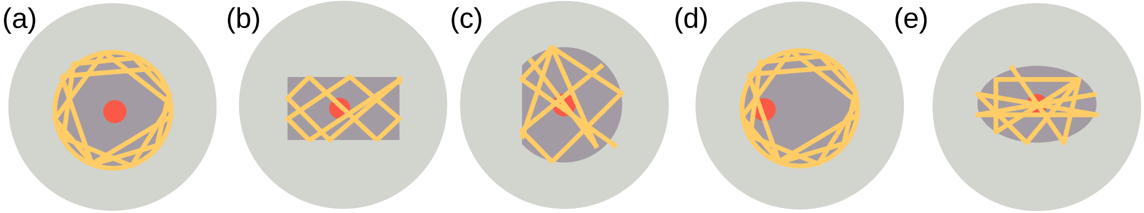

Fig 1.2. Different cladding design of DCFs. (a)~(d) are elliptic, square, D-shaped, and off-centered cladding while; (e) is a circular cladding.

### 1.1.3 Pumping schemes

The injected pump power usually determines the performance of a high-power fiber laser. The injected pump power is mainly depends on the pump schemes and can be divided into two categories: The end-pumping and side-pumping. They are distinguished from the point of DCFs injected of pump light. Below are several reported pumping schemes including the side-pumping and the end-pumping scheme.

#### Side-pumping scheme

Side-pumping means injecting the pump light along the side of the DC-fiber and therefore it leaves the fiber ends free for the access of the signal. These techniques are also called the notch coupling because of the coating and the clad at the injection have to be eliminated. They include the V-groove pumping [15], pumping with angle-polished fibers [16], microprism coupling [17], grating coupling [18], and embedded-mirror side-pumping [19].

*V-groove coupling*: V-groove is formed on the side of DCF where the coating, outer clad and some of the inner clad is removed. Pump light is coupled through reflection on the V facet. The coupling efficiency is typically higher than 75%. This technique has the advantage to be compact and few diodes can be launched at different points along the fiber length. The main drawback is that the groove weakens the fiber results in a loss.

*Pumping with angled-polished fibers:* a multimode angle-polished or tapered fibers connected onto the side of the DCF where the coating and outer clad is removed. This fiber could be embedded with an index matching gel or directly fused to the DCFs. The coupling efficiency could be up to 90% nevertheless there are no reports that lasers by this method radiate output power higher than 1 W.

*Micro-prism coupling*: Like the method above, this approach utilizes a micro-prisms instead of a multimode fiber to couple pump light into the DC fiber. Here the prism also contacts the inner clad by an index-matching gel. The main drawback is the difficulty in fabrication of the micro-prism.

*Grating coupling*: A binary grating is settled by the inner clad of a DCF. Incident pump light is diffracted into positive and negative order by the grating and propagating inside the clad if the incident angle is higher than the critical angle. Herda showed that the only TM polarized pump light could raise the coupling efficiency up to 57% owing to the polarization-dependent diffraction and the pump power was also limited by the index matching gel [18]. Zhang et al. recently theoretically showed that a maximum coupling efficiency is up to 94.7% with a TE polarized pump light or 93.94% with a TM one by use an “asymmetric dual-side-grating” and 72% with an un-polarized pump light by a “double-groove and two-depth dielectric transmission grating” in a multi-point pump scheme. However, to my best knowledge there are no stirring experimental results better than Herda’s record.

Besides, there are also other ingenious methods called *co-linear coupling* which injects pump light through side fiber in optical contact with the inner cladding of the active fiber. For example, the GTwave developed by SPI [22] and a novel method created by Peterka et al [23]. The former is to launch pump light into many passive fibers which are wound around an active fiber thus the pump is transferred to the active fiber. The later is similar to the former except it uses two passive fibers fused with the DC fiber at end facet. One is for transmitting the pump and the other is for signal. Both of them obtain high coupling efficiency and the former has been employed in commercial products.

### End-pumping scheme

*Lens-coupling*: Lens-coupling is the simplest method the couple the pump light directly into the inner cladding of the active fiber using free-space coupling optic. It is easy to implement in an experimental setup and the coupling efficiency is generally up to 70%~80% as long as the beam quality of the pump light is sufficient high. This method is very simple and flexible to various fiber-coupled laser diodes. Especially they can couple the pump light of diode bar or diode stack into an active fiber to scale the output power. For example the reported fiber laser of highest CW output power up to 1.36 kW was pumped by this method [13]. However this coupling scheme requires precise and stable alignment therefore lens-coupling is preferred as the laboratory pumping scheme.

*Tapered fiber coupling*: Direct fusing the active fiber with the injecting fiber possesses the merit of robustness. This method requires the NA and the diameters of the injection fiber and the DC fiber matching each other, however the cladding of a coupled fiber of a high-power laser diode are usually larger than that of the active fiber. A tapered or flared fiber is therefore introduced to connected two un-matching fibers. A conical shape at the end of a passive or active fiber enhanced the pumping efficiency even pumped by low-brightness LDs. Recently Filippov et al. [20] proposed a tapered DC Yb doped fiber, owning a gradual-varying core and cladding diameters, at the wide part of the tapered fiber are 27 and 834 μm respectively; at the narrow part are 5.8 and 177 μm. The fiber could be pumped by a pump source with BPP of 300 mm×mrad and the highest output CW power was 212 W.

*Fiber bundles coupling*: This technique is associated with coupling via many pump fibers and developed by DiGiovanni et al. at 1999 [21]. A DCF without outer clad is wound by several multimode fibers as a fiber bundles. The multimode fibers are spliced and tapered to match the cross section of the DC fiber. The bundles allow consisting of a single-mode fiber for accessing a signal of the DC fiber. This approach is rugged and convenient in commercial and industrial applications.

## 1.2 Motivations

To date the highest power of continuous-wave fiber laser is up to kW with multimode output [12, 24] and single mode output [14]. They have many applications in industry and potentially as laser weapons. On the other hand there are other applications such as medical lasers, micro-machining, or laser radar require mid-power-scale (dozens of watt) or pulsed laser. Consequently high-pulse-energy pulse from fiber lasers [25] and fiber amplifiers [26] demonstrated by Q-switching operation or by master oscillation power amplifier (MOPA) have attract much attentions as well. The performance of a pulsed laser is determined by the doping concentration of active fiber, the lifetime of doped rare-earth, and the fiber core area. The higher energy of a pulse requires a larger mode area. Therefore the large-mode-area (LMA) fibers are suitable for this purpose because their core owns the merits of large size ( diameter > 15 μm ) and low NA (< 0.07). Besides, a large mode-area also reduces the nonlinearity such as SBS or SRS effect. Consequently cladding-pumped LMA fiber lasers are no doubt potential and practical laser sources. Furthermore there are many techniques and experiences in crystal lasers are practical and can be merged with fiber lasers. Therefore this thesis is motivated mainly by combining the techniques of crystal lasers with cladding pumped $Yb^{3+}$ doped and $Er^{3+}/Yb^{3+}$ codoped LMA fiber lasers. Below are the researches in this thesis

### 1.2.1 CW tunable Yb-doped and Er/Yb codoped fiber lasers

Tunable narrow linewidth laser sources have potential applications in dense wavelength-division-multiplexed (DWDM) systems, nonlinear wavelength conversion, and medical instruments. Fiber lasers are one of the promising sources owing to the advantages as mentioned before. The rare earths ions $Yb^{3+}$ and $Er^{3+}$ radiate broadband linewidths. Although the broadband emission provides fiber lasers with adequate flexibility in operating wavelength, it is indispensable to develop a practical method for selecting and narrowing the lasing wavelength. The current approaches for wavelength selection can be categorized into two groups: one is to use an in-fiber Bragg grating (FBG) [27, 28] and the other is to use an external feedback cavity with a wavelength selector.

Although FBGs can be fused to the active fiber to obtain narrow line width operation without the need for alignment, it is difficult to splice FBGs to LMA fibers [29]. So far narrowband LMA fiber lasers are most realized with an external feedback cavity containing a replica diffraction grating [30, 31] or a volume-Bragg-grating (VBG) [32, 33]. The approach with a diffraction grating has the attraction of a wide wavelength tuning range; however, it usually requires a complicated and bulky external cavity to obtain a large spot-sized collimated beam for high diffraction efficiency. Recently, an alternative component for wavelength selection in an external feedback cavity is to use VBGs that are holographically produced 3D bulk grating and are used in a variety of lasers for spectral narrowing. Even so, it is still desirable to develop relatively inexpensive and simple methods for tunable narrow linewidth fiber lasers. In this section I proposed a wavelength selection technique by an all-dielectric coated Fabry-Perot (FP) bandpass filter formed by a space region sandwiched between two highly-reflecting multilayer stacks deposited on a glass substrate. They are well-developed and inexpensive, e.g. WDM systems are mostly realized with the FP bandpass filter. Nowadays the thin-film FP bandpass filters with a bandwidth of 50 GHz are commercially available for WDM applications.

### 1.2.2 Actively Q-switched fiber lasers

Q-switched fiber lasers are developed rapidly owing to Q-switching is an efficient and simple technique to generate high energy pulse lasers. Controlling the Q-value of a cavity would allow the oscillator to store higher gain than CW regime and can emit higher energy in a short duration. In the active Q-switching, electro-optics (EO) [34], acoustic-optics (AO) [25], or mechanical [35] modulators are used for Q-switching. Photonics crystal fibers with large mode area have also been invented to achieve high-power Q-switched lasers with short pulse durations [36]. It is noted that stored gain of a gain medium depends on the low-Q interval, meaning there is a trade-off between extractable pulse energy and the pulse repetition rate.

To date the highest reported un-amplified pulse energy in a Q-switched fiber laser is 7 mJ at pulse repetition rate of 500 Hz by using an AOM modulator and a LMA fiber with core size of 60 μm [25]. However the pulse repetition rates in many mJ-level reports are nearly 1 kHz or even lower, which somewhat limits their applications. Besides, the pulse energy might be overestimated due to the repetition rate is close to the recovery time of laser upper level, i.e. much amplified spontaneous emission (ASE) would exist and result in unstable pulse output, average-power loss and misunderstanding in determining the pulse energy. On the other hand the most popular method in active Q-switching is to feed back the periodic deflected beam from a Bragg-type acousticoptic modulator to prevent the pre-lasing or parasitic lasing resulted by the residual undeflected beam at low repetition rate. However the deflected beam is 85% at most of the incident beam leading to a power-wasting. Consequently, in addition to the Bragg-type one, I attempted to Q-switch a LMA ytterbium doped fiber (identical to the above) actively by a Raman-Nath type acousticoptic modulator which diffracts incident beam into several order beams. Although they can only be used for reflecting the un-diffracted beam (i.e. pre-lasing might exist at low repetition rate operation) they can really avoid power loss at most repetition rate. Besides it is cheaper and small compared with the Bragg-type one to simplify the cavity design.

### 1.2.3 Passively Q-switched fiber lasers

Asides from the active Q-switching, passive Q-switching is modulated by a saturable absorber (SA) and the pulse performance is related with modulation depth of the SA. Passive Q-switching is attractive for its simpler, inexpensive, and compact setup due to removal of external electronics. All-fiber passively Q-switched fiber lasers are realized by fusing the gain fiber with Cr$^{4+}$ [37] or Sm [38] doped fiber as saturable absorbers. In addition, Cr$^{4+}$- [39] and Co$^{2+}$- [40, 41] doped crystals and multi quantum well (MQWs) semiconductors have been also employed as SAs in passively Q-switched fiber lasers [42]. The performance of the developed system mentioned above, however, were constrained to low average power (<10 W) and low pulse energy (<0.1 mJ) by the fiber core size and especially for the mechanical stability such as thermal management and damage threshold of saturable absorbers.

In this part, I attempted to Q-switch a LMA ytterbium doped fiber (identical to the above) passively by a Cr$^{4+}$:YAG crystal with high modulation depth ~70% to Q-switch a Yb-doped fiber laser. Besides, a novel semiconductor AlGaInAs quaternary alloy was developed as saturable absorbers. AlGaInAs quaternary alloys own advantages of larger conduction band offset than InGaAsP materials at spectral region of 1.5 μm [43] and lattice-matching to their substrate InP in the region of 840 nm to 1600 nm. Besides, semiconductor materials can be tailored for specific wavelength by changing the ratio of compounds. These advantages reveal that AlGaInAs quaternary alloys are potentially applicable as saturable absorber in Q-switching lasers. Here I utilized AlGaInAs periodic multi quantum-well (MQW) saturable absorbers to Q-switch Yb-doped in the 1.06 μm and Er/Yb codoped fiber lasers in the 1.5 μm.

## 1.3 Achievements

### 1.3.1 CW tunable Yb-doped and Er/Yb codoped fiber lasers

By use of a FP filter (peaking at 1100nm, bandwidth of 5nm) and a LMA Yb-doped fiber with core diameter about 30μm, a tunable Yb-doped fiber laser with an output power of 16 W and spectral linewidth of 0.5 nm was generated. The tunability ranged from 1040nm~1100nm, where the lower limit was restricted by gain bandwidth and the longer one was bound by the filter. Besides, a narrowband Er/Yb codoped fiber laser employed a FP filter (peaking at 1564nm, bandwidth of 0.4 nm) for wavelength selection and narrowing. The gain fiber was an Er/Yb codoped LMA fiber with core diameter about 25μm. Output power of 3.5 W and spectral linewidth of 0.15 nm was generated. The tunability ranged from 1536nm~1564nm, where the lower limit and the longer one were bound by the same reasons as well.

Experimental results reveal that thin-film bandpass filter can reduce the lasing spectrum from a free-running wide band of >5 nm both for Yb fiber laser and Er/Yb fiber laser to be a narrow band of < 1.0 nm for Yb fiber laser and <0.15 nm for Er/Yb fiber laser without substantial losses. The efficiency of narrowing is higher than 90% for all tuning range for both lasers. Besides, the wide tuning range is achieved with tilting the incident angle to shift the passband curves. The resonant wavelengths were showed fitting well with the theory. The experiments emphasized that an efficient resonant-wavelength tuning and narrowing is simple to realize for a fiber laser.

### 1.3.2 Passively Q-switched Yb-doped fiber laser by a $Cr^{4+}$:YAG crystal

A laser output with pulse energy up to 350 μJ with pulse duration of 80 ns at pulse repetition rate of 43 kHz was obtained. By use of the FP filter, tunability was realized from 1055 nm to 1080 nm and the pulse energies were at 250 μJ at the maximum pump power. The Q-switching efficiency (average power of Q-switched laser/cw laser) was over 90% even if the average power exceeded 14W. The result reveal that the loss induced by a $Cr^{4+}$:YAG crystal with high modulation deptch~50% is quite low and the $Cr^{4+}$:YAG crystal is appropriate to Q-switch a high power fiber laser.

### 1.3.3 Passively Q-switched fiber lasers by AlGaInAs MQW semiconductor saturable absorbers

In the Q-switched Yb-doped fiber laser experiment, a pulse with energy of 450 μJ and duration of 60 ns was obtained at pulse repetition rate 30 kHz. The output performance was compared with that of Q-switched fiber laser by use of $Cr^{4+}$:YAG crystal. On the other hand, in the Q-switched Er/Yb codoped fiber laser experiment, a pulse with energy above 100 μJ with a Q-switched mode-locking (QML) pulse shape was obtained at pulse repetition rate 12 kHz. The FWHM of envelope of the QML pulse was 300ns, and the peak power was estimated by the highest pulse with energy of 17μJ and duration of 33ns to be 0.5kW. The Q-switching efficiencies in the two experiments exceeded 80 % and their pulse energies are the highest ones in 1.06 μm and 1.5 μm respectively. The remarkable performance confirms the prospect of using AlGaInAs QWs as saturable absorbers in passively Q-switched lasers.

### 1.3.4 Actively Q-switched Yb-doped fiber lasers

At first we demonstrated a high-power Q-switched fiber laser that can emits stably from 53 kHz to 200 kHz. The maximum pulse energy is 0.25 mJ with pulse duration of 100 ns with a spectral linewidth of 1.5 nm. The limit of the repetition rate was estimated to be pumping rate for the upper limit and pre-lasing for the lower. The loss modulation of the AO Q-switch is about 20% ~30% measured in a single pass. There occurred a pre-lasing within the low-Q state when we tried to operate at a lower repetition rate, which resulted in unstable pulse output and several spiking in spectral domain. To expand the pulse repetition rate as well as to obtain higher pulse energy, an AlGaInAs semiconductor saturable absorber was used to enhance the loss modulation. The hybrid Q-switch can enhance the modulation loss. Experimental results showed that the maximum pulse energy was raised to 0.56 mJ with timing jitter less than 1%.

On the other hand, due to the loss modulation of an AO Q-switch is dependent on polarization of the incident beam; it could be possible to enhance the loss modulation by employing a low-loss polarization optic inside the external cavity. Consequently we utilized a polarization beam splitter (PBS) settled before the AO Q-switch to control the polarization of incident beam into the AO Q-switch. A loss modulation exceeding 60% was realized in a single pass. However the loss induced by the PBS was about 20% and the efficiency of power of laser with and without the PBS was estimated to be 92% Q-switching regime. Consequently the experiment results manifested the PBS could increase the loss modulation efficiently, where the pulse repetition rate was could be operated to 20 kHz with output power of 12 W, the maximum pulse energy was up to 0.6 mJ with pulse width of 42 ns peak power of 14 kW. The wavelength was centered at 1075 nm with a FWHM linewidth of 1.5 nm and > 40 dB higher than the ASE which ensures the pulse energy is reasonable.

## 1.4 Outline

Chapter 1: Introduction to fiber lasers including the history of development, design of double clad fiber allowing pumping by high power laser diode for higher power-scaling. Besides, several pumping schemes including side-pumping and end-pumping are introduced. Finally the motivation for this thesis and the achievement are presented.

Chapter 2: In this chapter, the properties and importance of Yb ions and Er/Yb ions are introduced firstly. Afterwards a continuous wave tunable Yb fiber and an Er/Yb codoped fiber by use of thin film filters were demonstrated.

Chapter 3: In this chapter, I pay my attention to passively Q-switched fiber lasers. A fiber laser was Q-switch passively by $Cr^{4+}$:YAG crystal. Besides, an analytical model was demonstrated to optimizing an external Q-switch, which consisted of the saturable absorber, re-imagining focus lens, and a high reflection mirror. The influences of the parameters of the external Q-switch were discussed.

Chapter 4: In this chapter I demonstrated an Yb-doped and an Er/Yb codoped fiber laser by AlGaInAs based semiconductor periodic multi quantum wells, respectively. The pulse energies are to date the highest ones for both in the Yb-doped and Er/Yb codoped passively Q-switched fiber lasers.

Chapter 5: In this chapter, I demonstrated fiber lasers Q-switched by an AO Q-switch, hybrid Q-switch, and an AO Q-switch with polarization control respectively. The influences of a saturable absorber and polarization control on the performance of Q-switched fiber lasers by AO Q-switch were discussed.

Chapter 6: This is the final chapter in this thesis and I concluded all the results here. Besides, outlook for the fiber lasers are discussed.

# Reference

1. E. Snitzer, “Proposed fiber cavities for optical lasers,” J. Appl. Phys. **32,** 36-39 (1961).
2. E. Snitzer, “Optical maser action of $Nd^{3+}$ in a barium crown glass,” Phys. Rev. Lett. **7**, 444-446 (1961).
3. C. A. Burrus, J. Stone, “Neodymium –doped silica lasers in End-pumped fiber geometry,” Appl. Phys. Lett. **23**, 388-390 (1973).
4. S.B. Poole, D.N. Payne, and M.E. Fermann, “Fabrication of low loss optical fibers containing rare-earth ions,” Electron. Lett. **21**, 738-740 (1985).
5. R. J. Mears, L. Reekie, I. M. Juancey, D. N. Payne, “Low-noise erbium-doped fiber amplifier operating at 1.54μ m,” Electron. Lett. **23**, 1026-1028 (1987).
6. E. Snitzer, H. Po, F. Hakimi, R. Tumminelli, and B.C. McCollum,“Double-clad offset core Nd fiber lasers,” in Proc. Opt. Fiber Sensors, New Orleans, 1988, post-deadline, PD5.
7. D. Golla, M. Bode, S. Knoke, W. Schöne, and A. Tünnermann, “62-W cw $TEM_{00}$ Nd:YAG laser side-pumped by fiber-coupled diode lasers,” Opt. Lett. **21**, 210–212 (1996).
8. Y.F. Chen, “High-power diode-pumped Q-switched intracavity frequency-doubled Nd:YVO4 laser with a sandwich-type resonator,” Opt. Lett. **24**, 1032-1034 (1999).
9. J. Lu, M. Prabhu, J. Song, C. Li, J. Xu, K. Ueda, A.A. Kaminskii, H. Yagi and T. Yanagitani, “Optical properties and highly efficient laser oscillation of Nd:YAG ceramics,” Appl. Phy. B **71,** 469-473 (2000).
10. H. W. Etzel, H. W. Gandy, R. J. Ginther, “Stimulated emission of infrared radiation from Ytterbium-activated silica glass,” Appl. Opt. **1**, 534-536, (1962).
11. R. Paschotta, J. Nilsson, Anne C. Tropper, and D. C. Hanna, “Ytterbium-doped Fiber Amplifiers,” IEEE J. Quantum Electron. **33**, 1049-1056 (1997).
12. Y. Jeong, J. K. Sahu, D. N. Payne, and J. Nilsson, “Ytterbium-doped large-core fibre laser with 1 kW of continuous-wave output power,” Electron. Lett. **40**, 470-471 (2004).
13. A. Liem, J. Limpert, H. Zellmer, A. Tünnermann, V. Reichel, K. Mörl, S. Jetschke,

S. Unger, H.-R. Müller, J. Kirchhof, T. Sandrock, A. Harschak, “1.3 kW Yb-doped fiber laser with excellent beam quality,” in Proc. Conference on Lasers and Electro-Optics 2004, San Francisco, USA, May 16-21, 2004, postdeadline paper CPDD2.

14. Y. Jeong, J. K. Sahu, D. N. Payne, and J. Nilsson, "Ytterbium-doped large-core fiber laser with 1.36 kW continuous-wave output power," Opt. Express **12,** 6088-6092 (2004).
15. D.J Ripin and al,”High efficiency side-coupling of light into optical fibres using imbedded v-grooves”, Elec. Lett. **31**, 22042205 (1995).
16. J. J. Larsen and G. Vienne, “Side pumping of double-clad photonic crystal fibers”, Opt. Lett. **29**, 436-438 (2004).
17. T. Weber, W. Luthy, H.P. Weber, V. Neuman, H Berthou, G. Kotrotsios, "A longitudinal and side-pumped single transverse-mode double clad fiber laser with a special silicone coating", Optics Commun. **115**, 99-104 (1995).
18. R. Herda, A. Liem, B. Schnabel, A. Drauschke, H.-J. Fuchs, E.-B. Kley, H. Zellmer and A. Tuennermann, “Efficient side-pumping of fibre lasers using binary gold diffraction gratings,” Electron. Lett. **39**, 276-277 (2003).
19. J. P. Koplow, S. W. Moore and D. A. Kliner, “A new method for side pumping of double-clad fiber sources”, IEEE J. Quantum Electron. **39**, 529-540 (2003).
20. V. Filippov, Y. Chamorovskii, J. Kerttula, A. Kholodkov, and O.G. Okhotnikov, “Single-mode 212 W tapered fiber laser pumped by a low-brightness source,” Opt. Lett. **33**, 1416-1418 (2008).
21. D. Giovanni, “Tapered fiber bundles for coupling light into and out of cladding-pumped fiber devices”, US patent US5864644 (1999).
22. A. B. Grudinin, J. Nilsson, P. W. Turner, C. C. Renaud, W. A. Clarkson, and D. N. Payne, in *Conference on Lasers and Electro-Optic* (Optical Society of America, 1999), paper CPD26.
23. P. Peterka, I. Kašík, and V. Matejec, “Experimental demonstration of novel end-pumping method for double-clad fiber devices,” Opt. Lett. **31**, 3240-3242 (2006).

24. A. Liem, J. Limpert, H. Zellmer, A. Tünnermann, V. Reichel, K. Mörl, S. Jetschke, S. Unger, H.-R. Müller, J. Kirchhof, T. Sandrock, A. Harschak, “1.3 kW Yb-doped fiber laser with excellent beam quality,” in *Proc. Conference on Lasers and Electro-Optics 2004*, San Francisco, USA, May 16-21, 2004, postdeadline paper CPDD2.

25. C. C.Renaud, J. A.Alvarez-Chavez, J. K.Sahu, J. Nilsson, D.J. Richardson, W.A.Clarkson, "7.7mJ pulses from a large core Yb-doped cladding pumped Q-switched fiber laser", CLEO 2001 Baltimore 6-1 1 May 2001 CTuQ5 (2001).

26. K. H. Liao, K. C. Hou, G. Chang, V. Smirnov, L. Glebov, R. Changkakoti, P. Mamidipudi, and A. Galvanauskas, “Diffraction-limited 65-um core Yb-doped LMA fiber based high energy fiber CPA system,” postdeadline paper, presented at CLEO/QELS 2006, Long Beach (2006).

27. C. H. Liu, A. Galvanauskas, V. Khitrov, B. Samson, U. Manyam, K. Tankala, D. Machewirth, and S. Heinemann, “High-power single-polarization and single-transverse-mode fiber laser with an all-fiber cavity and fiber-grating stabilized spectrum,” Opt. Lett. **31**, 17-19 (2006).

28. N. Jovanovic, A. Fuerbach, G. D. Marshall, M. J. Withford, and S. D. Jackson, “Stable high-power continuous-wave $Yb^{3+}$-doped silica fiber laser utilizing a point-by-point inscribed fiber Bragg grating,” Opt. Lett. **32**, 1486-1488, (2007).

29. X. Feng, H. Y. Tam, W. H. Chung, and P. K.A. Wai, “Multiwavelength fiber lasers based on multimode fiberBragg gratings using offset launch technique,” Opt. Commun. **263**, 295-299 (2006).

30. D. Y. Shen, J. K. Sahu and W. A. Clarkson, “Highly efficient Er,Yb-doped fiber laser with 188W free-running and > 100W tunable output power,” Opt. Express **13**, 4916-4921 (2005).

31. W. A. Clarkson, N. P. Barnes, P. W. Turner, J. Nilsson, and D. C. Hanna, “High-power cladding-pumped Tm-doped silica fiber laser with wavelength tuning from 1860 to 2090 nm,” Opt. Lett. **27,** 1989-1991 (2002).

32. Timothy McComb, Vikas Sudesh, and Martin Richardson, “Volume Bragg grating stabilized spectrally narrow Tm fiber laser,” Opt. Lett. **33**, 881-883 (2008).

33. Pär Jelger and Fredrik Laurell, "Efficient narrow-linewidth volume-Bragg grating-locked Nd:fiber laser," Opt. Express **15,** 11336-11340 (2007).

34. C-P. Amado, J. F. D. Michel, and J. S. Herbert, "Miniature CW and active interally Q-switched Nd:MgO:LiNbO3 lasers," J. Quantum Electron. **23**, 262−266 (1987).

35. W. Shin, S. W. Han, C. S. Park, and K. Oh, "All fiber optical inter-band router for broadband wavelength division multiplexing," Opt. Express **12**, 1815-1822 (2004).

36. O. Schmidt, J. Rothhardt, F. Röser, S. Linke, T. Schreiber, K. Rademaker, J. Limpert, S. Ermeneux, P. Yvernault, F. Salin, and A. Tünnermann, "Millijoule pulse energy *Q*-switched short-length fiber laser," Opt. Lett. **32**, 1551-1553 (2005).

37. T. Tordella, H. Djellout, B. Dussardier, A. Saïssy, and G. Monnom, "High repetition rate passively Qswitched $Nd^{3+}$:$Cr^{4+}$ all-fibre laser," Electron. Lett. **39**, 1307-1308 (2003).

38. A. Fotiadi, A. Kurkov, and I. Razdobreev, "All-fiber passively Q-switched ytterbium laser," CLEO/Europe-EQEC 2005, Technical Digest, CJ 2-3, Munich, Germany (2005).

39. V. Philippov, J. Nilsson, W. A. Clarkson, A. Abdolvand, V. E. Kisel, V. G. Shcherbitsky, N. V. Kuleshov, V. I. Konstantinov, and V. I. Levchenko, "Passively Q-switched Er-Yb double clad fiber laser with Cr2+:ZnSe and $Co^{2+}$:MgAl2O4 as a saturable absorber," Proc. SPIE **5335**, 8-15 (2004).

40. V. N. Philippov, A. V. Kir'yanov, and S. Unger, "Advanced configuration of erbium fiber passively Qswitched laser with Co2+:ZnSe crystal as saturable absorber," IEEE Photon. Technol. Lett. **16**, 57–59 (2004).

41. M. Laroche, A. M. Chardon, J. Nilsson, D. P. Shepherd, W. A. Clarkson, S. Girard, and R. Moncorgé, "Compact diode-pumped passively Q-switched tunable Er-Yb double-clad fiber laser," Opt. Lett. **27**, 1980– 1982 (2002).

42. R. Paschotta, R. Häring, E. Gini, H. Melchior, U. Keller, H. L. Offerhaus, and D. J. Richardson, "Passively Q-switched 0.1 mJ fiber laser system at 1.53μm," Opt. Lett. **24**, 388-390 (1999).

43. K. Alavi, H. Temkin, W. R. Wagner, and A. Y. Cho, “Optically pumped 1.55-μm double heterostructure $Ga_xAl_yIn_{1-x-y}As/Al_uIn_{1-u}As$ lasers grown by molecular beam epitaxy,” Appl. Phys. Lett. **42**, 254-256 (1983).

44. T. Hakulinen and O. G. Okhotnikov, “8 ns fiber laser Q switched by the resonant saturable absorber mirror,” Opt. Lett. **32**, 2677-2679 (2007)**.**

# *Chapter 2 Continuous-wave tunable Yb doped and Er/Yb codoped fiber lasers*

## 2.1 Yb doped and Er/Yb codoped silica fiber lasers

Ytterbium (Yb) and Erbium (Er) are both rare earth elements of the lanthanide series. They are often used as doping materials in many hosts such as YAG, $YVO_4$, and various glasses such as silicate, borate, fluoride, and phosphate glasses. Here we qualitatively focus on silica glasses based fibers only because silica glass is the most popular and mature material for fabrication of fibers. Besides, we would also observe that both the dopants are suitable for tunable operation thanks to their broad emission spectrum.

### 2.1.1 Yb doped silica fiber

Ytterbium is the one of the lanthanons element with an atomic number of 70. The electronic configuration of an ytterbium atom is $[kr]4d^{10}4f^{14}5s^{2}5p^{6}6s^{2}$ while the outermost 6s and one of 4f electrons are removed when it is ionized as a trivalent ion. The optical active orbital 4f electrons are hence partly shielded by 5s and 5p shells. The main energy levels concerning the optical transitions of ytterbium ions ($Yb^{3+}$) are shown in Fig. 2.1. The $4f^{13}$ electrons possess only two energy levels where the higher, or say excited level is $^{2}F_{5/2}$ and the lower one is $^{2}F_{7/2}$. Both of them have split into three or four fine stark levels due to several reasons.

The L-S coupling (Russell-Saunders coupling) mainly determined the energy structure for that the optical electrons are shielded partly by 5s and 5p filled orbital. The shielding effect has optical transitions of $Yb^{3+}$ doped materials almost the same. The factors affecting finer split energy levels include local field of hosts, thermal phonons, electronic and magnetic interactions with each individual ions in its vicinity, and resonant interaction with neighboring Yb ions if the doping concentration is sufficiently high [1]. The calculations of fine structures are complicated and are not discussed in this thesis.

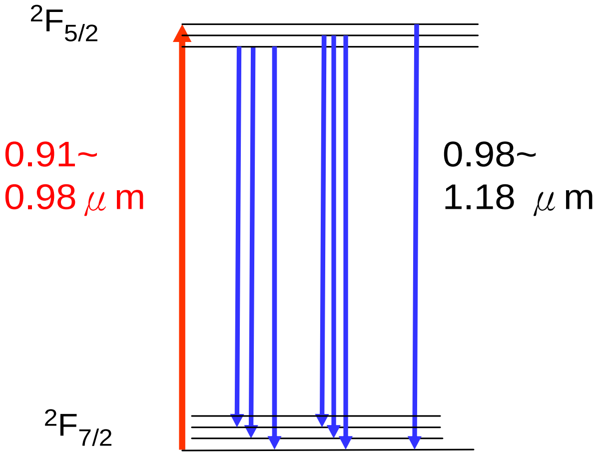

Fig. 2.1. $Yb^{3+}$ energy level diagram in silica fibers. The red line indicates the absorption line and the blue ones indicate emission line.

$Yb^{3+}$ ions are three or quasi-three stark levels structure, which means that they may have slight lower optical transition efficiency than the four levels. However the development of high power diode lasers help to efficiently depopulate the ions in ground level to the excited state. Besides there are some advantages making Yb attractive dopants in fiber gain medium:

A. Low quantum defect:

The simple energy levels structures also reveal that the usual pump wavelengths are close to the radiation showing the quantum defect is quite small, reducing thermal effect at high power operation.

B. Weak quench effect:

Some detrimental effects such as excited stimulated absorption (ESA), concentration quench, and upconversion are weak (still exist actually) due to no other 4f energy level of Yb doped gain medium [2], thus a high doping levels even for 10,000 ppm wt. is achievable in $Yb^{3+}$ doped fiber.

C. Broad emission region:

Broad optical emission and absorption profile as shown in Fig. 2.2 [2] showing Yb$^{3+}$ a potential gain medium in amplifier, tunable lasers, and ultrafast laser.

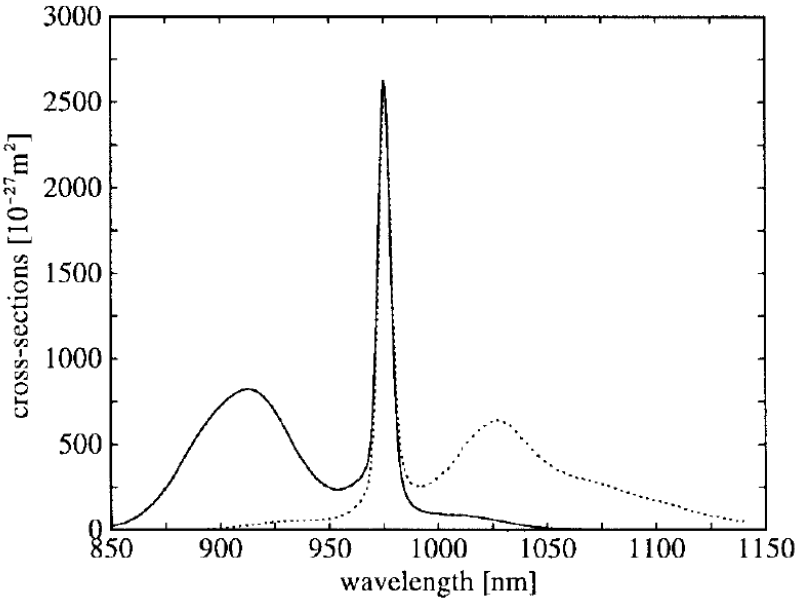

Fig. 2.2. Emission and absorption cross section of ytterbium ion. Solid: absorption cross section; dash: emission cross section. [2]

The stimulated emission and absorption cross-section of Yb doped silicate glass are shown in Fig. 1.2 as well, where the host was germanosilicate glass. The profiles of the optical absorption and emission cross sections are nearly mirror symmetry. The spontaneous emission extends from 0.9µm to 1.1µm continuously due to the strong homogeneous and inhomogeneous broadening. On the other hand the absorption band ranges from 0.8µm–1µm, which indicates a laser-diode or a Nd laser could be as a pump source. The fluorescence lifetime of a pure silicate glass based Yb$^{3+}$ medium is around 1.5 ms [2]. Usually some elements such as Ge, Al, or K are codoped to reduce concentration quench and the lifetime is reduced [2].

### 2.1.2 Er/Yb codoped silica fiber

Er$^{3+}$-dope materials are attractive for their useful gain region in 1.5~1.6 µm, as shown in Fig. 2.3. For high power output higher doping concentration is necessary due to the absorption of erbium ion is impractically low. A problem is followed that the reduction of gain and pump efficiency due to quench effects such as ion-pairing [3, 4] and upconversion, and the latter would be enhanced if ion-pairing is present [5]. It has been showed that $Er^{3+}$-ion pairs would act like a saturable absorber inducing self-pulsing effect in Er-doped fiber lasers at high paired ions level and that did reduce optical efficiency. Afterward several methods were proposed to improve those detrimental effects. An Er-doped fiber laser was shown theoretically and demonstrated simultaneously operating at a stable CW output utilizing a pump wavelength at 1.51μm instead of at 0.98μm [6,7], where self-pulsing was suppressed by a dumping (resonant pumping) of $Er^{3+}$-ions from excited state to ground state.

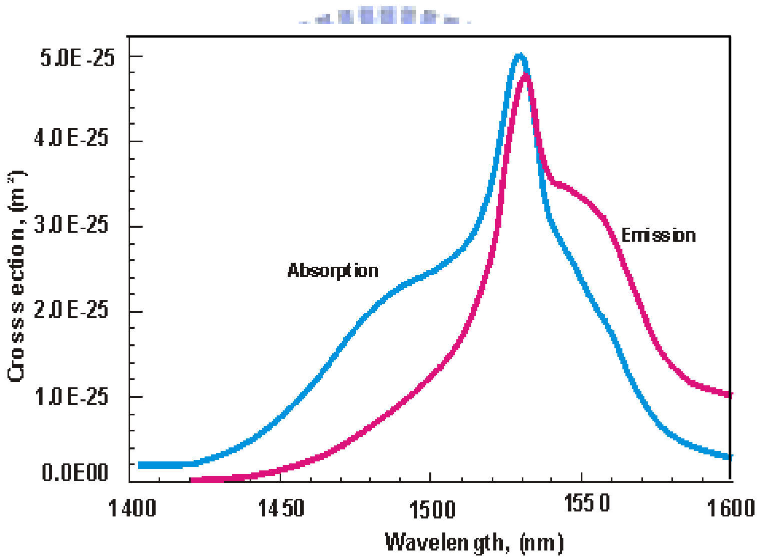

Fig. 2.3. Emission and absorption cross section of Erbium ion.

However the dumping effect significantly decreases pumping efficiency. Other methods to prevent ion-pairing includes low-temperature deposition technique or co-doping with Al or P; however they does not eliminate upconversion among the uniformly distributed ions. In addition, an efficient and practical method to solve this problem is co-doping with ytterbium to absorb the pump light around 980nm and then transferred to Er-ion nonradiatively. The proposal is based on the properties as the following:

A. The ionic radius of $Yb^{3+}$ (85.8 pm) is close to that of $Er^{3+}$ (88.1 pm) [8]. It is possible to surround each $Er^{3+}$ ion with several $Yb^{3+}$ ions to facilitate energy transfer process, especially ytterbium tends to cluster as a high concentration doping level.

B. As mentioned before $Yb^{3+}$-ion owns a simple electronic level, which means the sensitizer does not results in other detrimental effect.

These features increase the efficiency of energy transfer from $Yb^{3+}$ ion to $Er^{3+}$ ion. The pump energy is nonradiatively transferred from $Yb^{3+}$-ion to $Er^{3+}$-ion as shown in Fig 2.3. The pump light is absorbed mainly by $Yb^{3+}$-ion (partially by $Er^{3+}$-ion) and the electrons of the ground level $^2F_{7/2}$ are stimulated to excited level $^2F_{5/2}$, and due to clustering the excited $Yb^{3+}$-ions have a possibility to transfer their energy to their neighboring $Er^{3+}$ ion via elastic collision to indirectly excite, or pump the electrons at ground state $^4I_{15/2}$ to excited state $^4I_{11/2}$. It is worthwhile noting a back-transfer process is seldom cause of the lifetime of $^4I_{11/2}$ is quite short and for high-efficient Yb:Er codoped fibers and by the aid of codoping of phosphate and aluminum [9-14].

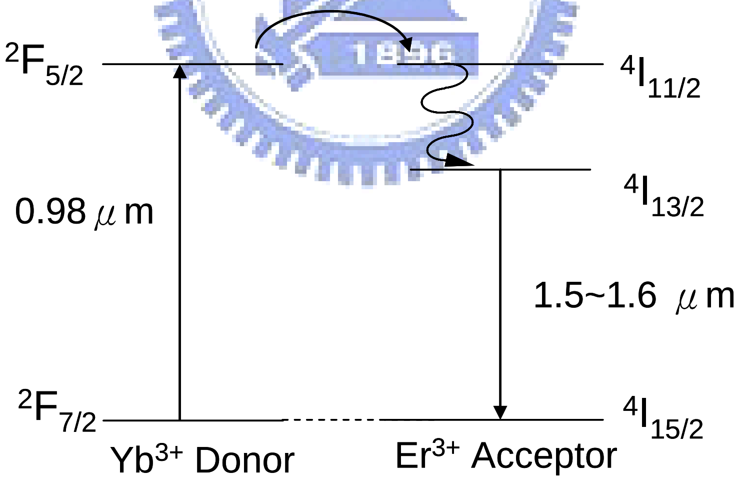

Fig. 2.4. Plot of Yb sensitized Er doped fibers. The energy is transferred nonradiatively from the excited state of $Yb^{3+}$ ion to the metastable state of $Er^{3+}$ ion to enhance pump absorption.

An important issue is ratio of the concentration for Yb and Er. As we mentioned above an $Er^{3+}$ ion is expected to be surrounded by several $Yb^{3+}$ ions, which obviously indicating a much higher concentration of $Yb^{3+}$ ion than that of $Er^{3+}$ ion. Nevertheless a too high concentration of Yb would waste pump energy and reduce the energy transfer efficiency, as well as the gain coefficient. The ratio of the concentration $N_{Yb}/N_{Er}$ is recommended to be between 4 and 20 [15]. Besides, some imperfections exist and are not understood yet so far. For example, isolated $Yb^{3+}$-ions would radiate 1.1-μm emission without transferring energy to $Er^{3+}$-ions and non-uniformly distributed concentration is harmful to energy-transferring as well.

## 2.2 All-dielectric thin film Fabry-Pérot filters

### 2.2.1 Introduction to dielectric thin film filters

Among the optical filters there are several types based on different principles such as absorbing glass filter and color filter are based on wavelength-dependent absorption, Lyot filters [16] are based on wavelength-dependent polarization change, and prisms are based on wavelength-dependent diffraction. On the other hand, interference effect based filters including etalon, Mach-Zehnder interferometers, acousticoptic filters [17-18], FBGs [19-20], VBGs [21-22], and AWGs [23]. They provide wavelength-selection and are well-developed and commercialized.

Dielectric thin film filter or multilayer interference filter is also based on interference effect and offer another approach for filtering. They are the first filter type to be widely deployed in wavelength division multiplexing (WDM) systems in the 1990s [24-25]. The technology has also been applied to a number of important optical network applications such as gain-flattening filters (GFFs), high performance band splitter-pump WDMs for erbium-doped fiber amplifiers (EDFAs), and wideband splitting filters for separating bands of channels. Thin film filter possess the merits of very low temperature coefficient, long stability, and small losses of chromatic dispersion and polarization-related dispersion. Thin film filter consists of an alternating sequence of layers of transparent dielectric material of high and low refractive indices deposited on a substrate.

The candidates for substrates are usually BK7 glass and fused silica and the coating materials are often categorized two types. One is oxides including $SiO_2$, $TiO_2$, and $Al_2O_3$, the other is fluorides including $MgF_2$, La $F_3$, and Al $F_3$. The fabrications of the thin films are based on the techniques such as electron beam deposition, ion-assisted deposition (IAD), and ion-beam sputtering (IBS) deposition. The technology is very flexible; AR, narrow bandpass, wide bandpass, edge, gain flattening, dispersion compensation, and other filters can be designed for applications.

### 2.2.2 All-dielectric Fabry-Pérot filters

In this section I pay my attention to narrow bandpass type thin film filter which realizes a narrowband transmission to be an efficient wavelength-narrowing element for broadband lasers. Figure 2.1 shows the structure of a typical bandpass dielectric thin film filter. The structure of is based on Fabry-Perot (FP) cavity type and is formed by a space region sandwiched between two highly-reflecting multilayer stacks deposited on a glass substrate. The basic design formula for the more commonly used all-dielectric version is:

$$\text{Substrate} \mid (LH)^m\ (2L)^n\ (HL)^m \mid \text{air}\ , \tag{2.1}$$

where m is the number of periods in the HRs; n is the order of the spacer.

The highly-reflecting stacks are composed of multi alternating sequence of high and low refractive indices with optical thickness of quarter-wave of central wavelength. The optical high spacer thickness at the centre wavelength for the first order (n = 1) is one halfwave, for the second order (m = 2) two halfwaves, etc. In a FP filter, only a small fraction of light normally penetrates the first reflector, but at certain resonant wavelengths, the light intensity builds up in the spacer layer until a significant fraction close to 100% of the input light is transmitted. The transmittance of thin film filter can be expressed as:

$$T(\theta) = T_{\max}\left[1 + F\sin^2\left(\frac{\phi_{\text{int}} + \phi_{out}}{2} - \delta(\theta)\right)\right]^{-1}\ , \tag{2.1}$$

where $T_{\max} = \dfrac{T_{in}T_{out}}{\left[1-\left(R_{in}R_{out}\right)^{1/2}\right]^2}$ ; $F = \dfrac{4\left(R_{\text{int}}R_{out}\right)^{1/2}}{\left[1-\left(R_{\text{int}}R_{out}\right)^{1/2}\right]^2}$ ; $\delta = \dfrac{2\pi}{\lambda} n_s d_s \cos\theta$, and

$R_{int}$ and $R_{out}$ are the reflectance at incidence and output side of filter respectively; $T_a$ and $T_b$ are the reflectance at incidence and output side of filter respectively; $\phi_{\text{int}}$ and $\phi_{out}$ are the phase change at incidence surface and output surface; $n_s$ is the refractive index of the filter; and $d_s$ is the thickness of the filter.

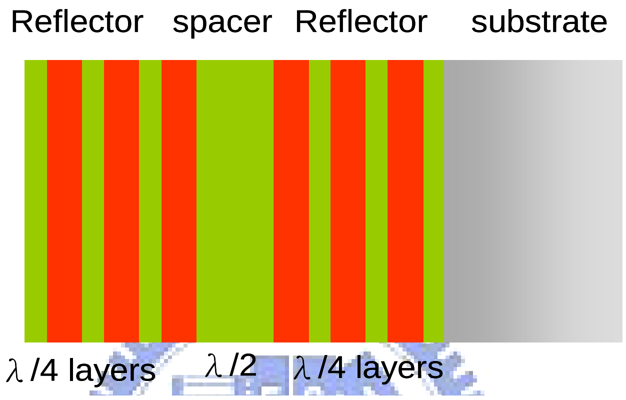

Fig. 2.5. The structure of a typical thin film Fabry-Perot filter.

The maximum transmission $T_{max}$ would equal unity only if all the materials do not absorb the light inelastically or the transmittance of the incidence side is equal to that of the output one. The highest transmission occurs at the total phase difference is m$\pi$ for $\lambda=\lambda_p$, the central wavelength, i.e.

$$\phi = \frac{2\pi}{\lambda_p} n_s d_s \cos\theta - \frac{\phi_a + \phi_b}{2} = m\pi,\ \text{m}=0,\ \pm 1,\ \pm 2 \ldots \tag{2.2}$$

which gives

$$\frac{1}{\lambda_p} = \frac{1}{2 n_s d_s \cos\theta}\left(m + \frac{\phi_a + \phi_b}{2\pi}\right). \tag{2.3}$$

If $\phi_{\text{int}}$ and $\phi_{out}$ are zero (2.3) can be rewritten as

$$\lambda_p = \lambda_p\left(\theta_{in}\right) = \frac{2}{m} n_s d_s \sqrt{1 - \frac{n_{air}^2}{n_s^2}\sin^2\theta_{in}} = \lambda_0 \sqrt{1 - \frac{n_{air}^2}{n_s^2}\sin^2\theta_{in}} \quad , \tag{2.4}$$

where $\lambda_0$ is the measured central wavelength at normal incidence. Hence the central wavelength of a FP filter is a function of the angle of incidence, which meaning it could be adopted as a tunable wavelength selector for optical measurement or wavelength tuning in a laser.

## 2.3 Tunable ytterbium doped fiber lasers

The wavelength selection in this section is achieved by an all-dielectric FP bandpass filter owning a bandwidth of approximately 1.24 THz or 5nm at 1100nm. In this part we demonstrated an efficient tunable Yb doped fiber laser with the FP bandpass filter. The efficiency from a free running lasing with a bandwidth of >10 nm to a narrow linewidth lasing with a linewidth < 1 nm can exceed 96%. By tilting the incidence angle, the lasing wavelength can be tuned from 1540 nm to 1100 nm with a tuning range up to 60 nm.

### 2.3.1 Experimental setup

Figure 2.6 displays the schematic of the experimental setup for the tunable Yb doped fiber laser, which consists of a 3-m Yb-doped fiber and an external feedback cavity including a saturable absorber. The fiber has an absorption coefficient of 10.8 dB/m at 976 nm and a double-clad structure with a diameter of 350 μm octagonal outer cladding, diameter of 250 μm octagonal inner cladding with a numerical aperture (NA) of 0.46, and 30μm circular core with a NA of 0.07. The low-intensity transmission of the narrowband dielectric filter is shown in figure 2.4.2, which peaks at 1100nm with FWHM around 5 nm measured by a monochromator with a resolution of 0.1 nm. The end facets of the fiber were cut to be normal incident. Therefore, the lasing by end facets usually occurred for the free-running operation.

The pump source was a 35-W 976-nm fiber-coupled laser diode with a core diameter of 400 μm and a NA of 0.22. A focusing lens with 25 mm focal length and 92% coupling efficiency was used to re-image the pump beam into the fiber through a dichroic mirror with high transmission (>90%) at 976 nm and high reflectivity

(>99.8%) at 1030~1100 nm. The pump spot radius was approximately 200 μm.

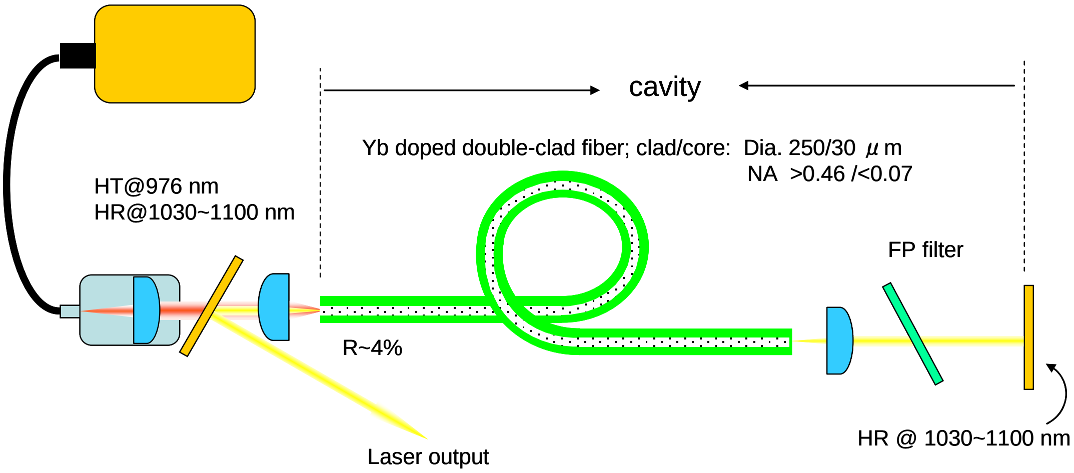

Fig. 2.6. Schematic configuration of the tunable and narrowband Yb doped fiber laser.

The spectral transmittance of the thin-film FP filter at normal incidence is shown in Fig. 2.7. The transmission bandwidth is approximately 5nm and the central wavelength is around 1102 nm with a transmission up to 96%. The thin-film FP bandpass filter used in this experiment had a clear aperture of 3 mm ×3 mm and was 0.5mm thick. The central wavelength can shift lower at oblique incidence. Therefore, the bandpass filter was mounted rigidly on a precision rotation stage to control the incident angle for wavelength tuning. In terms of the incident angle , the wavelength of peak transmittance is given by equation (2.4) with the parameters $\lambda_o=1.102\mu m$, $n_o=1$, and $n_{eff}$ is determined with the curve-fitting to the experimental measurement. As shown in Fig. 2.8. Eq. (2.4) can be used to express the wavelength dependence on angle of incidence up to $30^{o}$ with $n_{eff}=1.6$.

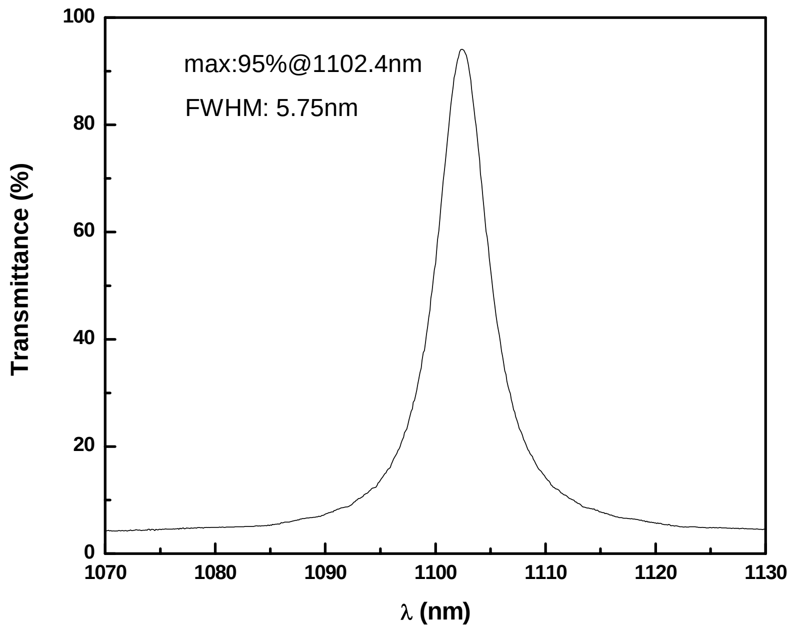

Fig. 2.7. Spectral transmittance of the thin-film FP 1.1-μm filter at normal incidence.

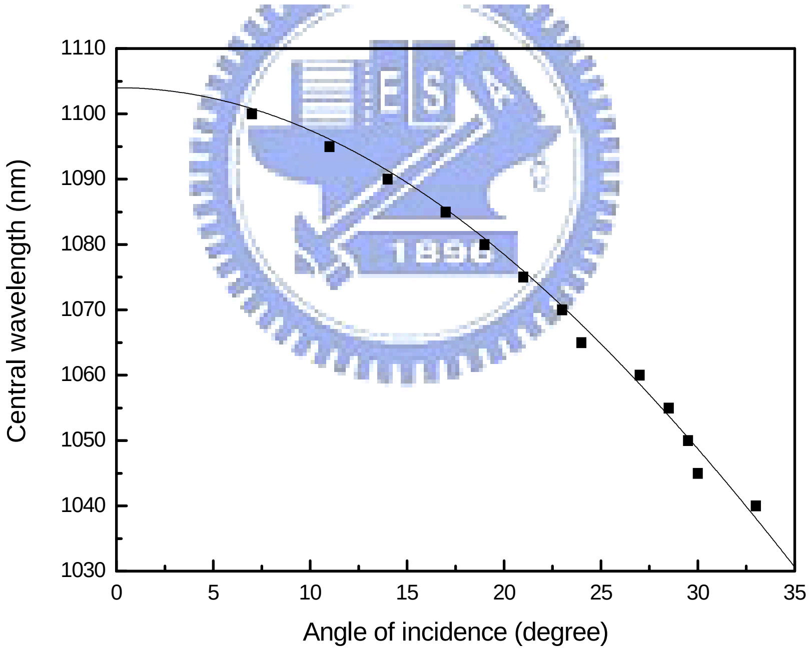

Fig. 2.8. Wavelength dependence on angle of incidence for the thin film FP 1.1-μm filter bandpass filter.

### 2.3.2 Results and discussions

The free-running performance of the present fiber laser was studied first. The external cavity only comprised a focusing lens and a high reflector without inserting the FP bandpass filter. The free-running performance was taken as a baseline to obtain the efficiency of the wavelength narrowing with the FP bandpass filter. Figure 2.9 shows the output powers with respect to the incident pump power in the free-running operation and the wavelength-narrowing operation at 1040nm, 1060nm, 1080nm, 1095nm, and 1100nm by changing the incident angle on the FP bandpass filter. In the free-running operation the maximum output power of was approximately 17 W at a pump power of 26 W. The slope and optical-to-optical efficiencies were 77% and 68%, respectively. The wavelength-narrowing operation had slightly lower slope efficiencies due to the insertion loss by the FP filter. The efficiency from the free running operation to the wavelength-narrowing operation can be generally greater than 90%.

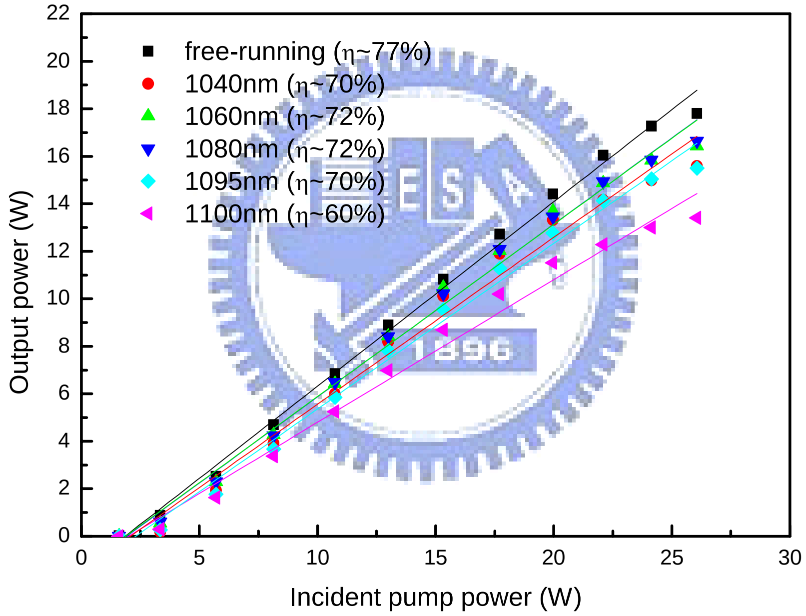

Fig. 2.9. Output powers with respect to the incident pump power in the free-running operation and the wavelength-narrowing operation of tunable Yb fiber laser.

The overall tuning range was shown in Fig. 2.10. The output powers were almost the same for the whole tuning range. Note that the upper wavelength was restrained by the peak transmission wavelength of the filter at normal incidence, whereas the lower wavelength was limited by the gain profile of the fiber. As we increased the AOI further, the Yb population required for lasing is higher that the gain at the gain peak becomes excessive, to the point where ASE at the gain peak starts to dominate the emission and a parasitic lasing occurred. It is noted that the gain profile is influence by the temperature of the core, the length of the fiber, and codoped dopants such as aluminates for refractive index controlling. Moreover the temperate-sensitive or length-sensitive property is due to the energy level of Yb ion as mentioned in 4.1. Sinha et al. at Stanford Univ. have produced a fiber laser emitting at 1150 nm by heating the fiber directly to red-shift the fluorescence of Yb fiber [26] and Dvoyrin et al. obtained an 1160-nm Yb fiber laser with a self-heating Yb fiber [27]. Oppositely a shorter-wavelength operation demands a shorter fiber or lower temperature of fiber itself.

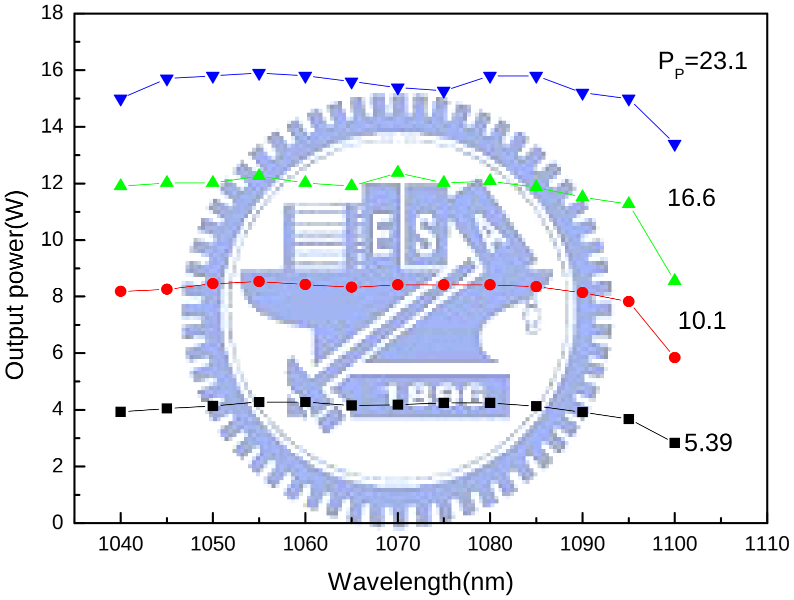

Fig. 2.10. Dependence of the output powers on the lasing central wavelength of tunable Yb fiber laser.

The laser spectral performance was recorded by an OSA with maximum resolution of 0.1 nm (Advantest Q3489). As depicted in Fig. 2.11, the lasing linewidth is narrower with a linewidth of 0.36 nm than 5 nm of the FP filter, due to the normal linewidth narrowing occurring in the multi-pass amplification. Figure 2.12 shows the spectral bandwidth of the free-running operation and narrowband operation at various wavelengths. Linewidth of free-running operation was wider than 10 nm while the lasing linewidth were narrower than 1 nm for all tuning range at narrowband operation.

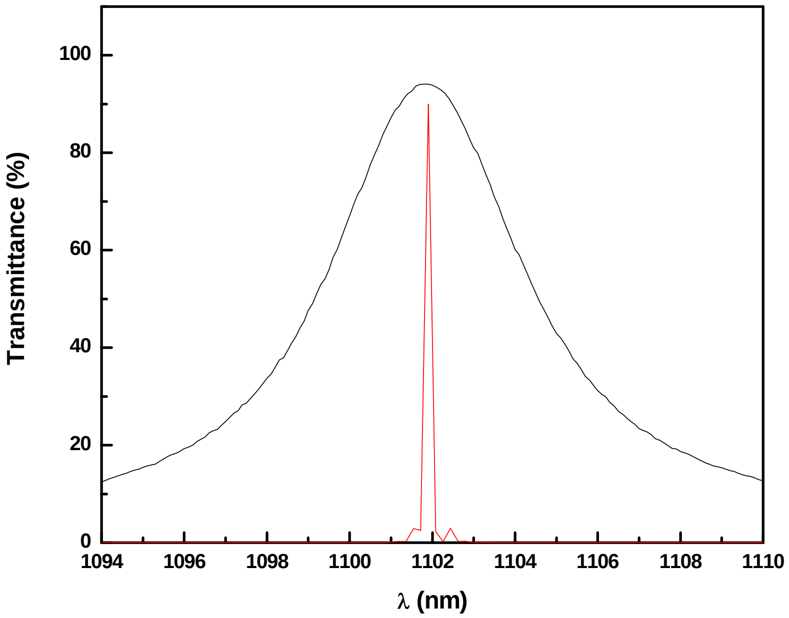

Fig. 2.11. Comparison of the linewidth of the thin-film FP1.1-μm filter and that of the narrow-linewidth Yb fiber laser.

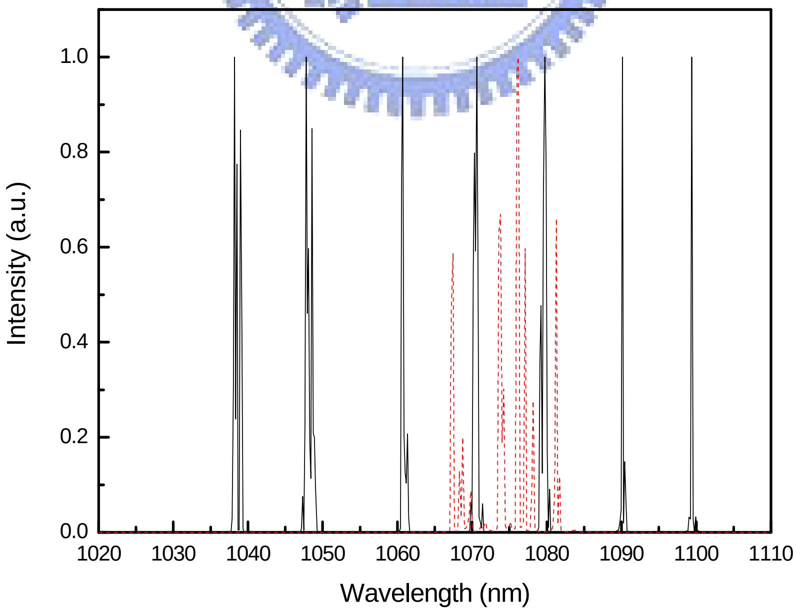

Fig. 2.12. Experimental spectra for the free-running and wavelength-narrowing operations of tunable Yb fiber laser. The solid lines present narrowing spectra; the dot line presents the free-running operation.

## 2.4 Tunable Er/Yb codoped fiber lasers

In this section the FP filter is a standard DWDM filter with a bandwidth of 50 GHz. We demonstrated that an efficient tunable Er/Yb doped fiber laser can be simply achieved with a 50 GHz FP bandpass filter. The efficiency from a free running lasing with a bandwidth of >5 nm to a narrow linewidth lasing with a linewidth < 0.15 nm can exceed 96%. With tilting the incidence angle, the lasing wavelength can be tuned from 1536 nm to 1564 nm with a tuning range up to 28 nm.

### 2.4.1 Experimental setup

Figure 2.13 depicts a schematic diagram of the experimental setup. The laser cavity comprised a 7-m double-clad Er/Yb codoped fiber and an external feedback cavity. The absorption coefficient of the gain fiber was lower than that of the Yb doped fiber, approximately 3dB/m at 976 nm. The fiber had a core diameter of 25 μm and a cladding diameter of 400 μm with corresponding numerical apertures (NA) of 0.07 and 0.46. The fiber was coiled with a 12-cm diameter to increase the losses for the higher order transverse modes and strengthen the single-spatial-mode operation.

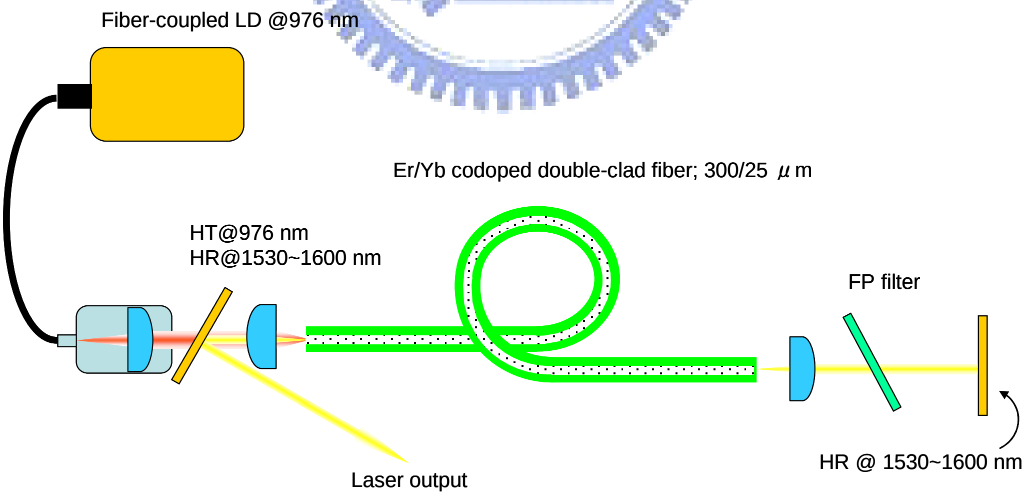

Fig. 2.13. Schematic configuration of the tunable and narrowband Er/Yb doped fiber laser.

The external cavity was composed of an aspherical lens with 8-mm focal length, a thin-film FP bandpass filter for selecting and narrowing the emission wavelength, and a rear dielectric mirror with high reflectivity at 1530-1570 nm. The whole cavity was bounded by the rear mirror and a perpendicularly cleaved fiber end facet as the output end with ~4% Fresnel reflection. The fiber end facet adjacent to the external cavity was not angled cleaved to suppress broadband feedback. The pump source and pump scheme were identical to those employed in the above section.

The spectral transmittance of the thin-film FP filter at normal incidence is shown in Fig. 2.14. It can be seen that the transmission bandwidth is approximately 50 GHz and the central wavelength is around 1564.2 nm with a transmission up to 98%. Note that the characteristics of the present bandpass filter are appropriate to the demand of WDM applications.

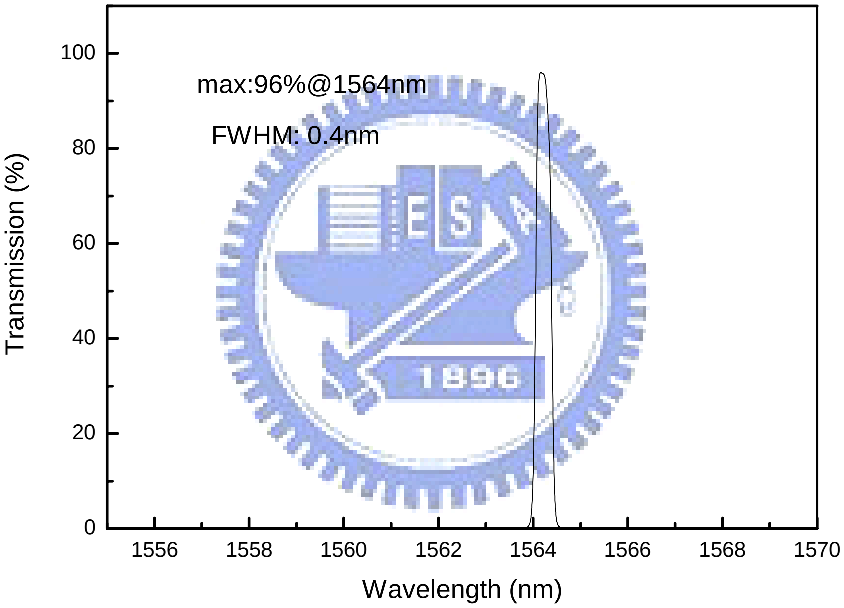

Fig. 2.14. Spectral transmittance of the thin-film FP 1.1-μm filter at normal incidence.

The thin-film FP bandpass filter used in our experiments had a clear aperture of 1.4 mm × 1.4 mm and was 0.5mm thick. The central wavelength can shift lower at oblique incidence. Therefore, the bandpass filter was mounted rigidly on a precision rotation stage to control the incident angle for wavelength tuning. In terms of the incident angle, the wavelength of peak transmittance is given by equation (1) with the parameters $\lambda_o$=1.56 $\mu m$, $n_o$=1, and $n_{eff}$ is determined with the curve-fitting to the experimental measurement. As shown in Fig. 2.15, Eq. (1) can be used to express the wavelength dependence on angle of incidence up to 15° with $n_{eff}$=1.37.

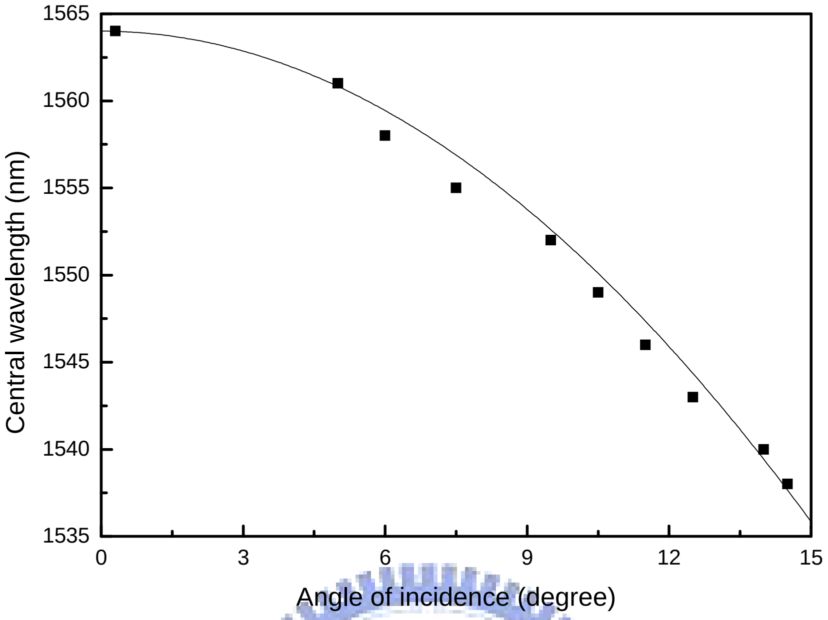

Fig. 2.15. Wavelength dependence on angle of incidence for the thin film FP 1.56-μm filter bandpass filter.

### 2.4.2 Results and discussions

The free-running performance of the present fiber laser was studied first. For this investigation, the external cavity only comprised a focusing lens and a high reflector without inserting the FP bandpass filter. The free-running performance provides the baseline for evaluating the efficiency of the wavelength narrowing with a FP bandpass filter. Figure 2.16 shows the output powers with respect to the incident pump power in the free-running operation and the wavelength-narrowing operation at normal incidence. In the free-running operation the maximum output power was approximately 3.7 W at a pump power of 18.5 W with a slope efficiency of 22%; while the slope efficiency was degraded to 7.9% at higher pump power owing to lasing of $Yb^{3+}$ ion mainly. The wavelength-narrowing operation had nearly the same performance at the output power. The corresponding output power and slope efficiency at 1564nm, 1552nm, and 1536 nm are shown in the Fig as well. The highest efficiency from the free running operation to the wavelength-narrowing operation can be generally greater than 92%. This result confirms the insertion loss of the thin film FP to be very low, comparable to the performance of VBGs in fiber lasers [chapter 1, 32-33].

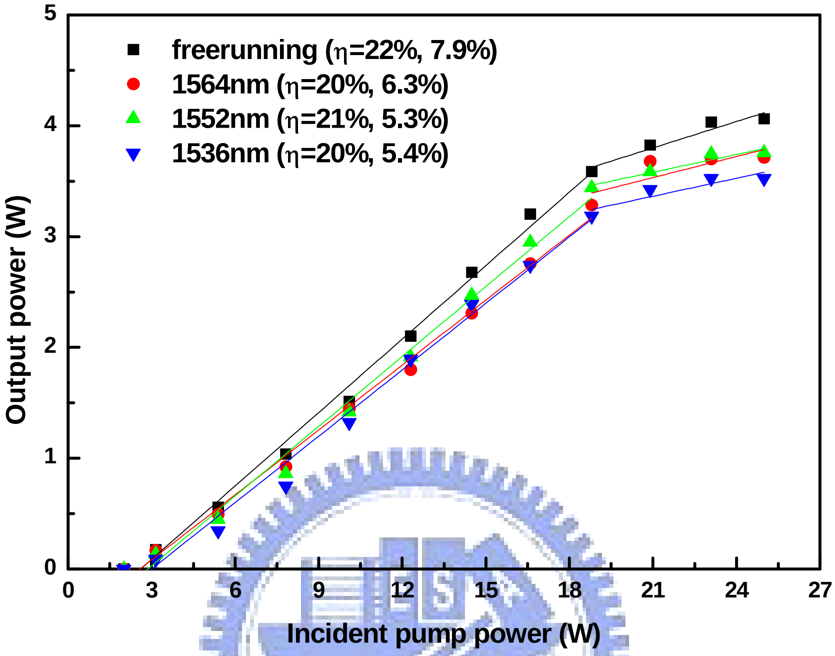

Fig. 2.16. Output powers with respect to the incident pump power in the free-running operation and the wavelength-narrowing operation of tunable Er/Yb fiber laser.

With changing the incident angle on the FP bandpass filter, the lasing central wavelength can be tuned from 1564.2 nm to 1536 nm, corresponding to the incident angle varying from 0° to 15°. The overall tuning range was shown in Fig. 2.17. The output powers were almost the same for the whole tuning range. Note that the upper wavelength was restrained by the peak transmission wavelength of the filter at normal incidence; whereas the lower wavelength was limited by the gain profile of the fiber.

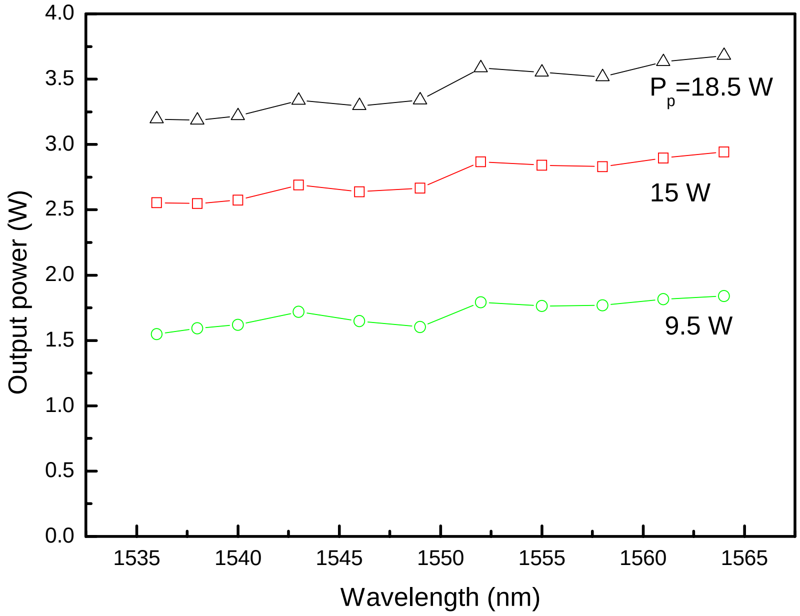

Fig. 2.17. Dependence of the output powers on the lasing central wavelength of tunable Er/Yb fiber laser.

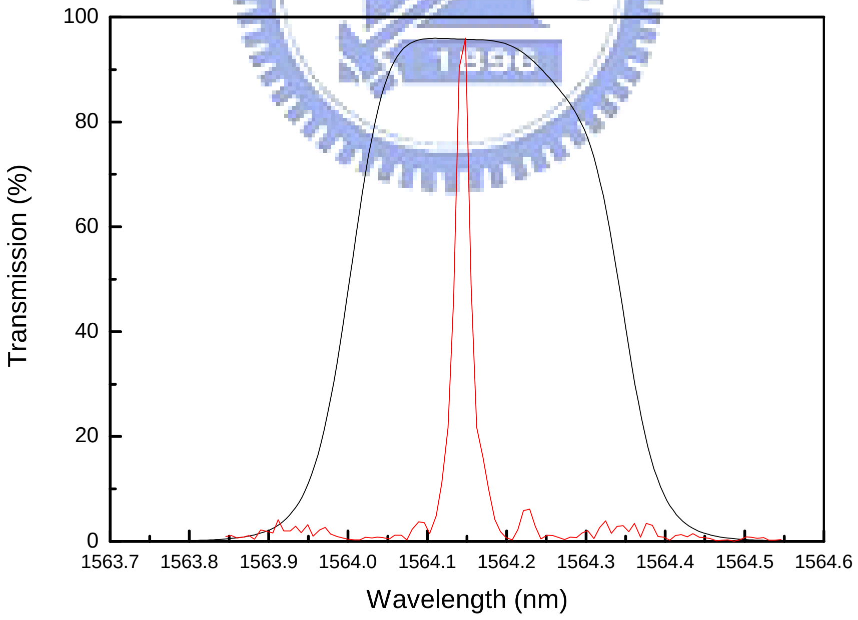

Fig. 2.18. Comparison of the linewidth of the thin-film FP 1.56-μm filter and that of the narrow-linewidth Er/Yb fiber laser.

The lasing spectra were measured by employing an optical spectra analyzer (Advantest Q8347) with a resolution of 0.007 nm. As depicted in Fig. 2.18, the spectral bandwidth of the narrowband operation was narrower with a linewidth <0.15 nm than 0.4 nm of the FP filter. Figure 2.19 shows the linewidth of the free-running mode and that of narrowband mode over all tunable range. Linewidth of free-running operation was wider than 5 nm while the lasing linewidth were narrower than 0.2 nm for all tuning range at narrowband operation.

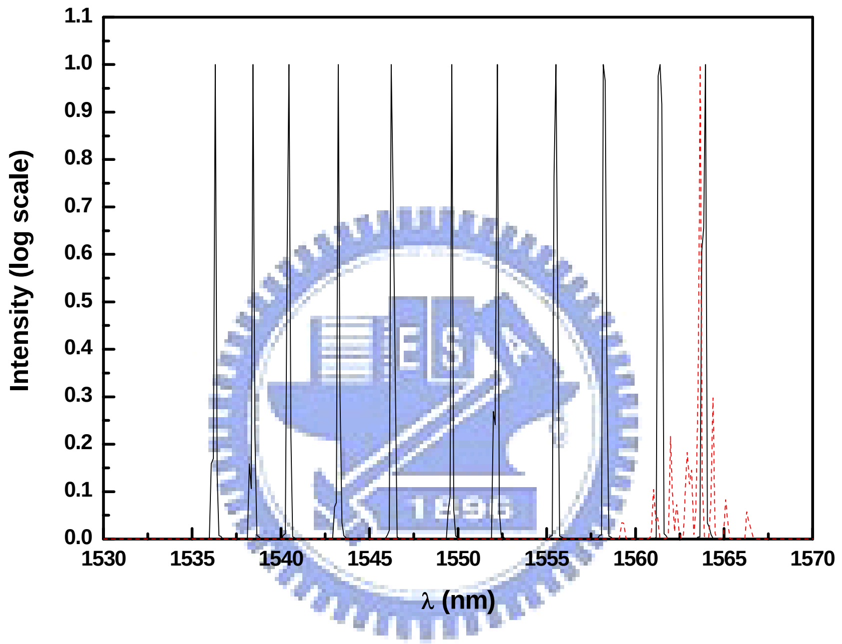

Fig. 2.19. Experimental spectra for the free-running and wavelength-narrowing operations of tunable Er/Yb fiber laser. The solid lines present narrowing spectra; the dot line presents the free-running operation.

## 2.5 Conclusion

An efficient tunable narrow-linewidth Yb and Er/Yb fiber lasers have been obtained with an all-dielectric FP bandpass filter as a wavelength selector. In Yb fiber experiment, the lasing spectrum can be reduced from a free-running wide band of 10 nm to a narrow band of <1 nm with a thin-film FP bandpass filter. The insertion loss introduced by the thin-film FP filter is so low that the overall output powers remain >93% of the free-running output power. With tilting the incident angle to shift the passband curve, the lasing wavelength can be tuned from 1040nm to 1100 nm with a tuning range greater than 60 nm. In the Er/Yb fiber laser experiments, an efficient tunable narrow-linewidth Er/Yb fiber laser has been obtained with an all-dielectric FP bandpass filter as a wavelength selector. The lasing spectrum can be reduced from a free-running wide band of >5 nm to a narrow band of <0.15 nm with a thin-film FP bandpass filter. More importantly, the insertion loss introduced by the thin-film FP filter is so low that the overall output powers remain >92% of the free-running output power. With tilting the incident angle to shift the passband curve, the lasing wavelength can be tuned from 1536nm to 1564.2 nm with a tuning range greater than 28 nm.

# Reference

1. K. Lu, N. K. Dutta, “Spectroscopic properties of Yb-doped silica lass,” J. Appli. Phy. **91**, 576-581, (2002).
2. Rüdiger Paschotta, Johan Nilsson, Anne C. Tropper, and David C. Hanna, “Ytterbium-dSoped Fiber Amplifiers,” IEEE J. Quantum Electro. **33**, 1049-1056 (1997).
3. F. Sanchez, P. Le Boudec, P. L. Francois, and G. Stephan, “Effects of ion pairs on the dynamics of erbium-doped fiber lasers,” Phys. Rev. A, **48**, 2220-2229 (1993).
4. J. L. Zyskind, V. Mizrahi, D. J. DiGiovanni, and J. W. Sulhoff, “Short single frequency erbium-doped fiber laser,” Electron. Lett. **28**, 1385-1387 (1992).
5. C. C. Ye, P.R. Morkel, E.R. Taylor, and D.N. Payne, “Direct observation of cooperative Upconversion mechanisms in erbium-doped fibre amplifiers,” ECOC ’93, Montreux, Sptember (1993).
6. W. H. Loh and J. P. de Sandro, “Suppression of self-pulsing behavior in erbium-doped fiber lasers with resonant pumping,” Opt. Lett. **21**, 1475–1477, (1996).
7. W. H. Loh, “Suppression of self-pulsing behavior in erbium-doped fiber lasers with resonant pumping,” Opt. Lett. **21**, 734–736 (1996).
8. http://www.3rd1000.com/
9. A. B. Grudinin, D. J. Richardson, A. K. Senatorov, and D. Payne, “Nd:YAG laser pumped picosecond Yb$^{3+}$/Er$^{3+}$ fibre laser,” Electron. Lett. **28,** 766–767 (1992).
10. D. C. Hanna, A. Kazer , M. W. Phillips, D. P. Shepherd, and P. J. Suni, “Active mode-locking of an Yb:Er fibre laser,” Electron. Lett. **19,** 95–96 1989).
11. D. U. Noske, A. Boskovic, M. J. Guy, and J. R. Taylor. “Synchronously pumped, picosecond, ytterbium-erbium fibre laser,” Electron. Lett. **29 ,**1863–1864 (1993).
12. J. E. Townsend, W. L. Barnes, and K. P. Jedrzejewski, “Yb$^{3+}$ sensitised Er$^{3+}$ doped silica optical fibre with ultrahigh transfer efficiency and gain,” Electron. Lett. **27 ,**1958–1959 (1991).

13. M. J. Guy, D. U. Noske and, J. R. Taylor, “Generation of femtosecond soliton pulses by passive mode locking of an ytterbium - erbium figure-of-eight fiber laser,” Opt. Lett. **18** **,**1447–1149 (1993).

14. M. E. Fermann, D. C. Hanna, D. P. Shepherd, P. J. Suni and J. E. Townsend, Efficient operation of an Yb-sensitised Er fibre laser at 1.56 µm,” Electron. Lett. **24,** 1135–1136 (1988).

15. F. M., and F. Di Psquale "The Effect of Pair-Induced Energy Transfer on the Performance of Silica Waveguide Amplifiers with High $Er^{3+/}Yb^{3+}$ Concentrations", IEEE Photon. Technol. Lett. **7**, 303-305 (1995).

16. B. Lyot, “Optical apparatus with wide field using interference of polarized light,” C. R. Acad, Sci. (Paris) 197, 1953 (1933).

17. I. C. Chang, “Noncollinear acousto-optic filter with large angular aperture,” Appl. Phy. Lett. **25**, 370-372 (1974).

18. H. S. Kim, S. H. Yun, I. K. Kwang, and B. Yoon Kim, "All-fiber acousto-optic tunable notch filter with electronically controllable spectral profile," Opt. Lett. **22**, 1476-1478 (1997).

19. K.O. Hill, and G. Meltz, “Fiber Bragg Grating Technology Fundamentals and Overview,” IEEE J. Lightwave Technol. **15**, 1263-1276 (1997).

20. A. D. Kersey, T. A. Berkoff, and W. W. Morey, "Multiplexed fiber Bragg grating strain-sensor system with a fiber Fabry - Perot wavelength filter," Opt. Lett. **18**, 1370-1372 (1993).

21. T. Chung, A. Rapaport, V. Smirnov, L. B. Glebov, M. C. Richardson, and M. Bass, "Solid-state laser spectral narrowing using a volumetric photothermal refractive Bragg grating cavity mirror," Opt. Lett. **31**, 229-231 (2006).

22. J. Lumeau, L. B. Glebov, and V. Smirnov, "Tunable narrowband filter based on a combination of Fabry-Perot etalon and volume Bragg grating," Opt. Lett. **31**, 2417-2419 (2006).

23. H. Takahashi, **S.** Suzuki, K. Katoh, and I. Nishi, “Arrayed-waveguide grating for wavelength division multi/demultiplexer with nanometer resolution,” Electron. Lett. **26**, 87-88 (1990).

24. C. K. Madsen and G. Lenz, “Optical all-pass filters for phase response design with applications for dispersion compensation,” IEEE Photon. Technol. Lett. **10**, 994–996 (1998).

25. G. Lenz, B. J. Eggleton, C. R. Giles, C. K. Madsen, and R. E. Slusher, “Dispersive properties of optical filters for WDM systems,” IEEE J. Quantum Electron. **34**, 1390–1402 (1998).

26. S. Sinha, C. Langrock, M. J. F. Digonnet, M. M. Fejer, and R. L. Byer, “Efficient yellow-light generation by frequency doubling a narrow-linewidth 1150 nm ytterbium fiber oscillator ,” Opt. Lett. **31**, 347-349 (2006).

27. V. V. Dvoyrin, V. M. Mashinsky, O. I. Medvedkov, and E. M. Dianov, “Yellow Frequency-Doubled Self-Heated Yb Fiber Laser,” Conference on Lasers and Electro-Optics (CLEO) San Jose, California, 1-2, May 4, (2008).

# *Chapter 3 Passively Q-switched Ytterbium Fiber Lasers by use of $Cr^{4+}$: YAG crystals*

## 3.1 Introduction to passively Q-switching

Passively Q-switching (PQS) is an important technique providing a compact method for generating pulse with duration of ns-scale normally or ps-scale for microchip type PQS lasers. PQS is modulated by a passive material such as organic dye, doped monolithic crystal, or semiconductor saturable absorber. These saturable absorbers can absorb light of their optical transition line and the absorption can be described simply by the equation:

$$\alpha_o(E) = \frac{\alpha_o}{1 + E_i / E_s}, \qquad (3.1)$$

where $\alpha_o$ is the small-signal absorption coefficient, $E_i$ is the incident energy density, and $E_s$ is a saturation fluence

$$E_{sat} = \frac{h\nu_s}{\left(\sigma_e + \sigma_a\right)} A_{mode}, \qquad (3.2)$$

where $\sigma_{gs}$ is the absorption cross section for the optical transition. The absorption is intensity dependent and saturable absorbers become more transparent when they absorb light. Figure 4.1 shows the transmission characteristics. The transmission is initially invariant and has a jump when $E_i$ close to $E_s$. At higher incident energy density saturable absorber is saturated or bleached and is nearly a constant. PQS is based on the behavior of the absorption which provides a high loss initially in a resonant to prevent resonating and to store population inversion in gain medium; as saturable absorber is pumped continuously by the fluorescence of gain medium, it is transparent finally and the gain exceeds the loss which results in a pulse output. There are a number of publications dealing with modeling of PQS lasers [1-5]. Here I will introduce and derive several important equations based on Ref. [1,4]

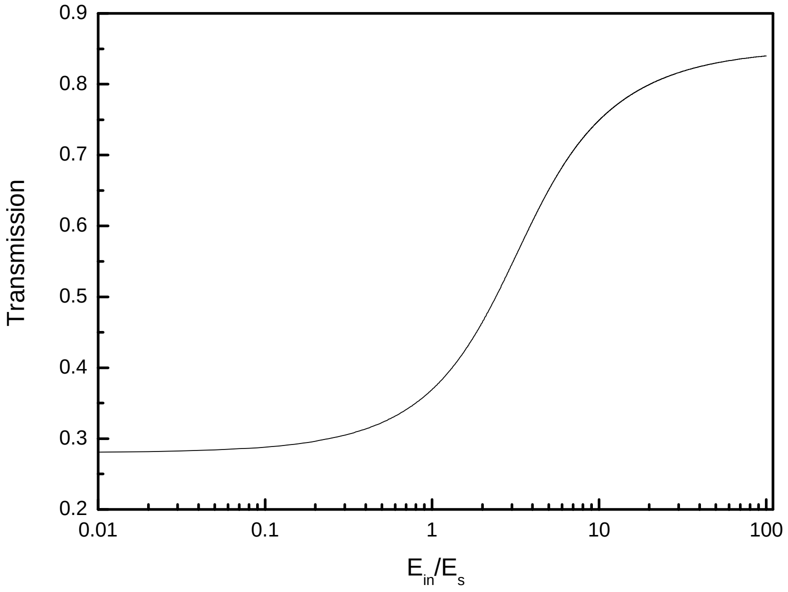

Fig. 3.1. Nonlinear transmission of a saturable absorber versus incident energy density normalized to its saturation energy density.

The parameters such as pulse energy, pulse peak power, and second threshold criterion will be obtained by including the parameters of intracavity focusing and the ESA effect into the rate equation. The coupled rate equations used here were based on that photon is axially uniformly distributed and the saturable absorber recovers completely.

$$\frac{d\phi}{dt}=\frac{\phi}{t_r}\left[2\sigma nl-2\sigma_{gs}n_{gs}l_{gs}-2\sigma_{es}n_{es}l_{es}-\left(\ln\left(\frac{1}{R}\right)+L\right)\right] \tag{3.3}$$

$$\frac{dn}{dt}=R_p-\frac{n}{\tau_f}-\gamma\sigma c\phi n \tag{3.4}$$

$$\frac{dn_{gs}}{dt}=\frac{n_{es}}{\tau_s}-\frac{A}{A_s}\sigma_{gs}c\phi n \tag{3.5}$$

$$n_{gs}+n_{es}=n_{so}, \tag{3.6}$$

where $\phi$ is the effective intracavity photon density; $R_p$ is the volumetric pump rate; n is population density of gain medium; $l_s$ is length of saturable absorber; $\tau_f$ and $\tau_s$ are the recovery time of upper laser level of gain medium and excited-state of saturable absorber, respectively; $A$ and $A_s$ are effective area in the gain medium and saturable absorber respectively; $n_{gs}$, $n_{es}$, and $n_{so}$ are ground, excited state, and total population densities respectively; $\sigma_{gs}$ and$\sigma_{es}$ are ground and excited state cross sections in the saturable absorber respectively; $R$ is reflectivity of the output coupler; $\gamma$ is inversion reduction factor, $\gamma$=1 and $\gamma$=2 correspond to respectively, four-level and three-level systems [1]; $t_r$ is round-trip transit time of light in the cavity optical length. Figure 3.2 shows the simulated results of development of passively Q-switched laser pulses. It is obviously seen that the gain exceeds the loss at some points, at which the photon number does not raise rapidly. The reason is that in passively Q-switched lasers there are two criterions for pulse-formation. 1st is the lasing criterion, i.e. gain surpasses loss. Satisfying the condition means there is probability to radiate photons, however it needs more condition to generate pulsed output, the condition is the so-called 2nd criterion. The details will be discussed later. Figure 3.3 shows the detail of Fig. 3.2 for a single pulse generation. It can be observed that the pulse peak occurs at the point that the gain equals the loss. After the point the loss exceeds gain again and continues to increase the population inversion of gain medium to output another pulse in the next cycle. The simulated results provides the view of the development of Q-switched pulse, however it is necessary to study this topic more analytically to give insight into the mechanism.

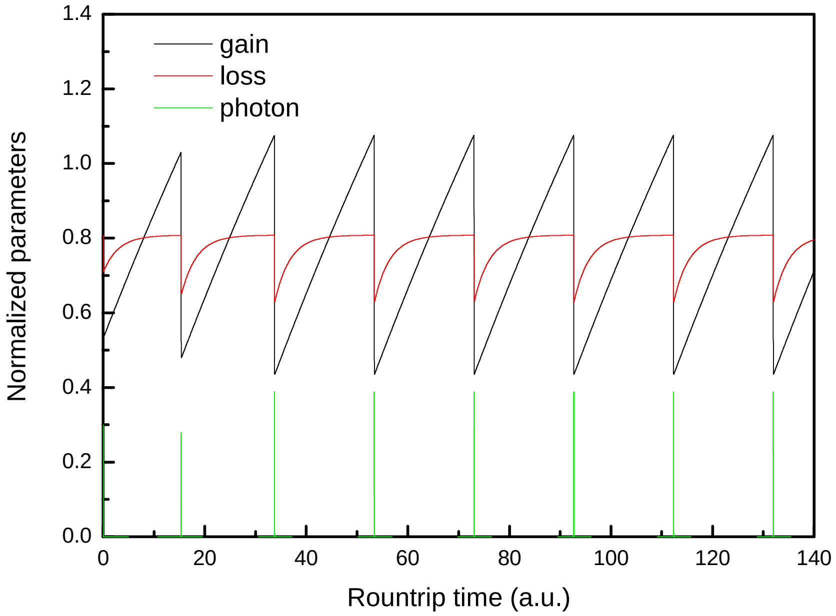

Fig. 3.2. The development of passively Q-switched laser pulses.

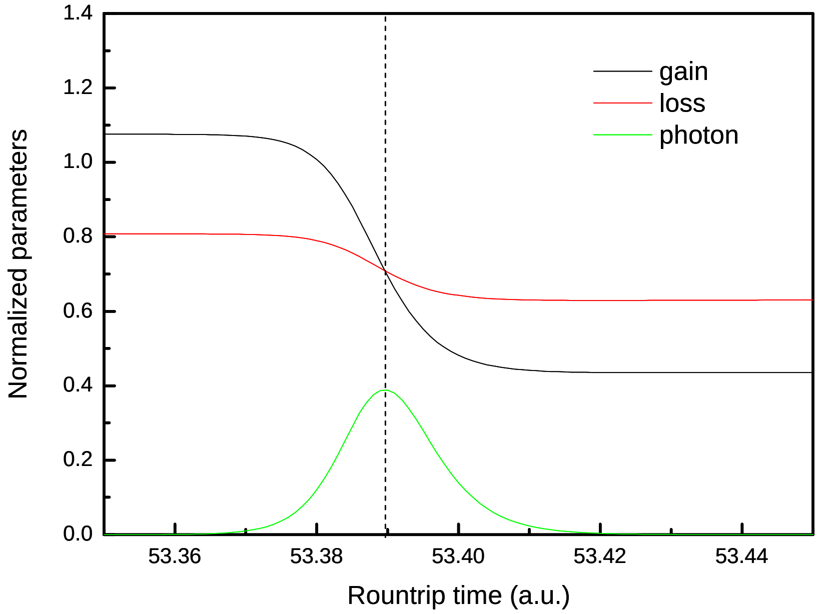

Fig. 3.3. The development of a single passively Q-switched pulse. The maximum value of photon density occurs at the gain equals the loss.

Firstly the terms $R_p$ and $n/\tau_f$ in (3.4) and $n_{es}/\tau_s$ in (3.5) are dismissed due to the build-up time of the Q-switched laser pulse is generally quite short compared with them. Now that (3.4) and (3.5) could be written as

$$\frac{dn}{dt} = -\gamma\sigma c\phi n, \tag{3.7}$$

and

$$\frac{dn_{gs}}{dt} = -\frac{A}{A_s}\sigma_{gs}c\phi n. \tag{3.8}$$

Dividing (3.7) by (3.8) and integrating gives

$$n_{gs} = n_{so}\left(\frac{n}{n_i}\right)^{\alpha}, \tag{3.9}$$

where

$$\alpha = \frac{1}{\gamma}\frac{\mathrm{A}}{\mathrm{A_s}}\frac{\sigma_{gs}}{\sigma}, \tag{3.10}$$

and $n_i$ is the initial population inversion density in the gain medium, which can be obtained by setting the right-hand side of (3.3) to zero and assume that $n(n_{gs}=n_{s0})=n_i$. The value of initial population inversion density $n_i$ can be expressed as

$$n_i = \frac{\ln\left(\frac{1}{R}\right) + L + \ln\left(\frac{1}{T_0^2}\right)}{2\sigma l}. \tag{3.11}$$

Here the relation of the initial transmission of saturable absorber $T_o = e^{-\sigma_{gs} n_{so} l_s}$ is used. The value of pulse energy can be obtained with the aid of (3.7) as

$$E = \int_0^\infty dt P(t) = \frac{h\nu A l'}{t_r}\int_0^\infty dt\,\phi(t) = \frac{h\nu A l'}{t_r}\int_{\mathrm{n_i}}^{\mathrm{n_f}} \frac{\mathrm{dn}}{-\gamma\sigma c\mathrm{n}} = \frac{h\nu A}{2\sigma\gamma}\ln(\frac{1}{\mathrm{R}})\ln(\frac{\mathrm{n_i}}{\mathrm{n_f}}). \tag{3.12}$$

The value of $n_f$ can be obtained as follows:

1. Dividing (3.3) by (3.7) and replacing (3.9) into the result gives

$$\frac{d\phi}{dn} = -\frac{l}{\gamma l'}\left[1 - \frac{(1-\beta)}{2\sigma n_i l}\ln(\frac{1}{T_o^2})(\frac{n}{n_i})^{\alpha-1} - \frac{\beta\ln(\frac{1}{T_o^2}) + \ln(\frac{1}{R}) + L}{2\sigma n l}\right]. \tag{3.13}$$

2. Integrating (3.13) gives

$$\phi(n) - \phi(n_i) \approx \phi(n) =$$
$$\frac{n_i l}{\gamma l'}\left[1 - \frac{n}{n_i} + \frac{\beta\ln(\frac{1}{T_o^2}) + \ln(\frac{1}{R}) + L}{\ln(\frac{1}{T_o^2}) + \ln(\frac{1}{R}) + L}\ln(\frac{n}{n_i}) - \frac{(1-\beta)\ln(\frac{1}{T_o^2})}{\ln(\frac{1}{T_o^2}) + \ln(\frac{1}{R}) + L}\frac{1}{\alpha}\left[1 - (\frac{n}{n_i})^{\alpha}\right]\right], \tag{3.14}$$

and then setting ψ(n=n$_f$)=0 [ψ(n=n$_i$)=0 is a trivial solution gives

$$1 - \frac{n_f}{n_i} - \frac{\beta\ln(\frac{1}{T_o^2}) + \ln(\frac{1}{R}) + L}{\ln(\frac{1}{T_o^2}) + \ln(\frac{1}{R}) + L}\ln(\frac{n_i}{n_f}) - \frac{(1-\beta)\ln(\frac{1}{T_o^2})}{\ln(\frac{1}{T_o^2}) + \ln(\frac{1}{R}) + L}\frac{1}{\alpha}\left[1 - (\frac{n_f}{n_i})^{\alpha}\right] = 0 \tag{3.13}$$

Eqs (3.15) can be solved numerically to obtain $n_f$.

Peak power is expressed as

$$P=\frac{h\nu A l^{'}\phi_{\max}}{t_r}\ln(\frac{1}{R})=\frac{h\nu A l^{'}\phi(n=n_{\phi\max})}{t_r}\ln(\frac{1}{R}), \tag{3.16}$$

where $n_{\phi\max}$ can be obtained by setting (3.13) to be zero with $n$=$n_{\phi\max}$ , which gives

$$1-\frac{n_{\phi\max}^{*}}{n_{\phi\max}}-\frac{(1-\beta)\ln(\frac{1}{T_o^2})}{\ln(\frac{1}{T_o^2})+\ln(\frac{1}{R})+L}\left(\frac{n_{\phi\max}}{n_i}\right)^{\alpha-1}=0, \tag{3.17}$$

with

$$n_{\phi\max}^{*}=\frac{\beta\ln(\frac{1}{T_o^2})+\ln(\frac{1}{R})+L}{2\sigma l}. \tag{3.18}$$

$n_{\phi\max}^{*}$ is the maximum photon density of fast saturable absorber where α is infinity. Besides it is necessary to derive a criterion for Q-switching as depicted in Ref. [4]. The author derived a modified 2nd threshold criterion for Q-switching by including the influence of intracavity focusing and the ESA effect into the rate-equation analysis. The threshold was obtained by setting $\left.\frac{d^2\phi}{dn^2}\right|_{n=n_i}$ be positive assuring a growth curve for photon intensity will turn upward.

With (3.13) and then replacing $n$ = $n_i$ gives

$$\left[\alpha\left(1-\beta\right)-1\right]\ln\left(\frac{1}{T_0^2}\right)-\ln(\frac{1}{R})-L>0, \tag{3.19}$$

which can be written as

$$\frac{\ln\left(\frac{1}{T_0^2}\right)}{\ln\left(\frac{1}{T_0^2}\right)+\ln(\frac{1}{R})+L}\frac{\sigma_{gs}}{\sigma}\frac{A}{A_s}>\frac{\gamma}{1-\beta}. \tag{3.20}$$

(3.19) can be expanded to discover the upper bound and lower bound for $T_o$ and $R$, respectively as follow:

$$T_o \le \exp\left[ -\frac{\ln(\frac{1}{R}) + L}{2(\alpha(1-\beta)-1)} \right] \tag{3.22}$$

$$R \ge \exp\left[ -(\alpha(1-\beta)-1)\ln(\frac{1}{T_0^2}) + L \right]. \tag{3.23}$$

The limits of the initial transmission and reflectivity of output coupler provide criterion more practically to design a laser cavity.

In a passively Q-switched laser the pump power do not affect much the pulse energy or pulse width but do increase the repetition rate. Degnan [1] have proposed that the initial population density at the start of Q-switching is expressed as

$$\mathrm{n_i} = \mathrm{r_p}\tau_\mathrm{f} \frac{1\text{-}\exp(-\tau_\mathrm{c}/\tau_\mathrm{f})}{1\text{-}\delta\exp(-\tau_\mathrm{c}/\tau_\mathrm{f})}, \tag{3.24}$$

where $\tau_c$ is the time interval between pulses and $\delta$ is the fraction of the population inversion left over at the start of the next pump cycle for CW-pumped Q-switched lasers. $\delta$ can be expressed as

$$\delta = 1\text{-}\frac{\mathrm{f_a}}{\gamma}(1\text{-}\frac{\mathrm{n_i}}{\mathrm{n_f}}), \tag{3.25}$$

where $f_a$ is the equilibrium fractional population of the upper level as determined by Maxwell-Boltzmann statistics. Now relate (3.24) with (3.11), we can find out the time interval between pulses can be expressed as

$$\tau_\mathrm{c} = \tau_\mathrm{f} \ln\left( \frac{R_p\tau_\mathrm{f} - \delta n_i}{R_p\tau_\mathrm{f} - n_i} \right). \tag{3.26}$$

## 3.2 $Cr^{4+}$:YAG crystals

Chromium-doped yttrium aluminum garnet ($Cr^{4+}$:YAG) crystals are the most recognized saturable absorbers at the spectral region of 0.9-1.2 μm during the last decade. Compared with the organic dyes saturable absorbers, they have the merits of reusability, chemical stability, and high heat conductivity for thermal management. The mechanical characteristics make them a reliable and durable device for high power operation. On the other hand, $Cr^{4+}$:YAG crystals own characteristics of large absorption cross-section and long excited-state lifetime required for optical absorption. The optical energy-level of $Cr^{4+}$:YAG crystals is shown in Fig. 3.4. $Cr^{4+}$:YAG crystal is a 4-level system at the absorption band of 1.0~1.1μm . The solid line and the dash line indicate radiative and non-radiative transitions respectively. The spontaneous emission occurs via transitions from level 3 to the metastable level 2 and the lifetime $\tau_{3-2}$ is in the order of 3~4μs [6-7]. ESA is included in this figure and the lifetime for the corresponding decay is of the order of ps [8-9]. The ESA acts a loss in the absorption process and results in a degradation of final transmission of saturable absorber. Fortunately the cross-section of ESA of $Cr^{4+}$:YAG is small compared to that of ground-state.  However the excited cross section can not be neglected and they have been studied for years. The values of the cross sections for ground state absorption, $\sigma_{gs}$, and excited state absorption, $\sigma_{es}$, are not known exactly so far and can

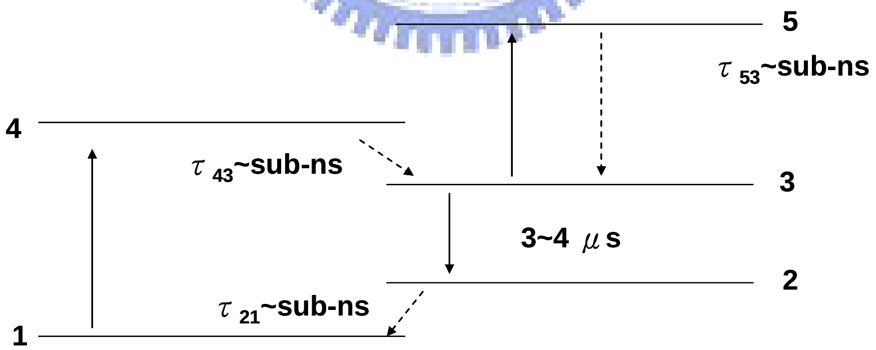

Fig. 3.4. Schematic energy-level diagram of $Cr^{4+}$: YAG with ESA. The solid lines indicate optical transitions and the dashed lines indicate non-radiative transitions. The non-radiative relaxation 4-3, 2-1, and 5-3 are much faster than the lifetime of the excited state 3.

vary by more than one order of magnitude due to measured cross-section depends on the property of incident pump beam such as the pulse repetition rate and pulse duration, and concentration and homogeneity of $Cr^{4+}$:YAG crystals. For example Ridderbusch et al. have used pulse laser of duration in continuous, ns- , and ps- scale to pump a $Cr^{4+}$:YAG crystal with initial transmission of 0.5 [10]. Experimental data revealed that the saturation behaviors as well as the cross-section differed for the three lasers. Besides, the deviation is also attributed to the fact that their fitting procedure and parameters such as concentration and the inhomogeneous intensity distribution of the probe beam. Table 3.1 shows the reported results for $\sigma_{gs}$ and $\sigma_{es}$.

Table 3.1. The reported values of $\sigma_{gs}$ and $\sigma_{es}$ of the $Cr^{4+}$:YAG crystal

| | | | |
|---|---|---|---|
| $\sigma_{gs}$ ($10^{-18}$ $cm^2$) | 7±0.8 | 2±0.4 | 0.87±0.08 |
| $\sigma_{es}$ ($10^{-19}$ $cm^2$) | 2±0.3 | 2±0.4 | 2.2±0.2 |
| $\sigma_{es}/\sigma_{gs}$ | **0.286** | **0.1** | **0.25** |
| **Ref.** | **[11]** | **[12]** | **[13]** |

Though the cross-section is not determined absolutely, we can approximately describe the transmission response with respect to incident energy density of $Cr^{4+}$:YAG crystals if the probe beam is a pulse of short duration with respect to the lifetime of excited state of $Cr^{4+}$:YAG crystals. As mentioned in 4.1 initial the transmission $T_o$ and maximum transmission $T_f$ can be expressed as

$$T_o=\exp(-n_{gs}\sigma_{gs}ls)\,, \tag{3.27}$$

and

$$T_f=\exp(-n_{so}\sigma_{es}ls)\,. \tag{3.28}$$

Burshtein et al. have proposed a approximate analytical expression to describe the transmission [11], which gives

$$T_{lossy}\ (\mathrm{E}_{\mathrm{in}})=\mathrm{T}_{\mathrm{o}}+\frac{\mathrm{T}_{\mathrm{FN}}(E_{in})-\mathrm{T}_{\mathrm{o}}}{1-\mathrm{T}_{\mathrm{o}}}(\mathrm{T}_{\mathrm{f}}\text{-}\mathrm{T}_{\mathrm{o}})\ , \tag{3.29}$$

where

$$\mathrm{T}_{\mathrm{FN}}(E_{in})=\frac{1}{\sigma_{\mathrm{gs}}E(0)}\ln\left[1+\mathrm{T}_0\left(e^{\sigma_{\mathrm{gs}}E(0)}-1\right)\right]\ , \tag{3.29}$$

which is derived by Frantz and Nodvik [14]. On the other hand if the duration of the probe beam is longer than the lifetime of excited state an analytical solution exists if all level populations reach steady-state much faster than change in the power density of the probe beam. The transmission T can be obtained by solving the equation

$$\mathrm{I}(0)=\frac{1}{\tau\sigma_{\mathrm{gs}}}\frac{1\text{-}\left(\frac{\mathrm{T}_0}{T}\right)^{\frac{\sigma_{es}}{\sigma_{gs}-\sigma_{es}}}}{\left(\frac{\mathrm{T}_0}{T}\right)^{\frac{\sigma_{es}}{\sigma_{gs}-\sigma_{es}}}-T}\ . \tag{3.30}$$

Besides the absolute value of cross section, the ratios of $\sigma_{es}/\sigma_{gs}$ are less duplicitous than the absolute values and were reported to be between 0.14 and 0.286 [8]. The ratio is important and is related to the parameter β in section 4.1. In the next section we will derive a simple and practical model to optimized a fiber laser with an external Q-switch and take a $Cr^{4+}$:YAG crystal to be saturable absorber.

## 3.3 Passively Q-switched Ytterbium Fiber Lasers by $Cr^{4+}$: YAG crystals

### 3.3.1 The $Cr^{4+}$: YAG crystal used in this experiment

The $Cr^{4+}$: YAG crystal used in this experiment has a thickness of 3mm and an initial or low-intensity transmission of 30% around 1040nm~1100nm corresponding a concentration of $5.3\times10^{18}$ $cm^{-3}$ as shown in Fig. 3.5. Fig. 3.6 shows the absorption saturation experiment and that reveals that the final transmission is 85% around and the modulation depth was observed to be approximately 50% in a single pass. With the foregoing results the ratio of the absorption excited state cross section to the ground of the $Cr^{4+}$:YAG crystal was calculated to be to be 0.124. Furthermore, the saturation fluence of the saturable absorber was estimated to be in the range of 0.6 J/cm$^2$ and its relaxation time was also on the order of 3 μs.

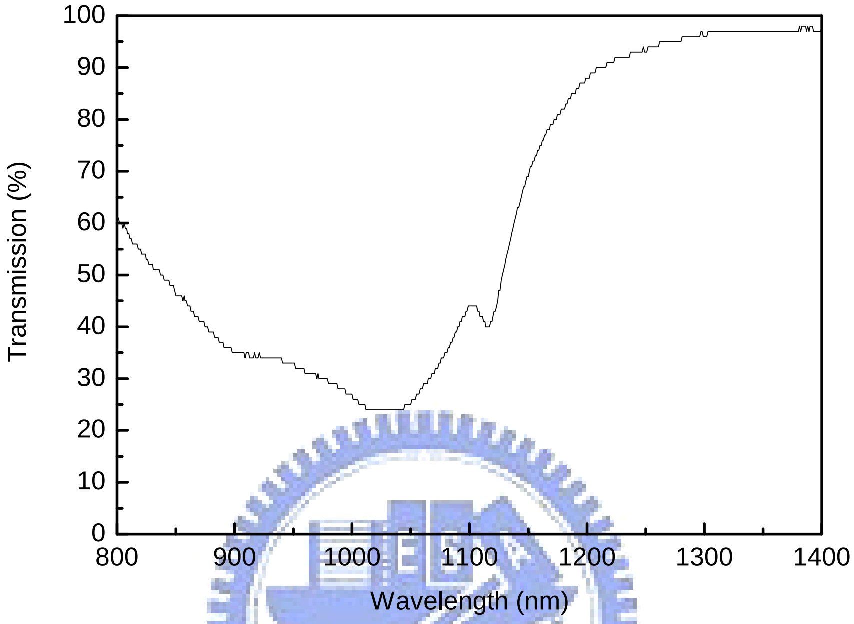

Fig. 3.5. The low-intensity transmission of the $Cr^{4+}$:YAG crystal used in this experiment.

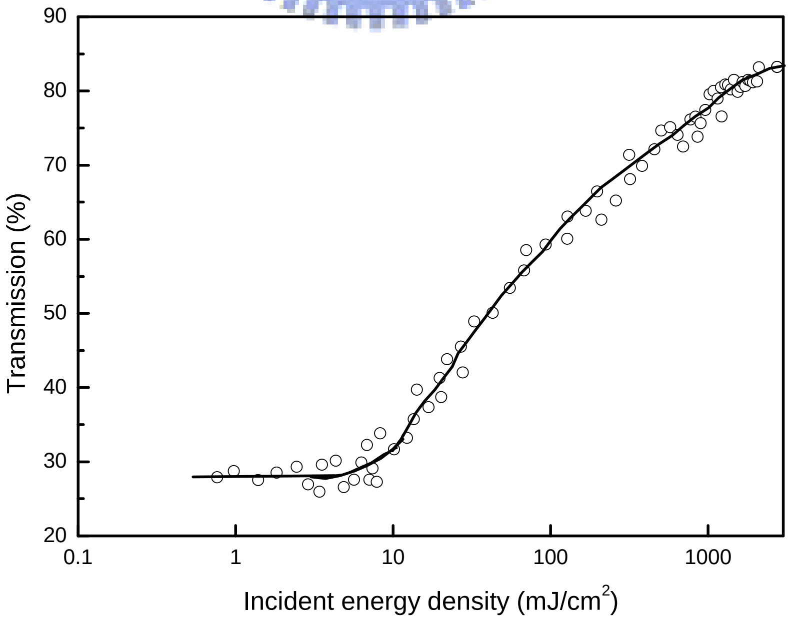

Fig. 3.6. Measured results of saturation of the $Cr^{4+}$:YAG crystal used in this experiment.

### 3.3.2 Experimental setup

Figure 4.7 displays the schematic of the experimental setup for the passively Q-switched Yb-doped fiber laser that consists of the 3-m Yb-doped fiber and an external feedback cavity including the $Cr^{4+}$:YAG crystal as a saturable absorber. The fiber has an absorption coefficient of 10.8 dB/m at 976 nm and a double-clad structure with a diameter of 350 μm octagonal outer cladding, diameter of 250 μm octagonal inner cladding with a numerical aperture (NA) of 0.46, and 30μm circular core with a NA of 0.07. The filter is a dielectric narrowband filter with peak at 1100nm, the same as that used in chap 2. The end facets of the fiber were cut to be normal incident. Therefore, the lasing by end facets usually occurred for the free-running operation.

The pump source was a 35-W 976-nm fiber-coupled laser diode with a core diameter of 400 μm and a NA of 0.22. A focusing lens with 25 mm focal length and 92% coupling efficiency was used to re-image the pump beam into the fiber through a dichroic mirror with high transmission (>90%) at 976 nm and high reflectivity (>99.8%) at 1030~1100 nm. The pump spot radius was approximately 200 μm. The pulse temporal behavior was recorded by a LeCroy digital oscilloscope (Wavepro 7100; 10G samples/sec; 1 GHz bandwidth) with a fast InGaAs photodiode.

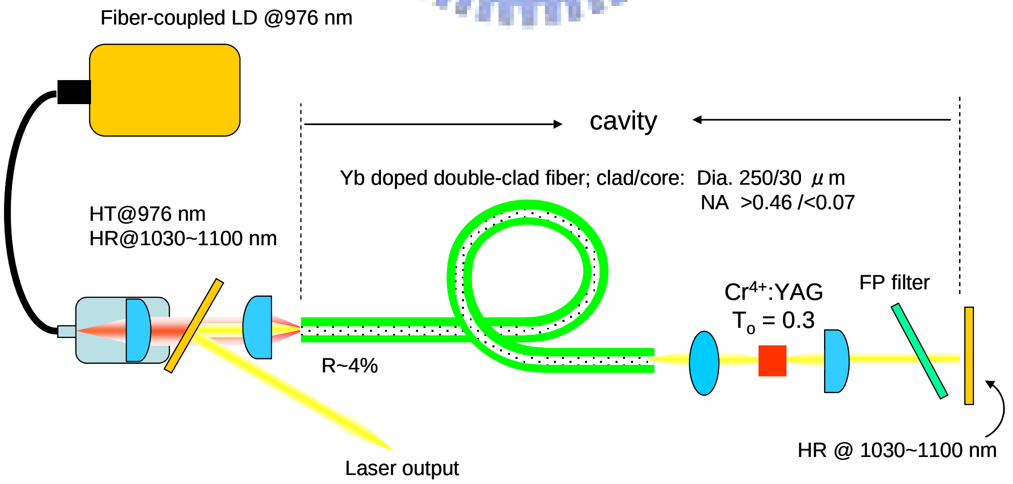

Fig. 3.7. The schematic configuration of the passively Q-switched fiber lasers by $Cr^{4+}$:YAG crystals.

### 3.3.3 Experimental results and discussions

Firstly the performance of average output power of continuous-wave and passively Q-switched modes were compared. For this investigation, the external cavity comprised a focusing lens and a high reflector. The narrowband filter was inserted inside the external cavity for narrowband operation. The cw performance provides the baseline for evaluating the passively Q-switched efficiency. Figure 3.8 (a) and Fig. 3.8 (b) shows the average powers with respect to the incident pump power for cw and PQS operations. The continuous-wave output power at 1080nm is lower than the others hence it is excluded in Fig. 3.8 (a) and was shown in Fig. 3.8 (b). The wavelength was experimentally tunable from 1055nm to 1080nm for all the power level. It is noted that the tunability was constrained by the loss introduced by the loss of the $Cr^{4+}$:YAG crystal. The slope efficiency of the CW laser in Fig. 3.8 (a) is 71%, slightly lower than that in chapter 2. The reason is attributed to the experimental setup in this chapter consisted more optics and is more complex in alignment. The slope efficiency ranged from 64%~68% in Fig. 3.8 (a) and is 60% in Fig. 3.8 (b). Consequently the Q-switching efficiency is 95% for 1055nm, 90% for 1060nm, 92% for 1070nm, and 95% for 1080nm. The Q-switching efficiency is superior to those of Yb-doped crystal lasers with $Cr^{4+}$:YAG crystals as saturable absorbers [15~20]. The $M^2$ beam-quality factor was measured to be <1.8 over the complete output power range.

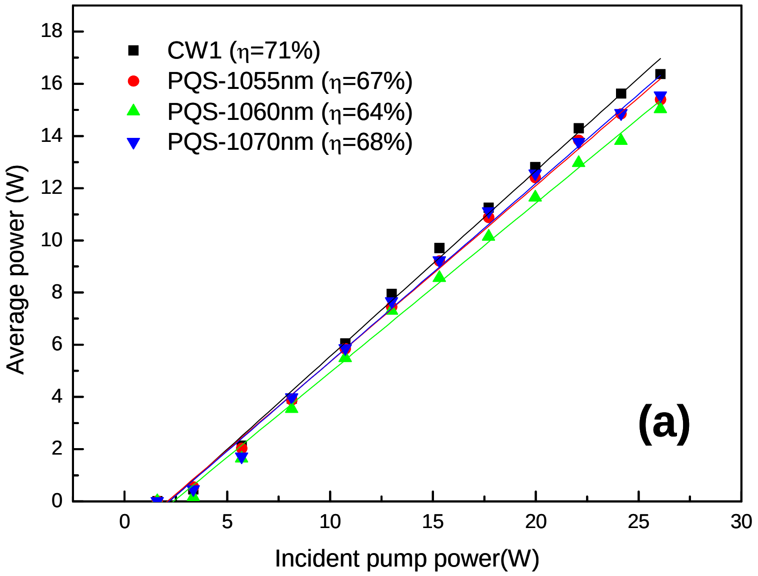

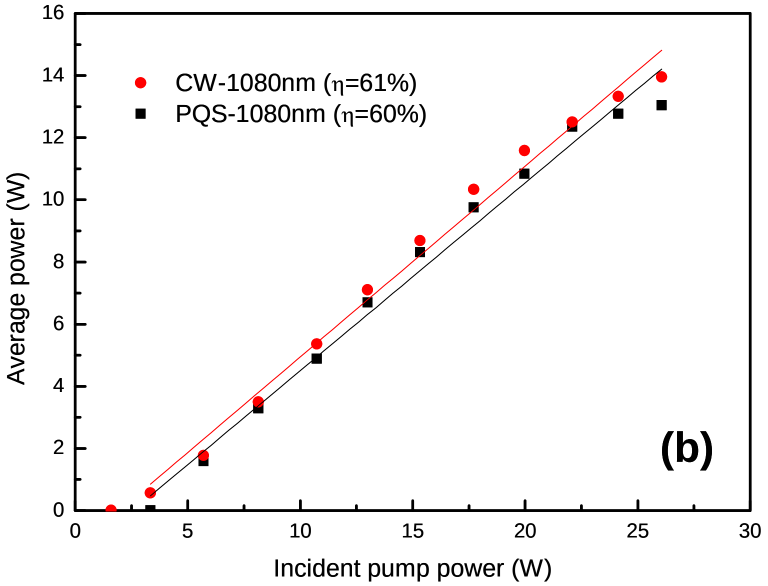

Fig. 3.8 The average power of CW and PQS regime for (a) 1055nm, 1060nm, and 1070nm; (b) 1080nm

It is noted that although the modulation depth of the $Cr^{4+}$:YAG crystal is between the four wavelengths, the performances are really different. Figure 4.9 shows the pulse repetition rate and pulse energy versus the incident pump power. As shown in Fig. 3.9 (a) the maximum pulse energy is at 1060nm, which increases slightly from 300μJ to 350μJ. The main reason is that we slightly tilted the $Cr^{4+}$: YAG crystal

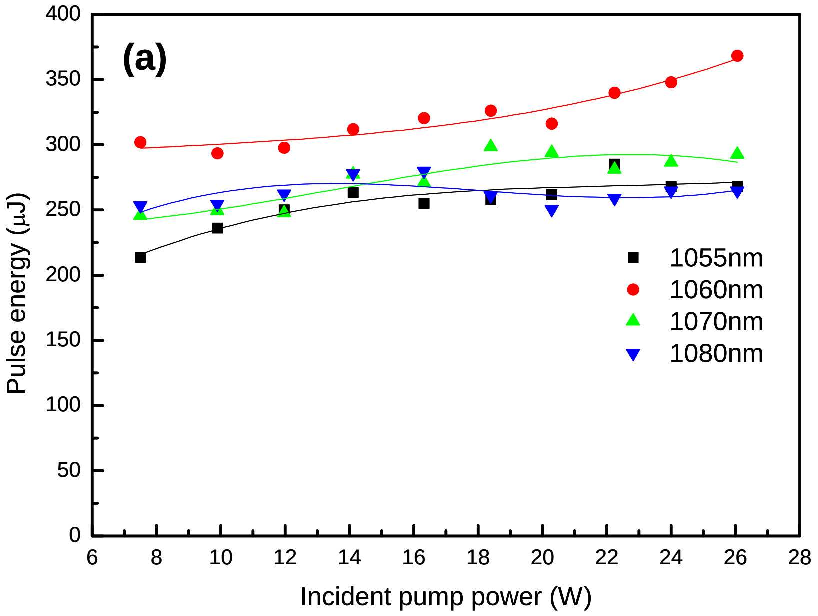

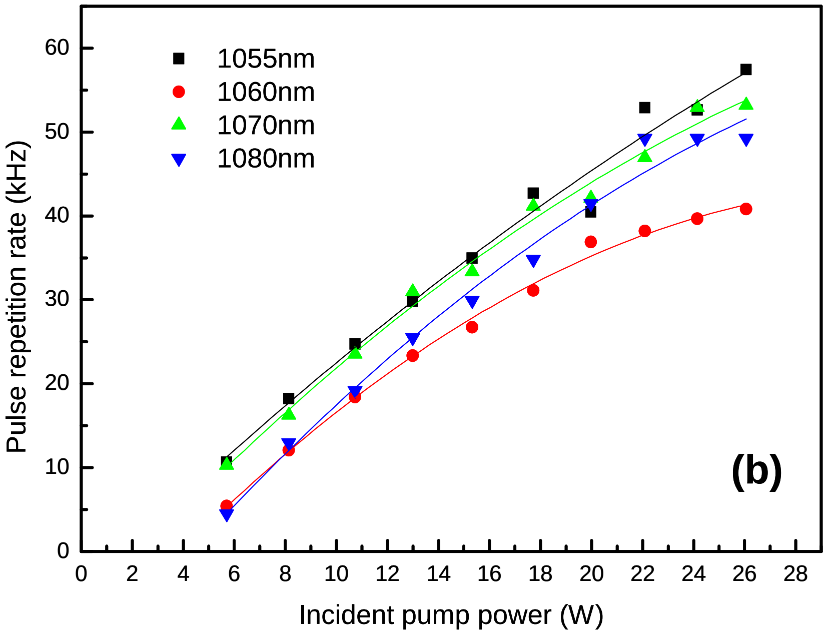

Figure 3.9. Pulse energy and pulse repetition rate versus the incident pump power.

with the model of the coupled rate equations, the expression for the pulse energy of the passively Q-switched has been derived to be given by Eq (3.12)

$$E = \frac{h\nu A}{2\sigma\gamma}\ln(1/R)x \quad , \tag{3.12}$$

with the values of parameters as in Table 3.1, the pulse energy could be found to be 289μJ, 312μJ, 274μJ, and 256 μJ for 1050nm, 1060nm, 1070nm, and 1080nm. These values agree well with the experimental result. Furthermore, the present pulse energies are comparable with the maximum energy storage capacity of the laser given by the saturation energy $E_{sat}=h\nu A/\sigma$ (for 1066nm)= 397μJ.

A typical oscilloscope trace of Q-switched pulse train is shown in Fig. 3.10(a). With the optimum alignment, the pulse-to-pulse stability was found to be approximately ±15%. The pulse-to-pulse stability may be improved by the angle-cleaved end facets of the fiber. Figure 4.10 shows the temporal domain of the 1060nm laser.

Table 3.2. The values of parameters of the $Cr^{4+}$:YAG crystal and Yb-doped fiber.

| | |
|---|---|
| $\sigma$ ($10^{-21}$cm$^2$) | 3.6 @1050nm, 3.3@1060nm,<br>3.3@1070nm, 3.2@1080nm [21] |
| $\sigma_{gs}$ ($10^{-19}$ cm$^2$ ) | 8.7 [13] |
| $\sigma_{es}$ ($10^{-19}$ cm$^2$ ) | 2.2 [13] |
| $T_o$ | 0.25@1050nm, 0.26@1060nm,<br>0.31@1070nm, 0.35@1080nm |
| R | 0.04 |
| L | 0.04 |
| A ($10^{-6}$cm$^2$) | 4.9 |
| $A_s$$10^{-6}$cm$^2$) | 4.9 |

Figure 3.10 (a) shows the temporal shape of a train of Q-switched pulses and (b) shows a single Q-switched pulse envelope. The present result indicates that the output peak power can be significantly enhanced by using a fiber with a larger core size and a saturable absorber with a lower initial transmission. The spectral information was measured by an optical spectrum analyzer (Advantest Q8381A) that utilizes a grating monochromator for the high speed measurement of pulse light with the resolution of 0.1 nm. Figure 3.11 shows the output spectrum of the passively Q-switched fiber laser at an average output power of 14 W. The experimental FWHM line width was approximately 1 nm.

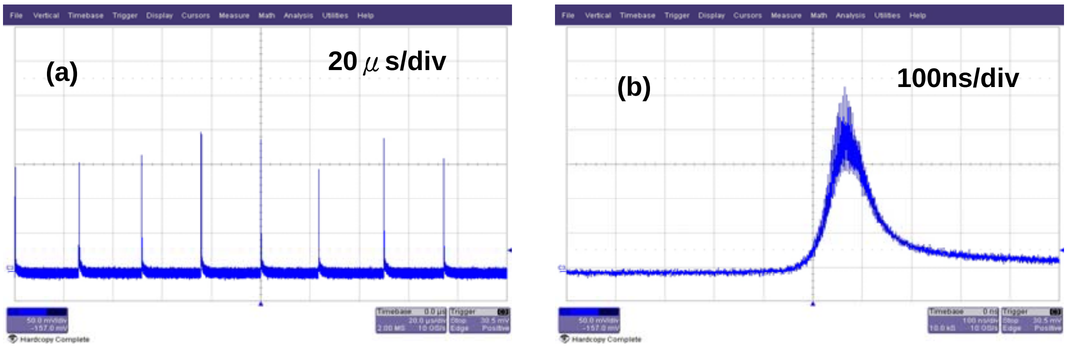

Fig. 3.10 (a) Oscilloscope traces of a train of Q-switched pulses, (b) Oscilloscope traces of a Q-switched envelope.

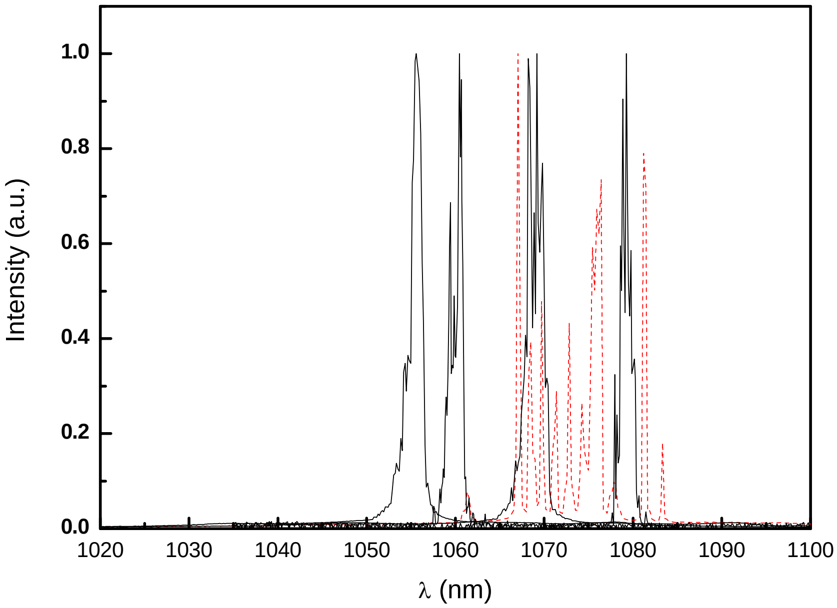

Fig. 3.11. Output spectrum of the Q-switched laser at an output power of 16 W. Dash line: broadband output; solid line: narrowband output

## 3.4 Analytical model for optimizing the external cavity of passively Q-switched fiber lasers

### 3.4.1 Introduction

Passive Q-switching of fiber lasers can be achieved by use of crystals as saturable absorbers. The external Q-switch in the cavity consists of a re-imaging optics to couple the laser mode into the saturable absorber. In most cases, the average mode area inside the saturable absorber, $A_s$, significantly affects the output pulse energy and efficiency as mentioned in section 3.1. Therefore, it is of great worth to develop a design model for optimizing the average mode area inside the saturable absorber. In this section, I will emphasize again the significance of $A_s$ for the passive Q-switching operation and then derive an analytical function to model the influence of $A_s$ on the Q-switched laser. The parameters included in this model are the focal position of the re-imaging mode, the numerical aperture and core size of the laser fiber, and the initial transmission and thickness of the saturable absorber.

The analytical function enables us to obtain an explicit expression for the optimum focal position of the re-imaging laser mode. Under the condition of minimum $A_s$, the optimum magnification of the re-imaging optics is exactly derived in terms of the physical parameters of the laser fiber and the saturable absorber. The present model provides a straightforward procedure to determine the optimum re-imaging magnification for the external cavity of a passively Q-switched fiber laser. A practical example of an end-pumped Yb-doped fiber laser with a $Cr^{4+}$:YAG crystal as a saturable absorber is considered to illustrate the utilization of the present model.

### 3.4.2 Background

In section 3.1 we have derived the relation between the population of gain medium and saturable absorber as

$$n_{gs} = n_{so}\left(\frac{n}{n_i}\right)^{\alpha}, \tag{3.9}$$

and

$$\alpha = \frac{1}{\gamma}\frac{\sigma_{gs}}{\sigma}\frac{A}{A_s}. \tag{3.10}$$

We denote the quantity to be the bleaching rate parameter (BRP) because its value determines the bleaching rate after the population inversion density reaches the initial threshold value. We replace $\ln(n_i / n_f)$ with $x$ in (3.12) and (3.15) as

$$E = \frac{h\nu A}{2\sigma\gamma}\ln\left(\frac{1}{R}\right)x, \tag{3.36}$$

and

$$1-e^{-x}-x+\frac{(1-\beta)\ln\left(\frac{1}{T_o^2}\right)}{\ln\left(\frac{1}{T_o^2}\right)+\ln\left(\frac{1}{R}\right)+L}\left(x-\frac{1-e^{-\alpha x}}{\alpha}\right)=0, \tag{3.37}$$

Note that in the calculation of the pulse energy with Eq. (3.36) the effect of cavity losses is included in the process of solving Eq. (3.37) with the parameter *L*. Furthermore, the nonlinear effects are not included in the present model because of the property of large mode areas of the fiber lasers studied here. Eq. (3.9) manifests that the larger is the BRP, the faster is the saturable absorber bleached. As a consequence, the larger is the BRP, the higher is the output efficiency of a passively Q-switching laser [1-4]. As indicated in Eq. (3.10), the BRP is proportional to the effective ratio $A/A_s$ for a given gain medium and a given saturable absorber. Therefore, the optimization of the effective ratio $A/A_s$ is essentially critical for developing an efficient passively Q-switched laser. For a given fiber laser, the maximization of the effective ratio $A/A_s$ is directly related to the minimum $A_s$, as illustrated in Fig. 3.12. Since the minimum $A_s$ is governed by the re-imaging magnification $\mathcal{M}$ of the external cavity, it is of practical usefulness to derive the optimum magnification in terms of the physical parameters of the laser fiber and the saturable absorber.

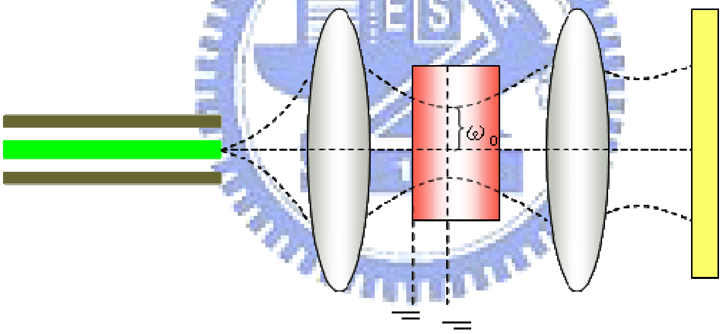

Fig. 3.12. Schematic illustration of the external cavity in a passively Q- switched fiber laser. $\omega_o$ is the beam waist of the laser mode; $Z_o$ is the position of the beam waist.

### 3.4.3 Optimization of Re-imaging Magnification

The laser mode size in the saturable absorber is generally given by [22]

$$\omega_s(z) = \omega_o\sqrt{1+[C(z-z_o)]^2} \tag{3.38}$$

with

$$C=\frac{M^2\lambda}{\pi\, n_r\omega_o^2} \tag{3.39}$$

where $\omega_o$ is the beam waist of the laser mode, $z_o$ is the position of the beam waist, is the laser wavelength, $M^2$ is the beam-quality factor, $n_r$ is the refractive index of the saturable absorber, and the point $z=0$ is set at the incident surface of the saturable absorber. For a given core radius $r_c$, the beam waist in the saturable absorber is directly related to the re-imaging magnification $\mathcal{M}$ by

$$\omega_o=\mathcal{M}\, r_c \quad . \tag{3.40}$$

With the brightness theorem, the beam-quality factor $M^2$ can be given by

$$M^2=(NA\cdot r_c)(\pi/\lambda), \tag{3.41}$$

where $NA$ is the numerical aperture of the laser fiber. Substituting Eqs. (3.40) and (3.41) into Eq. (3.39), the factor $C$ can be expressed as

$$C=\frac{NA}{n_r\,\mathcal{M}^2\, r_c}. \tag{3.42}$$

The average mode area in the saturable absorber, $A_s$, can be properly in terms of the mean square of the average mode size as

$$A_s=\pi\left\langle\omega_s^2\right\rangle \tag{3.43}$$

with

$$\left\langle\omega_s^2\right\rangle=\frac{\int_0^{l_a}\omega_s^2(z)\, e^{-n_{so}\sigma_{gs}z}\,dz}{\int_0^{l_a}e^{-n_{so}\sigma_{gs}z}\,dz}\quad , \tag{3.44}$$

where $l_a$ is the thickness of the saturable absorber and the weighting function $e^{-n_{so}\sigma_{gs}z}$ comes from the absorption effect. Eq. (3.44) is based on averaging along the decaying beam in the single-pass geometry. To take the round-trip effect into account, the effective beam area factor can be expressed as

$$\left\langle \omega_s^2 \right\rangle = \frac{\int_0^{l_a} \omega_s^2(z) \left[ e^{-n_{so}\sigma_{gs} z} + e^{-n_{so}\sigma_{gs}(2l_a - z)} \right] dz}{\int_0^{l_a} \left[ e^{-n_{so}\sigma_{gs} z} + e^{-n_{so}\sigma_{gs}(2l_a - z)} \right] dz} \tag{3.45}$$

Figure 3.13 shows a comparison for the calculated results $\left\langle \omega_s^2 \right\rangle$ obtained with Eqs. (3.44) and (3.45) for a typical case with the parameters of $NA = 0.04$, $r_c = 12.5$ μm, $n_r = 1.82$, $T_o = 0.4$, and $l_a = 2$ mm. The influence of the round-trip effect on the effective beam area can be clearly found to be insignificant. Since Eq. (3.44) for the single-pass approximation leads the derivation to be more concise, it is used for optimizing the effective beam area. On the other hand, the standing-wave effect is omitted because the multi-longitudinal mode operation of long fibers reduces this effect.

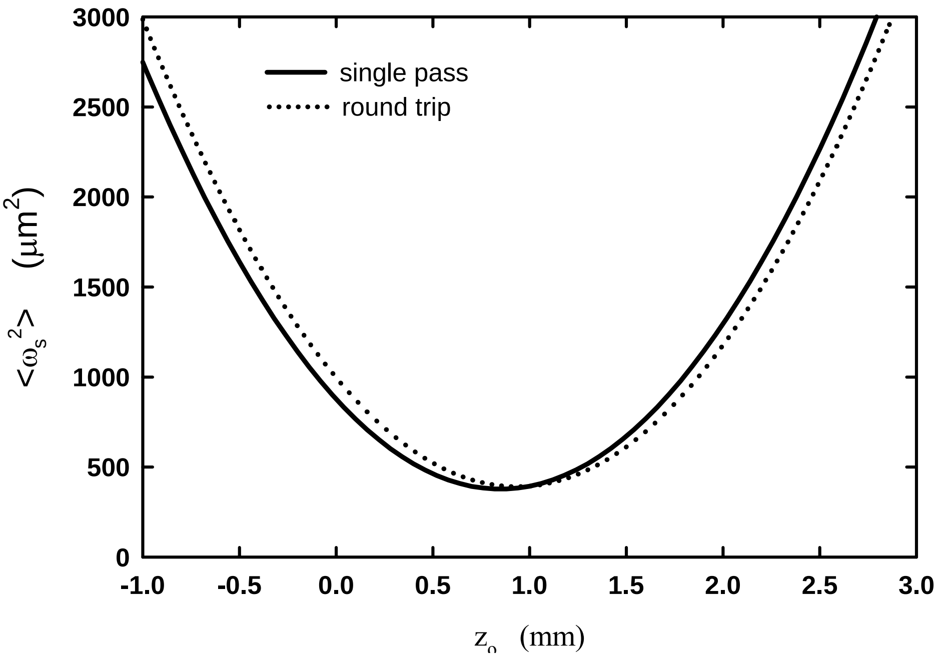

Fig. 3.13. A comparison for the calculated results $\left\langle \omega_s^2 \right\rangle$ obtained with Eqs. (16) and (17) for a typical case with the parameters of $NA = 0.04$, $r_c$=12.5 μm, $n_r$ = 1.82, $T_o$ =0.4, and $l_a$= 2mm.

Substituting (3.38) into (3.44), the integration can be exactly carried out and the average mode area is expressed as

$$A_s = \pi\omega_o^2 C^2 \left\{ z_o^2 - 2 z_o l_a \left[ \frac{1}{\ln(1/T_o)} - \frac{T_o}{1-T_o} \right] + \left[ \frac{1}{C^2} + \frac{2 l_a^2}{\left(\ln(1/T_o)\right)^2} - l_a^2 \left( \frac{T_o}{1-T_o} \right) \left( 1 + \frac{2}{\ln(1/T_o)} \right) \right] \right\} . \quad (3.46)$$

Note that the expression of Eq. (3.46) is in term of the initial transmission $T_o$ instead of $n_{so}\sigma_{gs}$ because $T_o$ is a macroscopic property of the saturable absorber and can be definitely measured.

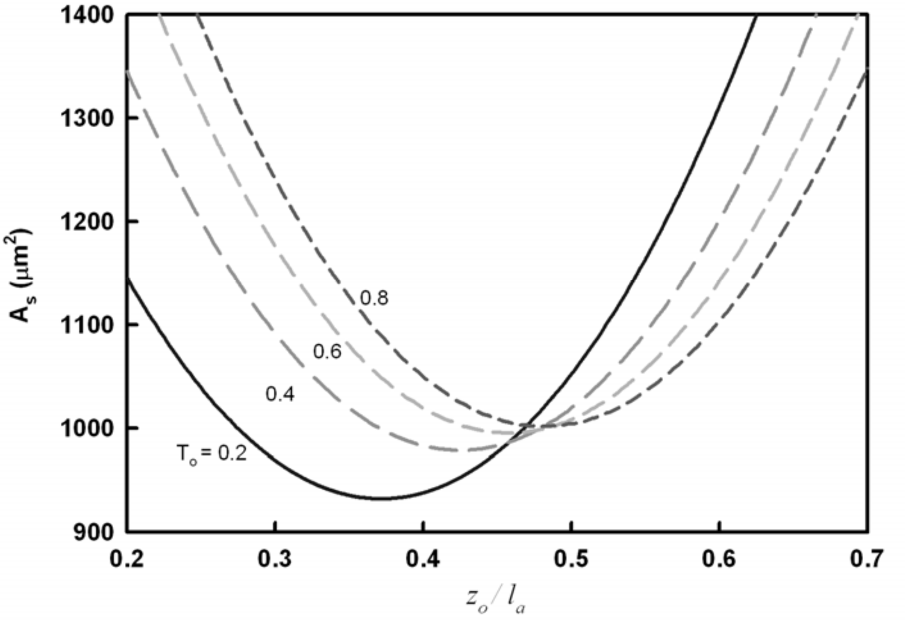

Fig. 3.14. Dependence of the average mode area on the focal position for several $T_o$ values.

Figure 3.7 shows a calculated example with Eq. (3.46) and the parameters of NA=0.04, $r_c$=12.5 μm, $n_r$=1.82, and $l_a$=2 mm to demonstrate the dependence of the average mode area on the focal position for several $T_o$ values. It can be seen that there is an optimum focal position for minimizing the average mode area. The optimum focal position, $z_{opt}$, for the minimum mode area can be analytically determined by partially differentiating Eq. (3.46) with respect to $z_o$ and setting the resulting equation equal to zero:

$$\left.\frac{\partial A_s}{\partial z_o}\right|_{z_o=z_{opt}} = 2\pi\omega_o^2\, C^2 \left\{ z_{opt} - l_a \left[ \frac{1}{\ln(1/T_o)} - \frac{T_o}{1-T_o} \right] \right\} = 0 \quad . \tag{3.47}$$

Eq. (3.47) leads to the $z_{opt}$ to be given by

$$z_{opt} = l_a \left[ \frac{1}{\ln(1/T_o)} - \frac{T_o}{1-T_o} \right] \quad . \tag{3.48}$$

Eq. (3.48) indicates that the optimum focal position depends only on $l_a$ and $T_o$, i.e. the properties of the saturable absorber. Substituting Eqs. (3.40), (3.42) and (3.48) into (3.46), the average mode area at the optimum focal position is then given by

$$A_s = \pi \left\{ \mathcal{M}^2\, r_c^2 + \frac{(NA)^2\, l_a^2}{n_r^2\, \mathcal{M}^2} \left[ \frac{1}{\left(\ln(1/T_o)\right)^2} - \frac{T_o}{\left(1-T_o\right)^2} \right] \right\} \quad . \tag{3.49}$$

The optimum magnification, $M_{opt}$, for minimizing the mode area can be analytically determined by partially differentiating Eq. (3.49) with respect to $M$ and setting the resulting equation equal to zero:

$$\left.\frac{\partial A_s}{\partial \mathcal{M}}\right|_{\mathcal{M}=\mathcal{M}_{opt}} = \pi \left\{ 2\mathcal{M}_{opt}\, r_c^2 - \frac{2(NA)^2\, l_a^2}{n_r^2\, \mathcal{M}_{opt}^3} \left[ \frac{1}{\left(\ln(1/T_o)\right)^2} - \frac{T_o}{\left(1-T_o\right)^2} \right] \right\} = 0 \quad . \tag{3.50}$$

Consequently, the $M_{opt}$ is given by

$$\mathcal{M}_{opt} = \left\{ \frac{(NA)^2\, l_a^2}{n_r^2\, r_c^2} \left[ \frac{1}{\left(\ln(1/T_o)\right)^2} - \frac{T_o}{\left(1-T_o\right)^2} \right] \right\}^{1/4} \quad . \tag{3.51}$$

Eq. (3.51) indicates that the optimum re-imaging magnification $M_{opt}$ can be straightforwardly determined with the NA and core radius of the laser fiber as well as the thickness and initial transmission of the saturable absorber. Figure 3.15 depicts a calculated example with Eq. (3.49) and the parameters of, NA=0.04, $r_c$=12.5 μm, $n_r$=1.82, and $T_o$=0.5 to reveal the dependence of the average mode area on the magnification $M$ for several $l_a$ values. The dashed line in Fig. 3.15 shows the minimum average mode areas corresponding to the optimum magnification $M_{opt}$.

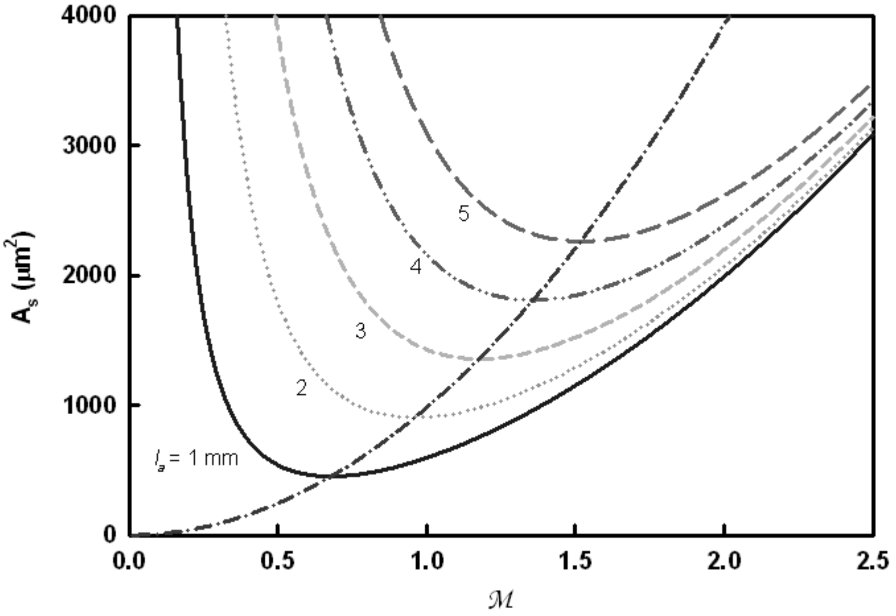

Fig. 3.15. Dependence of the average mode area on the magnification for several $l_a$ values.

### 3.4.4 Experimental Results

To illustrate the utility of the present model, a Yb-doped fiber laser with a $Cr^{4+}$:YAG crystal as a saturable absorber is considered. The experimental setup was the same as that in section 3.3 except the fiber used here was a 1.5-m long fiber with a core diameter of 25 μm and a numerical aperture of 0.04. The pump source was a 13-W 976-nm fiber-coupled laser diode with a core diameter of 400μm and a NA of 0.22. A focusing lens with 25 mm focal length and 92% coupling efficiency was used to re-image the pump beam into the fiber through a dichroic mirror with high transmission (>90%) at 976 nm and high reflectivity (>99.8%) at 1075 nm. The pump spot radius was approximately 200μm. The $Cr^{4+}$:YAG crystal has a thickness of 1.57 mm with 40% initial transmission at 1075 nm. Both sides of the $Cr^{4+}$:YAG crystal were coated for antireflection at 1075 nm (R<0.2%). The saturable absorber was wrapped with indium foil and mounted in a copper block without active cooling.

Substitution of the experimental parameters of $NA = 0.04$, $r_c = 12.5\ \mu$m, $n_r = 1.82$, $T_o = 0.4$, and $l_a = 1.57$ mm into Eq. (3.47) yields $M_{opt} = 0.88$. With the available optics, we setup an external cavity to obtain a re-imaging magnification of $M_a = 0.9$ that nearly achieves the optimum value of $M_{opt} = 0.88$. A translation stage was used to adjust the longitudinal position of the Cr$^{4+}$:YAG crystal for investigating the influence of the focal position on the average mode area as well as the output performance.

Figure 3.16 shows the experimental results for the dependence of the output pulse energy on the focal position at an incident pump power of 10 W. The theoretical calculations based on Eqs. (3.36) and (3.37) and the parameters of $\sigma = 2.4\times10^{-21}$ cm$^2$ [21], $\sigma_{gs} = 8.7\times10^{-19}$ cm$^2$ [13], $\sigma_{es} = 2.2\times10^{-19}$ cm$^2$ [13], $R = 0.04$, and $L = 0.04$ are also shown in this figure for comparison. It can be seen that the output energy is significantly influenced by the focal position and the optimum focal position agrees very well with the theoretical analysis of $z_{opt} = 0.67$ mm.

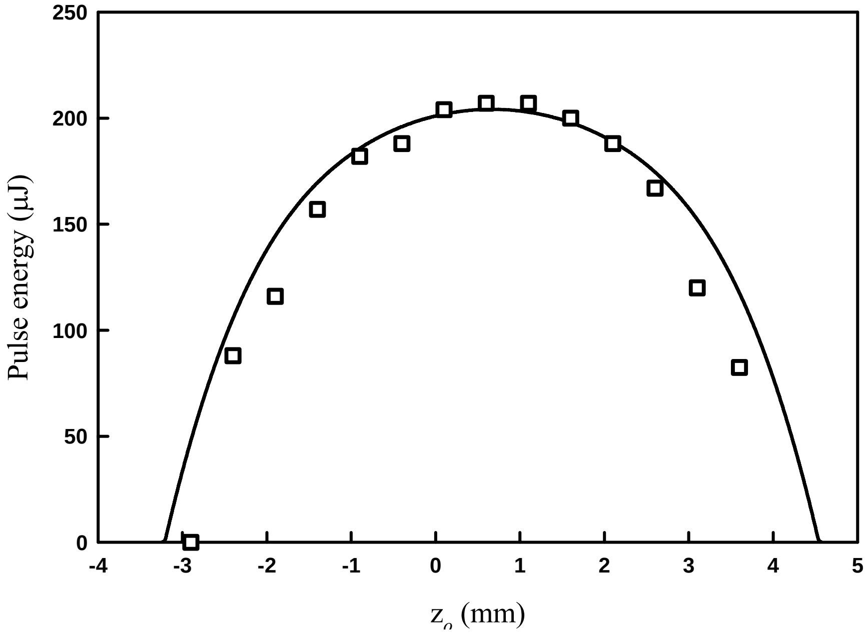

Fig. 3.16. Experimental and theoretical results for the output pulse energy as a function of the focal position. Symbols：Experimental data. Solid line：Calculated results .

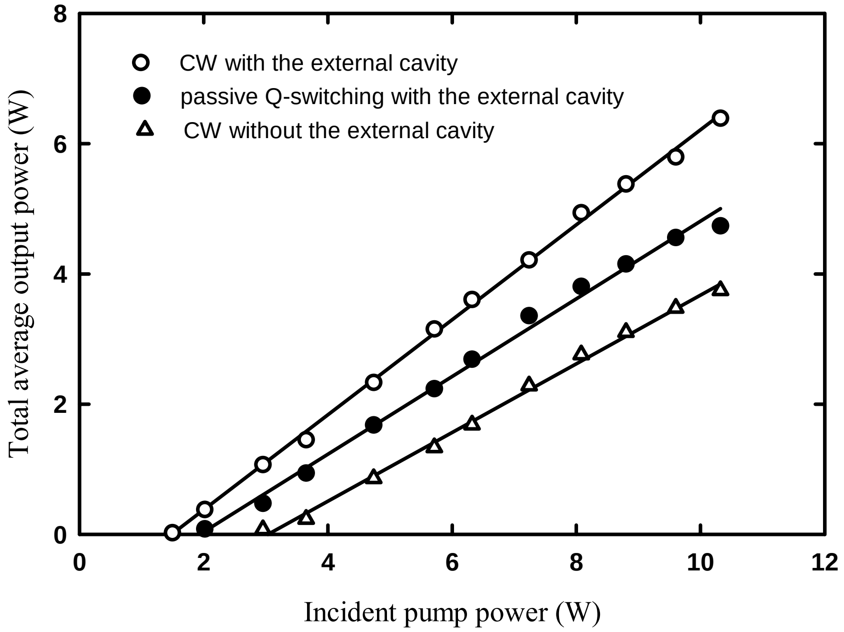

Fig. 3.17. Average output powers versus the incident pump power for CW lasing between the three cases depicted in the text.

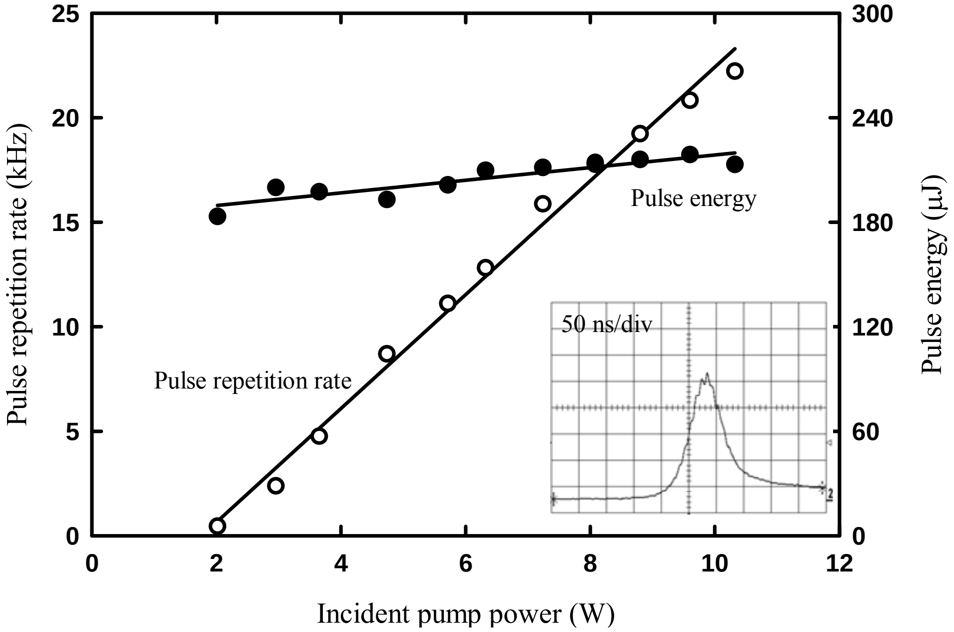

Fig. 3.18. Pulse repetition rate and pulse energy versus the incident pump power at the optimum focal position.

Although most of the fiber lasers can get CW lasing between facets without the external high-reflection cavity, the threshold of the fiber laser with an external high-reflection cavity is considerably lower than that of the fiber laser without external feedback. Experimental results reveal that the threshold of the passively

Q-switched fiber laser with an external cavity is also usually lower than that of CW free-running operation between facets, as shown in Fig. 3.17. Therefore, the CW lasing between facets can be completely prevented in the presence of the external high-reflection cavity with a saturable absorber. Since the external cavity dominates the lasing, the couple-cavity effect arising from facets is insignificant in the performance of the passive Q-switching operation. Figure 3.18 shows the pulse repetition rate and the pulse energy versus the incident pump power at the optimum focal position. The pulse repetition rate initially increases with pump power, and is approximately up to 22 kHz at an incident pump power of 10 W. Like typically passively Q-switched lasers, the pulse energies weakly depend on the pump power and their values are found to be approximately 210 $\mu$J. The pulse width is found to be in the range of 60−70 ns, as shown in the inset of Fig. 3.18.

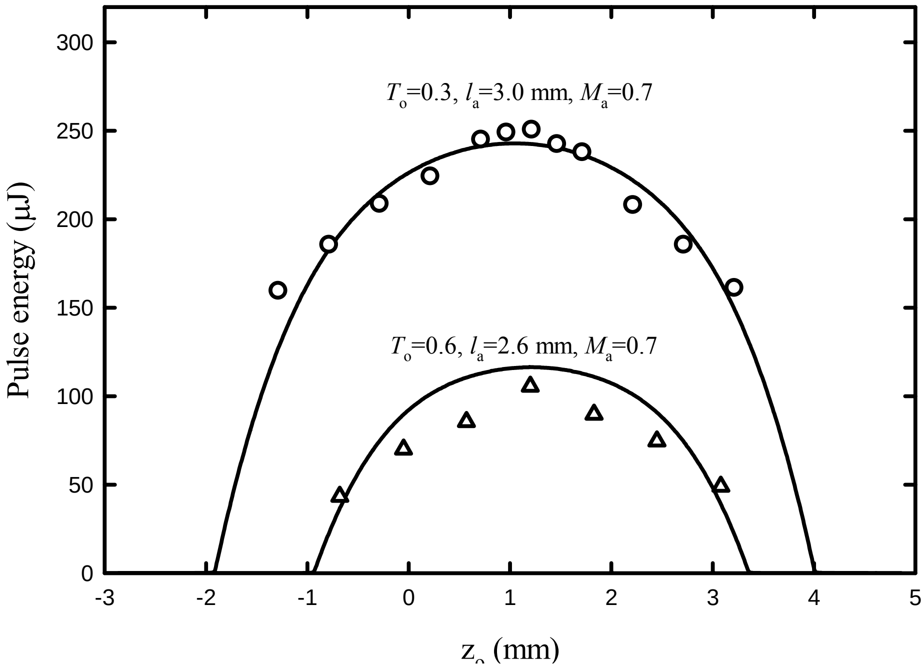

Fig. 3.19. Experimental and theoretical results for the dependence of the output pulse energy on the focal position at incident pump power of 10 W. Symbols : experimental data. Solid line : calculated results.

To validate the developed models, two more experiments were performed with other saturable absorbers ($T_o = 0.3$, $l_a = 3.0\,\text{mm}$ and $T_o = 0.6$, $l_a = 2.6\,\text{mm}$ ) and a re-imaging magnification of $M_a = 0.7$. Figure 3.19 shows the experimental results for the dependence of the output pulse energy on the focal position at an incident pump power of 10 W. The good agreement between experimental results and theoretical predictions confirms the validity of our physical analysis.

## 3.5 Conclusion

In this chapter we have developed an analytical model for the optimization of the external cavity with a saturable absorber in a passively Q-switched fiber laser. From the criterion of the minimum average mode area inside the saturable absorber, the optimum focal position was derived to be an analytical function of the thickness and initial transmission of the saturable absorber. With the expression of the optimum focal position, the optimum magnification of the re-imaging optics was exactly derived to be a compact close form in terms of the physical properties of the laser fiber as well as the saturable absorber. The present model provides a straightforward procedure to determine the key parameters for optimizing passively Q-switched fiber lasers. Based on the analytical model, we have demonstrated an efficient high-pulse-energy and high-average-power passively Q-switched Yb-doped fiber laser with a $Cr^{4+}$:YAG crystal as a saturable absorber in an external-Q-switch configuration. Greater than 14 W of an average output power at a repetition rate of 39 kHz was generated with a 26-W diode pump power. It is believed that this efficient Q-switched fiber laser should be a useful light source for technical applications because of its high average power as well as high peak power.

# Reference

1. J. J. Degnan, “Optimization of passively Q-switched lasers,” IEEE J. Quantum Electron. **31**, 1890-1901 (1995).
2. X. Zhang, S. Zhao, Q. Wang, Q. Zhang, L. Sun, and S. Zhang, “Optimization of $Cr^{4+}$-doped saturable-absorber Q-switched lasers,” IEEE J. Quantum Electron. **33**, 2286-2294 (1997).
3. G. Xiao and M. Bass, “A generalized model Q-switched lasers including excited state absorption in the saturable absorber,” IEEE J. Quantum Electron. **33**, 41-44 (1997).
4. Y. F. Chen, Y. P. Lan, and H. L. Chang, “Analytical model for design criteria of passively Q-switched lasers,” IEEE J. Quantum Electron. **37**, 462-468 (2001).
5. J. J. Zayhowski and P. L. Kelley, “Opimization of Q-switched Lasers,” IEEE J. Quantum Electron.27, 2220-2225 (1991).
6. Y. Shimony, Z. Burshtein, and Y. Kalisky, “ Cr :YAG as passive Q-switch and brewster plate in a pulsed Nd:YAG laser,” *IEEE J. Quantum Electron.* **31**, 1738–1741 (1995).
7. Z. Burshtein, P. Blau, Y. Kalisky, Y. Shimony, and M. R. Kokta, “Excited-state absorption studies of Cr ions in several garnet host crystals,” IEEE J. Quantum Electron. **34**, 292–299 (1998).
8. S.-H. Yim, D.-R. Lee, B. K. Rhee, and D. Kim, “Nonlinear absorption of Cr :YAG studied with lasers of different pulsewidth,” Apl. Phys. Lett. **73**, 3193–3195 (1998).
9. N. I. Borodin, V. A. Zhitnyuk, A. G. Okhrimchuk, and A. V. Shestakov, “Oscillation of a $Y_3$ $Al_5$ $O_{12}$ : $Cr^{4+}$ laser in wave length region of 1.34–1.6 µm,” Izvestiya Akademii Nauk SSSR, **54**, 1500–1506 (1990).
10. H. Ridderbusch and T. Graf, “Saturation of 1047- and 1064-nm absorption in $Cr^{4+}$:YAG Crystals,” IEEE J. Quantum. Electron. **43**, 168-173 (2007).
11. Z. Burshtein, P. Blau, Y. Kalisky, Y. Shimony, M.R. Kokta, “Excited-State Absorption Studie of $Cr^{4+}$ Ions in Several Garnet Host Crystals,” IEEE J. of Quantum Electron. **34,** 292–299 (1998).
12. R. Moncorge, H. Manna, F. Deghoul, Y. Guyot, Y. Kalisky, S.A. Pollack, E.V.

Zharikov, M. Kokta, “Saturable and excited state absorption measurements in $Cr^{4+}$:LuAG single crystals,” Optics Commun. **132,** 279–284 (1996).

13. Y. Shimony, Z, Burshtein and Y. Kalisky, “$Cr^{4+}$:YAG as passive Q-switch and Brewster plate in a pulsed Nd:YAG laser,” IEEE J. Quantum Electron. **31**, 1738-1741 (1995).
14. L. M. Frantz and J. S. Nodvik, “Theory of pulse propagation in a laser amplifier,” J. Appl. Phys. **34**, 2346-2349 (1963).
15. J. Dong, P. Deng, Y. Liu, Y. Zhang, J. Xu, W. Chen and X. Xie, “Passively Q-switched Yb:YAG laser with $Cr^{4+}$:YAG as the saturable absorber,” Appl. Opt. **40**, 4303-4307 (2001).
16. J. I. Mackenzie and D. P. Shepherd, “End-pump, passively Q-switched Yb:YAG double-clad waveguide laser,” Opt. Lett. **27**, 2161-2163 (2002).
17. H. Wu, P. Yan, M. Gong and Q. Liu, “A passively Q-switched diode pumped Yb:YAG microchip laser,” Chin. Opt. Lett. **1**, 697-698 (2003).
18. V. E. Kisel, A. E. Troshin, N. A. Tolstik, V. G. Shcherbitsky, N. V. Kuleshov, V. N. Matrosov, T. A. Matrosova and M. I. Kupchenko, “Q-switched $Yb^{3+}$:YVO4 laser with Raman self-conversion,” Appl. Phys. B **80**, 471-473 (2005).
19. X. Zhang, A. Brenier, Q. Wang, Z. Wang, J. Chang, P. Li, S. Zhang, S. Ding and S. Li, “Passive Q-switching characteristics of $Yb^{3+}$:Gd3Ga5O12 crystal,” Opt. Express **13**, 7708-7719 (2005).
20. Y. Kalisky, O. Kalisky, U. Rachum, G. Boulon and A. Brenier, “Comparative performance of passively Q-switched diode-pumped Yb:GGG, Yb:YAG and Yb-doped tungstates lasers using $Cr^{4+}$-doped garnets,” Proc. of SPIE Vol. 6100, 61001K (2006).
21. K. Lu and N. K. Dutta, “Spectroscopic properties of Yb-doped silica galss,” J. Appl. Phys. 91, 576-581 (2002).
22. A. E. Siegman, Laser, (University Science Books, Mill Valley, 1986).

# *Chapter 4 Passively Q-switched Ytterbium Fiber Lasers by AlGaInAs semiconductor saturable absorbers*

## 4.1 Semiconductor saturable absorbers

In addition to transition mental-doped crystals such as Cr$^{4+}$:YAG crystals mentioned in chapter 4, semiconductors based saturable absorber is an alternative material for passively Q-switched laser. Q-switching by semiconductor saturable absorbers offers more flexible parameters such as operating wavelength, modulation depth, unsaturated and saturated absorption, and recovery time. They are achieved by controlling band gap parameters, number of QWs, co-doping or growth technology [1~2]. To date semiconductors have been employed many optical elements such as lasers, LEDs, solar cells. Besides, they have proved to be excellent candidate for self-starting of passively mod-locked fiber lasers [3] and Q-switched fiber lasers [4~5]. The main advantage of taking semiconductors material as saturable absorber is their short recovery time in the time scale of ns to ps. Compared with Cr$^{4+}$: YAG crystals or other monolithic crystals, semiconductors are able to provide continuous-wave mode-locking and their large absorption cross section profit capturing photons in Q-switched lasers. Among the semiconductor saturable absorbers, InGaAs and AlGaInP materials are the most common in Q-switched lasers [4, 6-7]. Recently AlGaInAs quaternary alloys semiconductors have been confirmed with the merits of larger conduction band offset [8] (meaning a better electron confinement than InGaAsP materials) and lattice-matching to the InP substrate. It is note that choice of InP based alloys provides higher thermal conductivity than GaAs or AlGaAs based alloys [9, 10]. On the other hand the available range of operating wavelength of AlGaInAs can be seen in Fig. 4.1. AlGaInAs can be alloyed with the ternary alloys of InAlAs and InGaAs. It is noted they are both lattice-matched to InP substrates with lattice constant of 5.67A. The energy gap of AlGaInAs is determined by the composition of InAlAs and InGaAs and is tunable from 0.75eV to

1.37eV (1.65μm to 0.9μm). The advantages reveal that AlGaInAs quaternary alloys are potentially applicable as gain mediums in semiconductor lasers or saturable absorber in Q-switching or mode-locking lasers. Recently AlGaInAs have been employed as semiconductor lasers [11, 12] and saturable absorbers for Q-switching a solid-sate laser [13].

In this section, two periodic AlGaInAs multi quantum wells have been employed as saturable absorbers for Yb-doped and Er/Yb codoped fiber lasers. The structure of semiconductor saturable absorber is shown in Fig. 4.2, which was grown on Fe-doped InP substrate by metalorganic chemical-vapor deposition (MOCVD). Instead of the conventional S-doped InP substrate, a Fe-doped InP substrate is used because it is almost transparent in the region of 940 nm~1.6 μm. The region of the saturable absorbers consist periodic groups of several QWs, spaced at half-wavelength intervals by barrier layers. It is worthwhile to mention that, compared with a conventional SESAM structure, the missing DBR significantly simplifies the structure and thus growth and yield.

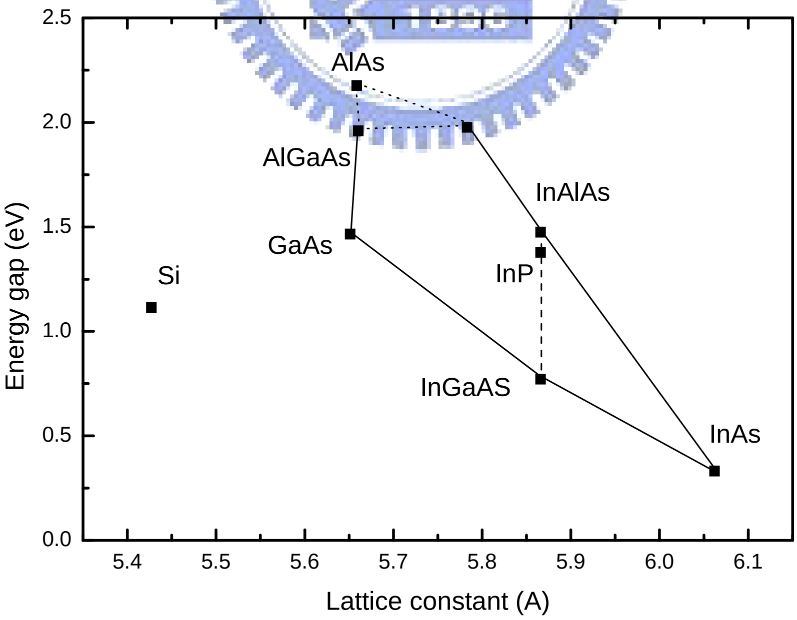

Fig. 4.1. Energy gap versus lattice constant in InGaAs-InP-InAlAs system

Since the cavity modes with lower losses always dominate the lasing output, the lasing modes are naturally the modes with the electric field minima along the periodic QWs. Therefore the barrier layers are used not only to confine the carriers but also to locate the QW groups in the region of the nodes of the lasing standing wave. An InP window layer was deposited on the QW/barrier structure to avoid surface recombination and oxidation.

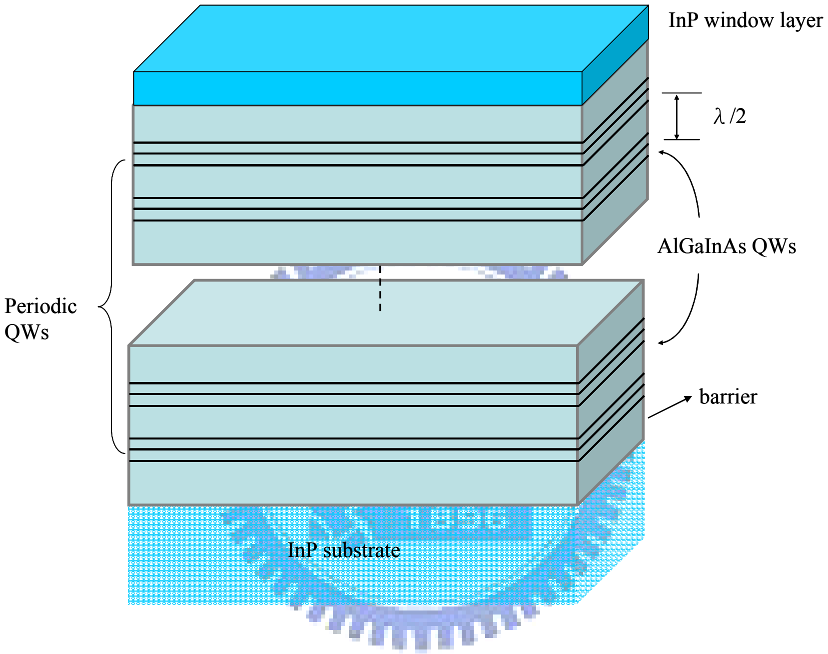

Fig. 4.2. Structure of periodic AlGaInAs QWs saturable absorbers. The periodic structure means the region of the saturable absorbers consist periodic groups of several QWs, spaced at half-wavelength intervals by barrier layers.

## 4.2 Passively Q-switched Yb-doped fiber lasers with AlGaInAs MQW saturable absorbers

In this section I demonstrated a high-pulse-energy passively Q-switched Yb-doped fiber laser with an AlGaInAs/InP QW saturable absorber. With an incident pump power of 24 W, an average output power of 14 W with a Q-switched pulse width of 80 ns at a pulse repetition rate of 33 kHz was obtained; consequently, the maximum pulse energy was up to 450 μJ. More importantly, the overall Q-switching efficiency could exceed 90% because of a low nonsaturable loss.

### 4.2.1 The AlGaInAs periodic MQW semiconductor saturable absorber for 1μm

The structure of the semiconductor saturable absorber was grown on InP substrate and is consisted of 50 groups of three QWs, spaced at half-wavelength intervals by InAlAs barrier layers with the band-gap wavelength around 805 nm. Figure 4.3 shows the measured result for photoluminescence in (a) and the low-intensity transmittance spectrum in (b) of the QW saturable absorber. The initial transmission of the absorber at the wavelength of 1066 nm was found to be approximately 40%. Fig. 4.4 shows the absorption saturation experiment and that reveals that the absorption change between low and high intensities was observed to be approximately 65% in a single pass and the total nonsaturable losses were lower than 9%. It is noted that there is roll-over in transmission at higher incident energy fluence of over 70mJ/cm$^2$. That is explained as nonlinear optical effects such as two photon absorption by Keller et al [14]. The roll-over provides some advantages in mode-locked lasers. However in Q-switching experiment a intracavity-induced lowered modulation depth would diminish pulse energy and may affects pulse stability. Furthermore, the saturation fluence of the saturable absorber was estimated to be in the range of 3mJ/cm$^2$ and its relaxation time was on the order of 100 ns. An InP window layer was deposited on the QW/barrier structure to avoid surface recombination and oxidation. The backside of the substrate was mechanically polished after growth. The both sides of the semiconductor saturable absorber were antireflection coated to reduce back reflections and the couple-cavity effects.

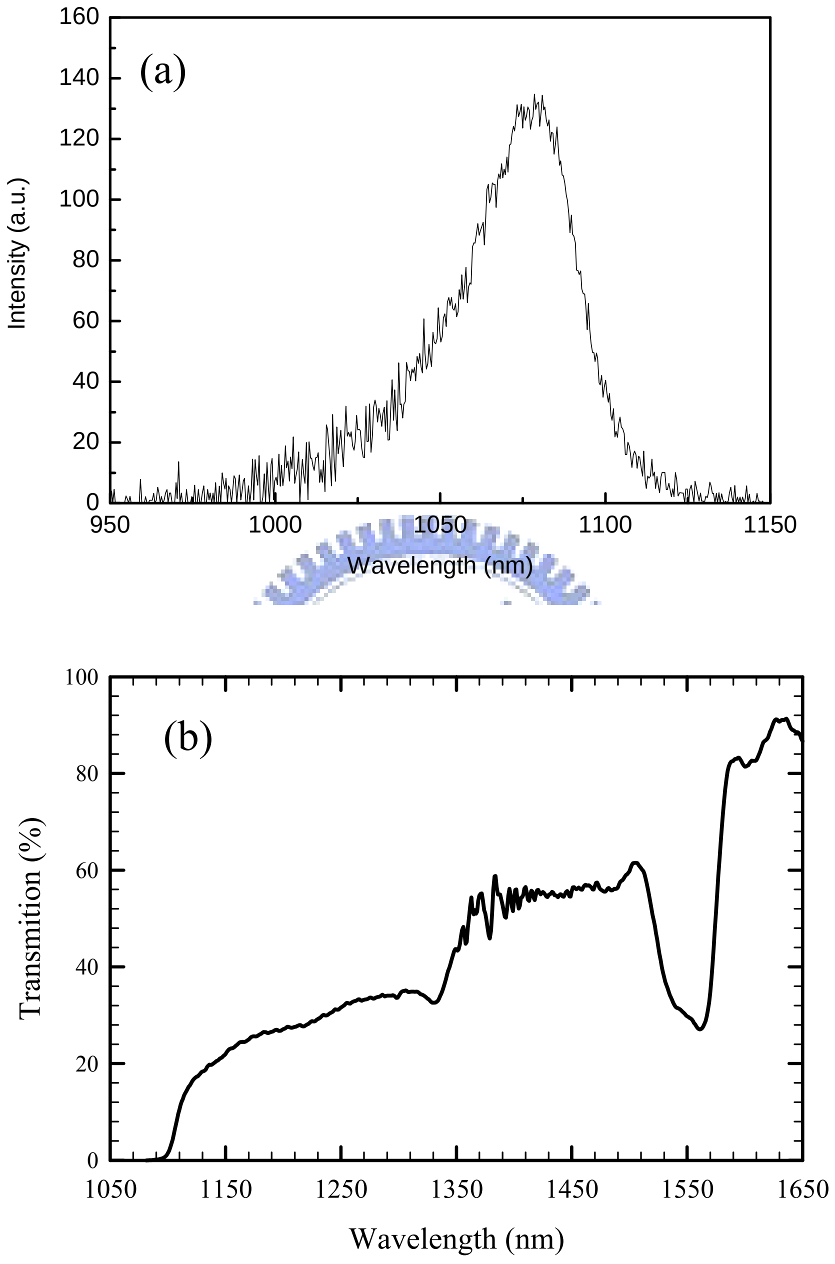

Fig. 4.3. (a) Photoluminescence and (b) low-intensity transmission spectrum of the AlGaInAs semiconductor saturable absorber for 1.06 μm.

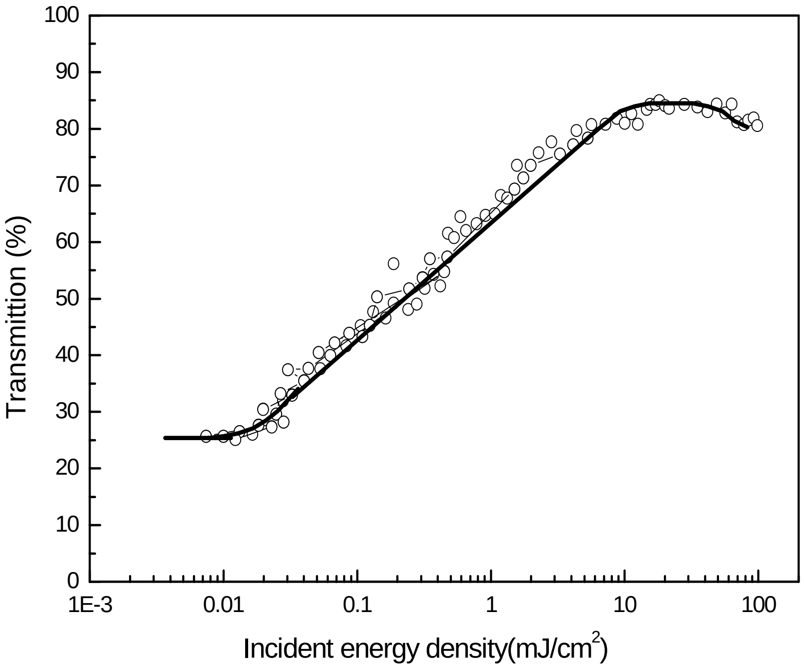

Fig. 4.4. Measured results of saturation of the AlGaInAs semiconductor

### 4.2.2 Experimental setup

The schematic of the experimental setup for the passively Q-switched Yb-doped fiber laser is shown in Fig. 4.5. The setup comprises a 3-m Yb doped fiber and an external feedback cavity with a periodic AlGaInAs QW/barrier structure as a saturable absorber. The external cavity comprises a re-imaging lens, a saturable absorber, a Fabry-Pérot etalon for controlling the lasing wavelength, and a highly reflective mirror at 1.06μm for feedback. The end facets of the fiber were cut to be normal incident. The fiber has a peak cladding absorption coefficient of 10.8 dB/m at 976 nm and a double-clad structure with a diameter of 350 μm octagonal outer cladding, diameter of 250 μm octagonal inner cladding with a numerical aperture (NA) of 0.46, and 25-μm circular core with a NA of 0.07. Note that the robust single-mode output was achieved with a unique low NA feature of the core.

The pump source was a 10-W 976-nm fiber-coupled laser diode with a core diameter of 400 μm and a NA of 0.22. A focusing lens with 25 mm focal length and 90% coupling efficiency was used to re-image the pump beam into the fiber through a dichroic mirror with high transmission (>90%) at 976 nm and high reflectivity

(>99.8%) at 1066 nm. The pump spot radius was approximately 200 μm. With launching into an undoped fiber, the pump coupling efficiency was measured to be approximately 80%. The pulse temporal behavior was recorded with a digital oscilloscope (LeCroy Wavepro 7100; 10G samples/sec; 1 GHz bandwidth) and a fast InGaAs photodiode. The laser spectrum was measured by an optical spectrum analyzer with 0.1-nm resolution (Advantest Q8381A).

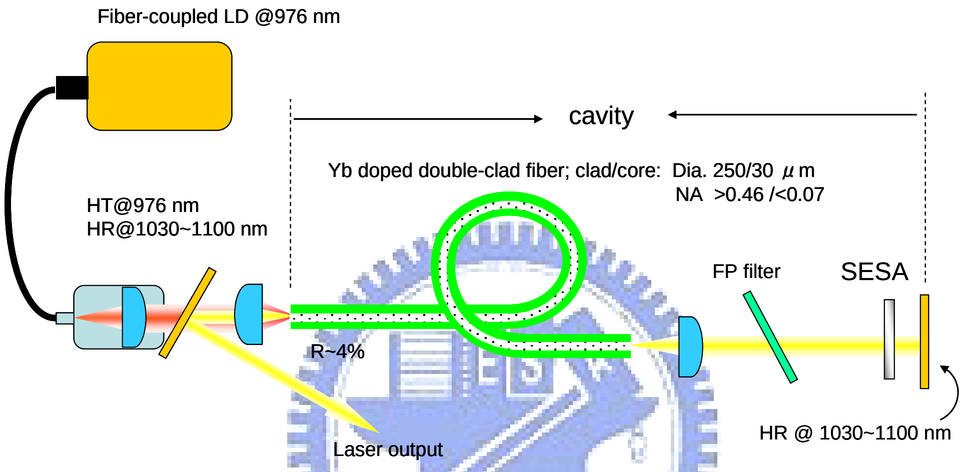

Fig. 4.5. The schematic plot of the fiber lasers passively Q-switched by AlGaInAs semiconductor saturable absorbers

### 4.2.3 Results and discussions

Figure 4.6 shows the average output powers with respect to the incident pump power in cw and passive Q-switching operations for resonant wavelength at 1066nm, 1073nm, 1079nm, and 1083nm. The cw operation was performed to make an evaluation for the passively Q-switched efficiency. Without the saturable absorber in the cavity, the laser had an output power of 16 W at an incident pump power of 24 W in a cw operation and the corresponding slope efficiency was 77%. In the passive Q-switching operation, average output power over 14 W were obtained for all resonant wavelengths at incident pump power of 24 W. The corresponding Q-switching efficiencies can be found to exceed 90%. It is emphasized again due to the lasing modes are naturally the modes with the electric field minima along the periodic QWs. Consequently, compared with the resonant design in the SESAM structure [4], the anti-resonant one owns a higher damage threshold due to the optical intensity is lower and can be operated at high power regime. The superior Q-switching efficiency confirms that the AlGaInAs QW material can be exploited to be an efficient saturable absorber. The lasing linewidth was narrower than 2.0 nm with the help of a FP bandpass filter with a bandwidth of 5 nm, as shown in the inset of Fig. 4.7. The $M^2$ factor was also measured to be less than 1.5 over the complete output power range thanks to the low NA feature of the fiber.

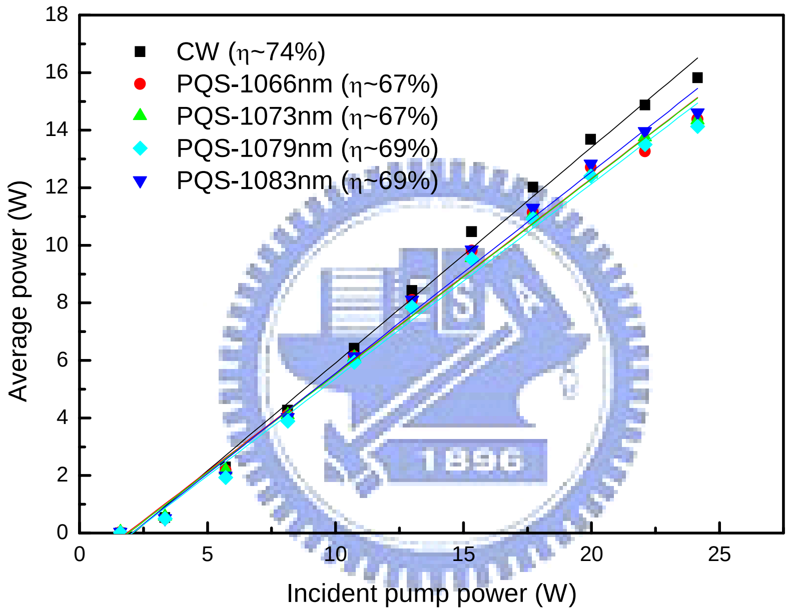

Fig. 4.6. Average output powers with respect to the incident pump power in cw and passive Q-switching operations for resonant wavelength at 1066nm, 1073nm, 1079nm,

Figure 4.8 shows the pulse repetition rate versus the incident pump power. It can be seen that the pulse repetition rate increases monotonically with the pump power. The pulse repetition rates for the 4 wavelengths at the highest pump power are 90 kHz at 1083nm, 35 kHz at 1073nm, 68 kHz at 1079nm, and 30 kHz at 1066nm. It is worthy-noting that according to the PQS theory, there exists a lowest modulation depth for generating a giant pulse stably. For resonant wavelengths at 1079nm and 1083nm, they achieved first laser threshold at the pump power over 3.8 W and radiated laser with slightly and randomly modulated pulse. With the increasing incident pump power, they did not obtain giant pulse periodically until the pump power exceeds 8W.

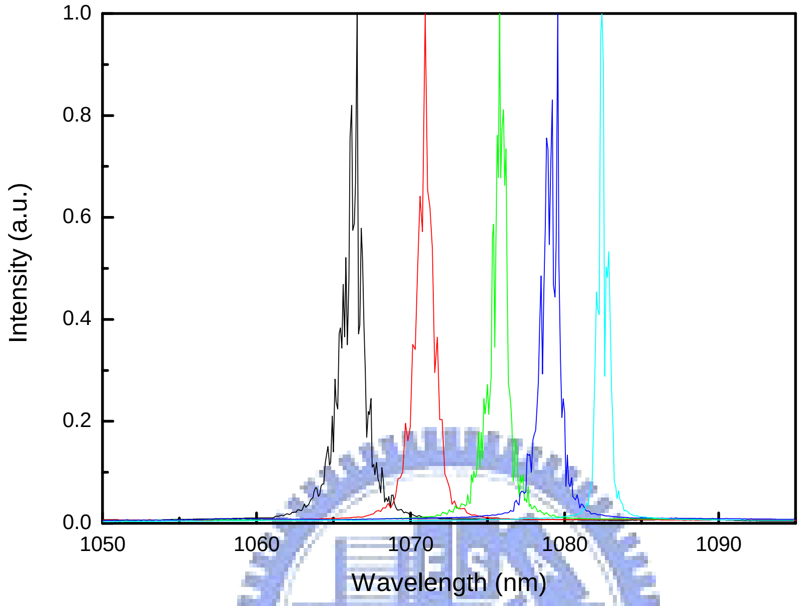

Fig. 4.7. Output spectral spectrum of the passively Q-switched fiber laser.

Besides, the pulse energies is shown in Fig. 4.9 for the 4 wavelengths: 160 μJ at 1083nm, 170 μJ at 1073nm, 350 μJ at 1079nm, and 450 μJ at 1066nm at maximum pump power. It is noted that the pulse energies are increasing with the incident pump power, which shows that saturable absorber is not totally transparent before pump power of 23W. The experimental results are compared with the theoretical prediction in Fig. 4.10. The experimental results shown in Fig. 4.10 are the pulse repetition rate and pulse energy versus resonant wavelength at the maximum pump power. The simulation parameters used here are identical to those employed in chapter 4 except that the absorption cross-section $\sigma_{SA}$ of saturable absorbers, which was taken as $8.7\times10^{-14}$ cm$^2$, and the parameter of $\beta$ is zero here due to semiconductors are 2-level systems [15]. It is noted that the cross-section of semiconductors is much larger than the $Cr^{4+}$:YAG crystal due to their short recovery time. Fig. 4.10 (a) and (b) show the comparisons of the experimental and theoretical results of pulse repetition rate and pulse energy respectively. The outcomes of prediction agree well with the experimental results.

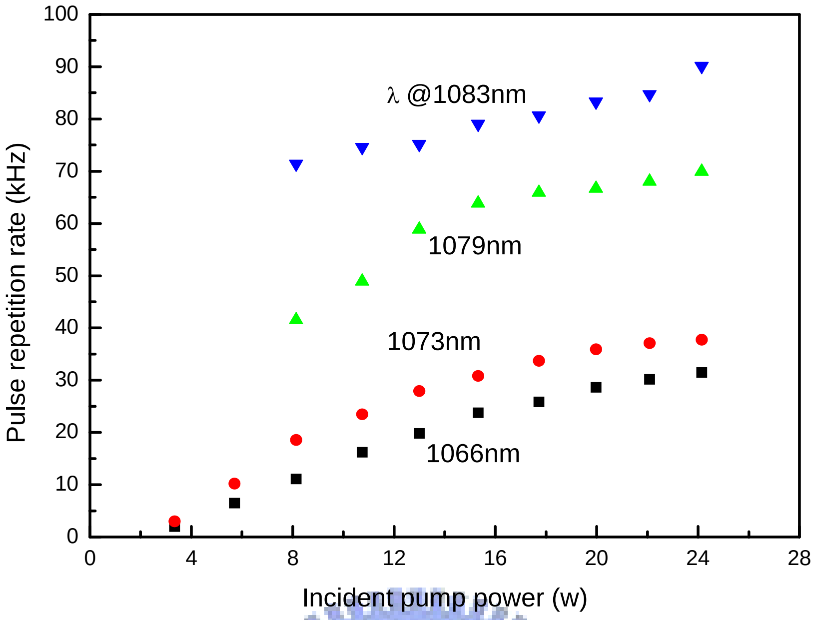

Fig. 4.8 The pulse repetition rate versus the incident pumping power.

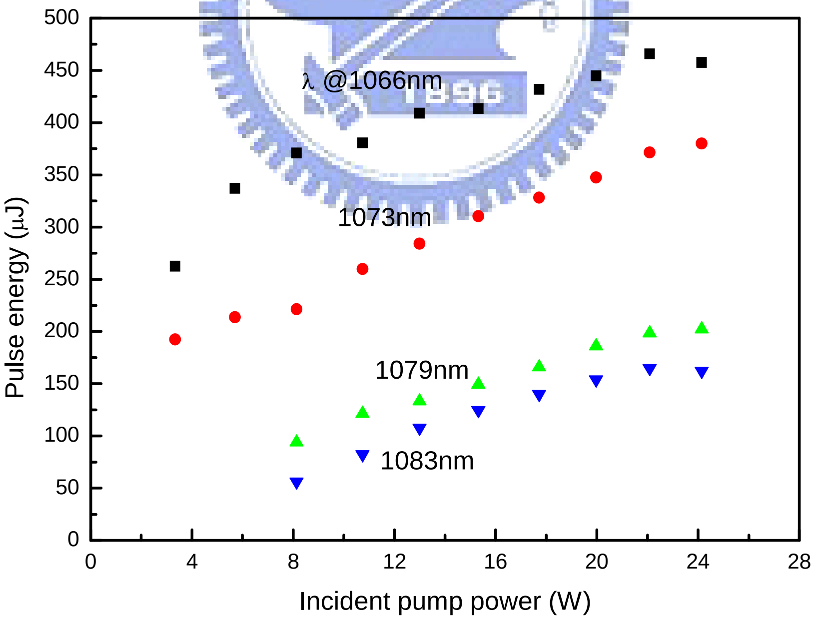

Fig. 4.9 The pulse energy versus the incident pumping power.

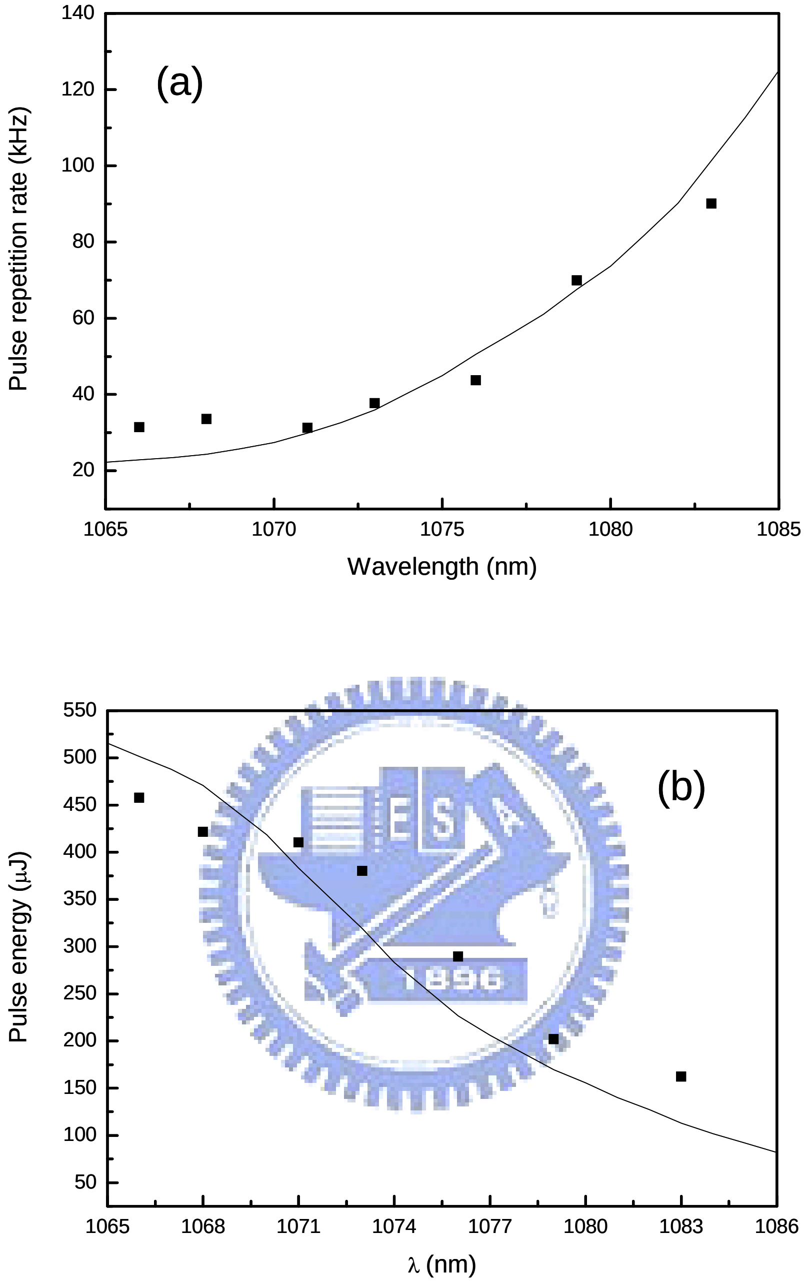

Fig. 4.10. The predictions of the pulse repetition rate (a) and the pulse energy (b) versus resonant wavelength at maximum pump power. Dots: the experimental results; solid line: the theoretical predictions.

The pulse duration at the 1066nm, as shown in Fig. 4.11 (a), was found to be almost constant at 75 ns at maximum pump powers. As a consequence, the maximum peak power reaches approximately 6 kW. A typical oscilloscope trace of a train of output pulses is shown in Fig. 4.11 (b). Under the optimum alignment condition, the pulse-to-pulse amplitude fluctuation was found to be within ± 10%. In passively Q-switched Yb-doped fiber lasers, on the whole, the performances with AlGaInAs QW saturable absorbers are superior to the results obtained with $Cr^{4+}$:YAG crystals .

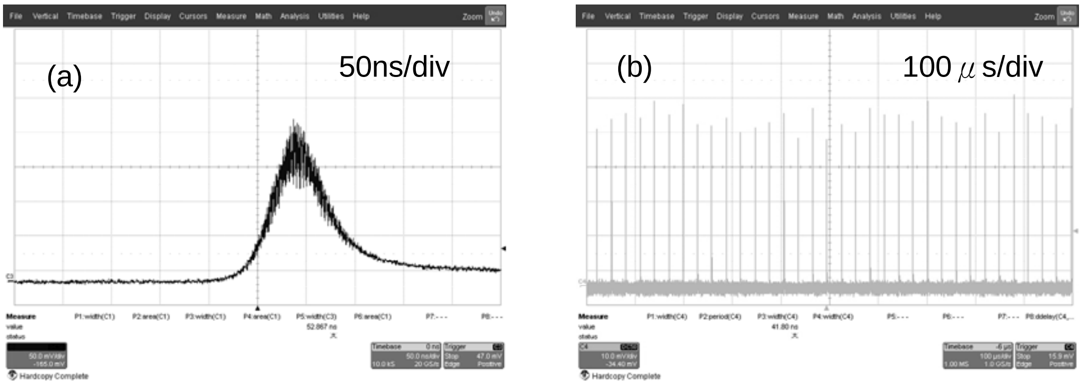

Fig. 4.11. (a). Oscilloscope traces of a train of Q-switched pulses, (b) Oscilloscope traces of a typical Q-switched envelope.

## 4.3 Passively Q-switched Er/Yb codoped fiber lasers with AlGaInAs saturable absorbers

In this section I introduced at first several saturable absorbers of Q-switched fiber lasers in the region of eyesafe. Then I report on a high-pulse-energy passively Q-switched Er/Yb codoped fiber laser with an AlGaInAs/InP QW saturable absorber. With an incident pump power of 13 W, an average output power of 1.26 W with a Q-switched pulse width of 300 ns at a pulse repetition rate of 33 kHz was obtained; consequently, the maximum pulse energy was up to 100μJ. A mode-locking phenomenon enhances the peak power higher than 0.5 kW. The overall Q-switching efficiency could exceed 84% because of a low nonsaturable loss.

### 4.3.1 Introduction to saturable absorbers used in Q-switched eye-safe lasers

Nowadays, the most common monolithic saturable absorbers in the eye-safe wavelength regime are the transition metal-doped crystals, including $Co^{2+}$:ZnSe [16], $Co^{2+}$:ZnS [17], $Cr^{2+}$:ZnSe [18], and $Co^{2+}$:$MgAl_2O_4$ [18]. The absorption band of $Co^{2+}$ ion and $Cr^{2+}$ ion ranges from 1.4 μm~2.5 μm and 1.4 μm~2.5 μm respectively.

Table 4.1. The monolithic saturable absorbers in the region of 1.5 μm.

| **SA** | **Lifetime (μs)** | **$\sigma_{es}/\ \sigma_{gs}$ ($10^{-19}cm^2$)**<br>**$\beta$ , $\alpha$, $T_o$** | **Results** | **Fiber parameters** | **Active medium** |
|---|---|---|---|---|---|
| $Co^{2+}$:$MgAl_3O_4$ [18] | 0.34 | NA<br>2.4-two level<br>40, 45% | **22μJ, 370 ns**<br>**60W@60kHz** | **12μm, NA=0.22** | **Er/Yb** |
| $Cr^{2+}$:ZnSe[18] | 8 | 0.2/3.4<br>0.06, 57, 30% | **18μJ, 380 ns**<br>**45W@70kHz** | **same as above** | **Er/Yb** |
| $Co^{2+}$:ZnS[17] | 200 | 1.1/10<br>0.11, 102,67% | **60μJ, 3.5 ns**<br>**>10 kW@6kHz** | **11 μm, NA~ 0.21** | **Er/Yb** |
| $Co^{2+}$:ZnSe[16] | 290 | 1.1/11.5<br>0.096, 117, 92% | **15 nJ, 43 mW,**<br>**350 ns @235kHz** | **2.7 μm, NA~ 0.27** | **Er** |

In addition to the transition metal-doped crystals, semiconductors are one of the candidates for saturable absorbers in the eyesafe region. The semiconductor saturable-absorber materials for passively Q-switched fiber lasers at 1.5 μm are merely so far based on the InGaAsP thick layer [19] and the InGaAs quantum well (QW) [20]. As mentioned before AlGaInAs semiconductors possess larger conduction band offset and lattice-matching to the InP substrate, which benefits operation in high power regime.

### 4.3.2 The AlGaInAs periodic MQW semiconductor saturable absorber for 1.5 μm

The structure of the semiconductor saturable absorber was grown on InP substrate and consisted of 30 groups of two QWs, spaced at half-wavelength intervals by AlGaInAs barrier layers with the band-gap wavelength around 1.1 μm. Figure 4.12 shows the measured result for photoluminescence in (a) and the low-intensity transmittance spectrum in (b) of the QW saturable absorber. The initial transmission of the absorber at the wavelength of 1560 nm was found to be approximately 23%. Fig. 4.13 shows the absorption saturation experiment and that reveals that the absorption change between low and high intensities was observed to be approximately 70% in a single pass and the total nonsaturable losses were lower than 5%. Furthermore, the saturation fluence of the saturable absorber was estimated to be in the range of 4mJ/cm$^2$ and its relaxation time was also on the order of 100 ns.

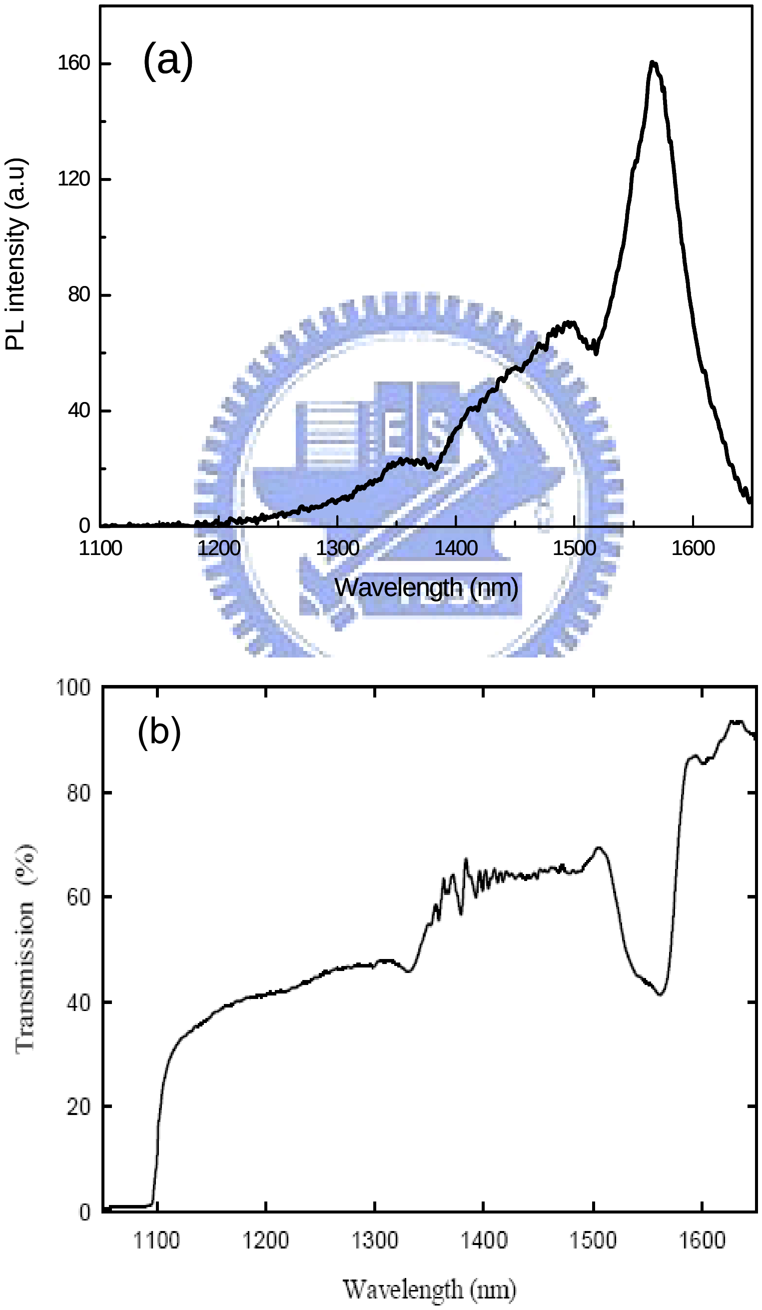

Fig. 4.12. (a) Photoluminescence and (b) low-intensity transmission spectrum of the AlGaInAs semiconductor saturable absorber for 1.5 μm.

An InP window layer was deposited on the QW/barrier structure to avoid surface recombination and oxidation. The backside of the substrate was mechanically polished after growth. The both sides of the semiconductor saturable absorber were antireflection coated to reduce back reflections and the couple-cavity effects.

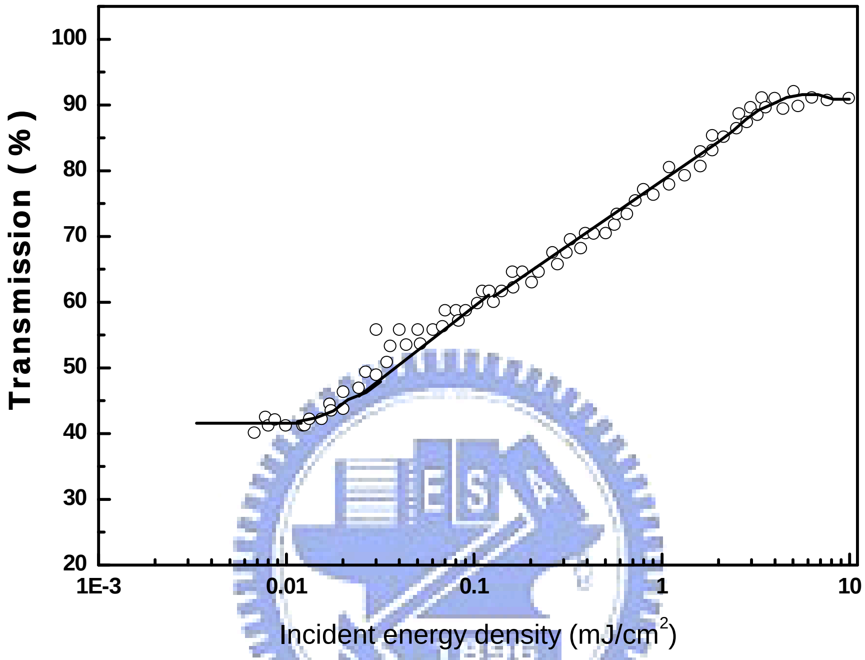

Fig. 4.13. Measured results of saturation of the AlGaInAs semiconductor

### 4.3.3 Experimental setup

Figure 4.14 depicts the schematic of the experimental setup for EYDFL that comprises a 7-m Er-Yb codoped fiber and an external feedback cavity with a periodic AlGaInAs QW/barrier structure as a saturable absorber. The fiber has an absorption coefficient of 3.0 dB/m at 976 nm and a double-clad structure with a diameter of 450-μm octagonal outer cladding, diameter of 300-μm octagonal inner cladding with a numerical aperture (NA) of 0.46, and 25-μm circular core with a NA of 0.1. Note that the LMA fiber featuring a unique low NA core design is used to achieve the robustly single-mode output beam quality with high pulse energies. The external cavity consists of a focusing lens of 25-mm focal length to focus the fiber output into the SESA device and a highly reflective mirror for feedback. The focusing lens was arranged to have a beam waist of 50 µm inside the SESA. The SESA was mounted in a copper block without active cooling. The pump source was a 16-W 976-nm fiber-coupled laser diode with a core diameter of 400 µm and a NA of 0.22. A focusing lens with 25 mm focal length and 85% coupling efficiency was used to re-image the pump beam into the fiber through a dichroic mirror with high transmission (>90%) at 976 nm and high reflectivity (>99.8%) at 1560 nm. The pump spot radius was approximately 200 µm.

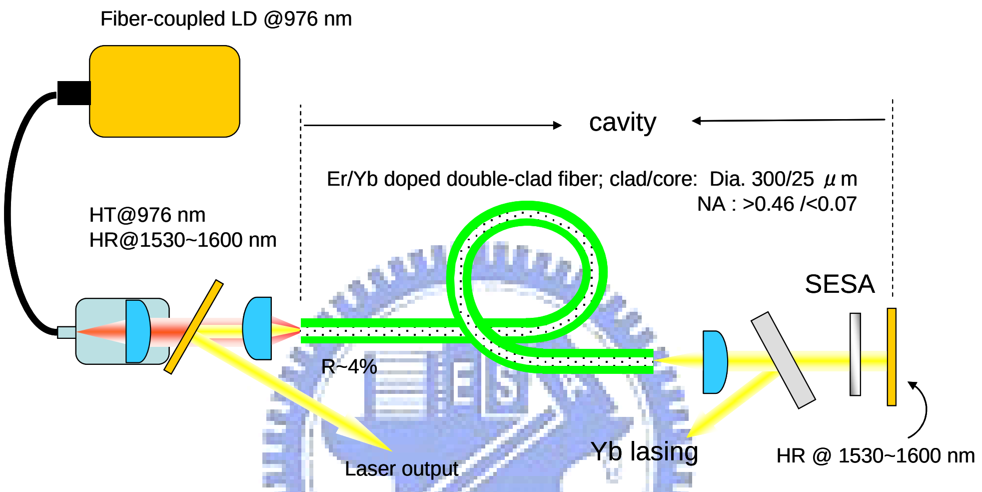

Fig. 4.14. The schematic plot of the fiber lasers passively Q-switched by AlGaInAs semiconductor saturable absorbers.

### 4.3.4 Experimental results and discussions

Figure 4.15 shows the average output powers at 1560 nm with respect to the incident pump power in cw and passively Q-switching operations. The cw performance at 1560 nm provides the baseline for evaluating the passively Q-switched efficiency. Without the semiconductor saturable absorber in the cavity, the cw laser at 1560 nm had an output power of 1.50 W at an incident pump power of 13.5 W. In the passively Q-switching regime, an average output power of 1.26 W was obtained at an incident pump power of 13.5 W. As a consequence, the Q-switching efficiency was found to be as high as 84%. The pulse temporal behavior was recorded by the LeCroy digital oscilloscope with a fast InGaAs photodiode. Figure 4.16 shows the pulse repetition rate and the pulse energy versus the incident pump power. The pulse repetition rate increases monotonically with the pump power up to 12 kHz. Like typically passively Q-switched lasers, the pulse energy is almost unrelated to the pump power and its value is 105 μJ on average.

A typical oscilloscope trace of Q-switched pulse train is shown in Fig. 4.17 (a). With the optimum alignment, the pulse-to-pulse stability was found to be approximately ±15% as the pump power is higher than 8 W. The pulse-to-pulse stability may be improved by the angle-cleaved end facets of the fiber. Figure 4.17 (b) shows the temporal shape of a single Q-switched pulse envelope, which was recorded at the maximum pump power. It can be seen that the self-mode-locking effect [21, 22] leads to the formation of the mode-locked pulses inside the Q-switched pulse envelope. The separation of the mode-locked pulses was found to be 80 ns, which matched exactly with the cavity roundtrip time and corresponded to a repetition rate of 12.4 MHz.

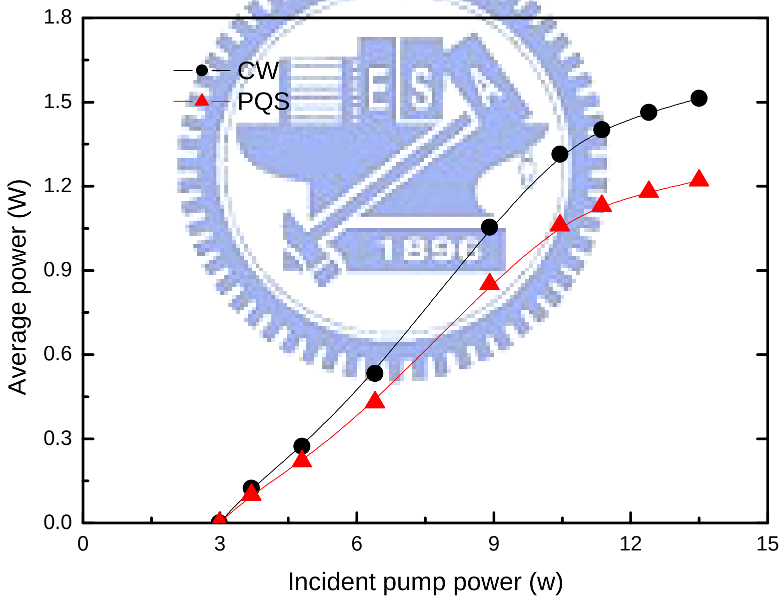

Fig. 4.15. Average output powers with respect to the incident pump power in cw and passive Q-switching operations.

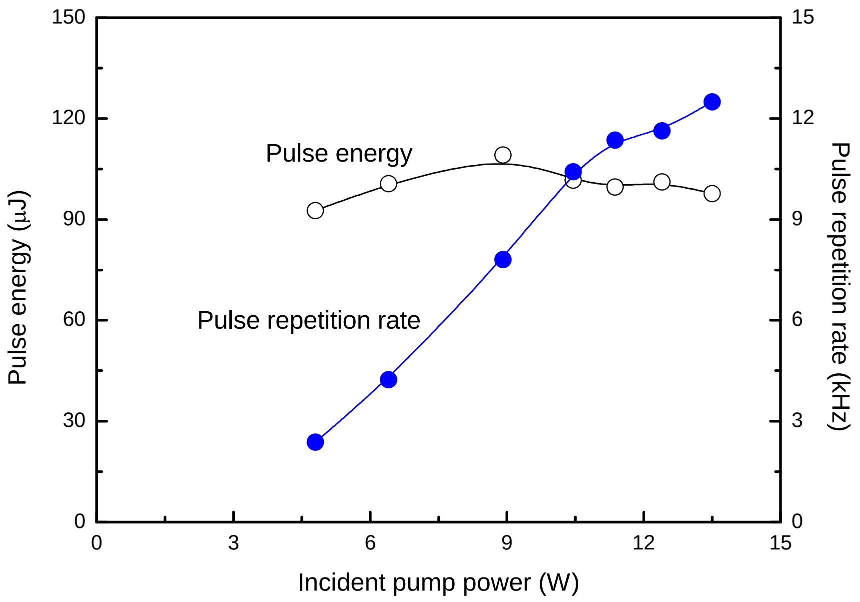

Fig. 4.16. The pulse repetition rate and the pulse energy versus the incident pump power.

The estimated energy of the highest pulse inside envelope was found to be close to 17μJ. The expanded oscilloscope traces reveal that the mode-locked pulse width is approximately 33 ns. As a result, the peak power can be found to be greater than 0.5 kW.

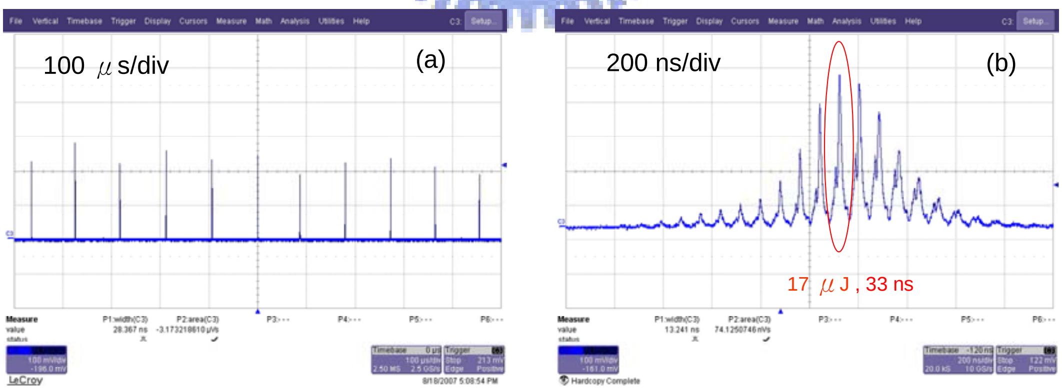

Fig. 4.17. (a) Oscilloscope traces of a typical Q-switched envelope; (b) Oscilloscope traces of a train of Q-switched pulses.

## 4.4 Conclusion

In this chapter we employed AlGaInAs semiconductor saturable absorbers to Q-switch Yb doped and Er/Yb doped fiber lasers. Semiconductor saturable absorbers possess the merits of tailored gain region and higher absorption cross-section than bulk saturable absorbers. By use of the semiconductor saturable absorbers, high-pulse-energy passively Q-switched Yb-doped and Er/Yb codoped fiber lasers have been developed. The Yb Q-switched fiber laser generated stable pulses of 75 ns duration with an average output power of 14 W and a repetition rate of 30 kHz at an incident pump power of 24 W. The overall Q-switching efficiency was found to exceed 87 %. Besides, tunability was also performed to confirm the validity of the PQS theory. The Excellent results substantiate that the AlGaInAs QW material can be exploited to be an efficient absorber with a large modulation change and a quite low nonsaturable loss. Compared with performances of the Q-switched laser by a $Cr^{4+}$:YAG crystal, the 87 % of Q-switching efficiency is slightly slower owing to the nonsaturable loss of semiconductor such as 8% of facet reflection even with AR-coated layer. On the other hand Q-switched by the AlGaInAs/InP QW saturable absorber, higher gain is stored due to the ESA effect limit the $Cr^{4+}$:YAG crystal to achieve higher transparency, i.e. higher modulation depth. Therefore the pulse energy in obtained here is higher than that in the Q-switched laser by $Cr^{4+}$:YAG crystal. The Er/Yb Q-switched fiber laser can emit greater than 1.26 W of an average output power at a repetition rate of 12 kHz at 13.5-W pump power. Moreover, mode-locking phenomenon enhances the peak power higher than 0.5 kW. The remarkable performance confirms the prospect of using AlGaInAs QWs as saturable absorbers in passively Q-switched fiber lasers in the region of 1.06 μm and 1.5 μm.

# Reference

1. M. Haiml, R. Grange, U. Keller, “Optical characterization of semiconductor saturable absorbers” Appl. Phys. B **79**, 331 (2004).
2. U. Keller, K. J. Weingarten, F. X. Kärtner, D. Kopf, B. Braun, I. D. Jung, R. Fluck, C. Hönninger, N. Matuschek, J. Aus der Au, "Semiconductor saturable absorber mirrors (SESAMs) for femtosecond to nanosecond pulse generation in solid-state lasers," IEEE J. Selected Topics in Quantum Electronics (JSTQE) **2**, 435-453 (1996).
3. K. Tamura, E. P. Ippen, H. A. Haus, and L. E. Nelson, “77-fs pulse generation from a stretched-pulse mode-locked all-fiber ring laser,” Opt. Lett. **18**, 1080-1082 (1993).
4. T. Hakulinen and O. G. Okhotnikov, “8 ns fiber laser Q switched by the resonant saturable absorber mirror,” Opt. Lett. **32**, 2677-2679 (2007**).**
5. S. Kivistö, R. Koskinen, J. Paajaste, S. D. Jackson, M. Guina, and O. G. Okhotnikov, “Passively Q-switched $Tm^{3+}$, $Ho^{3+}$-doped silica fiber laser using a highly nonlinear saturable absorber and dynamic gain pulse compression,” Opt. Express **16,** 22058-22063 (2008).
6. J.Y. Huang, H.C. Liang, K.W. Su, H.C. Lai, Y.F. Chen and K.F. Huang, “InGaAs quantum-well saturable absorbers for a diode-pumped passively Q-switched Nd:YAG laser at 1123 nm,” Appl. Opt. **46**, 2, 239-242 (2007).
7. A. Li, S.C. Liu, K.W. Su, Y.L. Liao, S.C. Huang, Y.F. Chen, K.F. Huang, “InGaAsP quantum-wells saturable absorber for diode-pumped passively Q-switched 1.3-μm lasers,” Appl. Phys. B **84**, 3, 429-431 (2006).
8. K. Alavi, H. Temkin, W. R. Wagner, and A. Y. Cho, “Optically pumped 1.55-μm double heterostructure $Ga_xAl_yIn_{1-x-y}As/Al_uIn_{1-u}As$ lasers grown by molecular beam epitaxy,” Appl. Phys. Lett. **42**, 254-256 (1983).
9. S.T. Huxtable, A. Shakouri, C. Labounty, X. Fan, P. Abraham, Y.J. Chiu, J.E. Bowers and A. Majumdar, “Thermal conductivity of indium phosphide based superlattices,” Microscale. Thermophys Eng, **4**, 197–203 (2000).
10. V. Spagnolo, M. Troccoli, C. Gmachl, F. Capasso, A. Tredicucci, A. M. Sergent, A. L. Hutchinson, D. L. Sivco, A. Y. Cho, and G. Scamarcio, “Temperature

profile of GaInAs/AlInAs/InP quantum cascade-laser facets measured by microprobe photoluminescence," Appl. Opt. Lett. **78**, 20952097 (2001).

11. S. R. Selmic, T. Chou, J. Sih, J. B. Kirk, A. Mantie, J. K. Butler, D. Bour, and G. A. Evans, "Design and characterization of 1.3-μm AlInGaAs/InP multiple-quantum-well lasers," IEEE J. Sel. Topics Quantum Electron. **7**, 340-349 (2001).
12. C. E. Zah, R. Bhat, B. N. Pathak, F. Favire, W. Lin, M. C. Wang, N. C. Andreadakis, D. M. Hwang, M. A. Koza, T. P. Lee, Z. Wang, D. Darby, D. Flanders, J. J. Heieh, "High-performance uncooled 1.3-μm AlxGayIn1-x-yAs/InP strained-layer quantum-well lasers for subscriberloop applications," IEEE J. Quantum Electron. **30**, 511-523 (1994).
13. S. C. Huang, S. C. Liu, A. Li, K. W. Su, Y. F. Chen, and K. F. Huang, "AlGaInAs quantum-well as a saturable absorber in a diode-pumped passively Q-switched solid-state laser," Opt. Lett. **32**, 1480–1482 (2007).
14. R. Grange, M. Haiml, R. Paschotta, G.J. Sp¨uhler, L. Krainer, M. Golling, O. Ostinelli, U. Keller, "New regime of inverse saturable absorption for self-stabilizing passively mode-locked lasers" Appl. Phys. B **80**, 151-158 (2005).
15. Y. F. Chen, J. L. Lee, H. D. Hsieh, and S. W. Tsai, "Analysis of passively Q-switched lasers with simultaneous mode-locking," IEEE J Quan. Electro. **38**, 312-317 (2002).
16. V. N. Philippov, A. V. Kir'yanov, and S. Unger, "Advanced configuration of erbium fiber passively Q-switched laser with Co$^{2+}$:ZnSe crystal as saturable absorber," IEEE Photon. Technol. Lett. **16**, 57–59, (2004).
17. M. Laroche, A. M. Chardon, J. Nilsson, D. P. Shepherd, W. A. Clarkson, S. Girard, and R. Moncorgé, "Compact diode-pumped passively Q-switched tunable Er-Yb double-clad fiber laser," Opt. Lett. **27**, 1980–1982 (2002).
18. V. Philippov, J. Nilsson, W. A. Clarkson, A. Abdolvand, V. E. Kisel, V. G. Shcherbitsky, N. V. Kuleshov, V. I. Konstantinov, and V. I. Levchenko, "Passively Q-switched Er-Yb double clad fiber laser with Cr$^{2+}$:ZnSe and Co$^{2+}$:MgAl$_2$O$_4$ as a saturable absorber," Proc. SPIE, **5335**, 8-15, (2004).
19. R. Paschotta, R. Häring, E. Gini, H. Melchior, U. Keller, H. L. Offerhaus, and D.

J. Richardson, “Passively Q-switched 0.1 mJ fiber laser system at 1.53μm,” Opt. Lett. **24**, 388-390 (1999).

20. J. B. Lecourt, G. Martel, M. Guézo, C. Labbé, and S. Loualiche, “Erbium-doped fiber laser passively Q-switched by an InGaAs/InP multiple quantum well saturable absorber,” Opt. Commun., **263**, 71–83, (2006).
21. L. A. Zenteno, H. Po, and N. M. Cho, “All-solid-state passively Q-switched mode-locked Nd-doped fiber laser,” Opt. Lett. **15**, 115-117 (1990).
22. Y. F. Chen and S. W. Tsai, “Simultaneous Q-switching and mode-locking in a diode-pumped Nd:YVO4-Cr$^{4+}$:YAG laser,” IEEE J. Quantum Electron. **37**, 580-586, (2001).

# *Chap 5 Actively Q-switched Fiber Lasers*

## 5.1 Introduction to active Q-switching

As depicted in section 1.2, the methods to achieve actively Q-switched lasers are so far by use of mechanical, EO, and AO modulators. Among these Q-switches, the mechanical type modulators could be manifested by rotating mirrors or prisms [1-2], modulated mechanically FBGs [3-4], or micro-actuating optical modulators [5]. The later are developed for all-fiber Q-switched lasers. They are less insensitive to polarization and wavelength so that they could be operated at longer wavelength (e.g. several μm). However the noise, short lifetime of the bearings, and weaker performance makes them uncommon in most applications. EO modulators (EOM) are based on electro-induced birefringence in a medium to modulate the phase, polarization, and amplitude of incident beams. However EOM with the high-voltage driver and the wave plates for Q-switching are more expensive and bulky. On the other hand, AOM possesses the merits of lower cost, lower driving voltage, high-speed, and high damage threshold; those advantages make AOM the most common Q-switch in fiber lasers [6-9].

The rate equations describing the active Q-switching are similar with (2.3) and (2.4) except the terms relative to saturable absorbers are dismissed and the modulation loss is now $\varepsilon(t)$ instead. $\varepsilon(t)$ represents the loss induced by the active Q-switch. For simplicity we assume that the modulator is so fast that no significant change of population inversion occurs within the switching process. Then the output pulse energy $E_p$ is the same as that in the PQS:

$$E_P = \frac{h\nu A}{2\sigma\gamma}\ln\left(\frac{1}{R}\right)\ln\left(\frac{n_i}{n_f}\right). \qquad (5.1)$$

Furthermore we can derive the expression of the population inversion density at threshold $n_t$ as in section 2.1:

$$n_t = \frac{\ln(1/R) + L}{2\sigma l}, \tag{5.2}$$

and the relation of the initial and final population inversion densities, $n_i$ and $n_f$, as

$$n_i - n_f = n_t \ln\left(\frac{\mathrm{n_i}}{\mathrm{n_f}}\right). \tag{5.3}$$

The pulse peak power $P$ is obtained again by setting $d\phi / dn$ to be zero to get the $n_{\phi\max}$.

And we found that $n_{\phi\max}$ happens to equals $n_t$ and the peak power is

$$P = \frac{h\nu A l' \phi_{\max}}{t_r} \ln(\frac{1}{R}) = \frac{h\nu A l'}{t_r} \ln(\frac{1}{R}) \left[ n_i - n_t \left( 1 + \ln \frac{n_i}{n_t} \right) \right]. \tag{5.4}$$

Hence the pulse width can be obtained as

$$\tau_p = \frac{P}{E_p} = \frac{t_r / \gamma}{\ln(1/R) + L} \frac{\ln(n_i / n_f)}{n_i / n_t - 1 - \ln(n_i / n_t)}. \tag{5.5}$$

To determine $n_i$ and $n_f$ we have to solve equation (5.3) with the following one, which indicates the initial population in a CW pumped Q-switched laser with repetition rate f:

$$\mathrm{n_i} = \mathrm{R_p} \tau_\mathrm{f} \left[ 1 - \exp\left( \frac{-1}{\tau_\mathrm{f} f} \right) \right] + \mathrm{n_f} \exp\left( \frac{-1}{\tau_\mathrm{f} f} \right). \tag{5.6}$$

As a consequence we can obtain the average power as

$$P_{avg} = \frac{h\nu A}{2\sigma\gamma} f \ln\left(\frac{1}{R}\right) \ln\left(\frac{n_i}{n_f}\right). \tag{5.7}$$

Fig. 5.1 shows the numerical results of the pulse energy, the pulse width, and the average power of a Q-switched laser. The average power is close to the CW at high repetition rate and is proportional to the repetition rate at lower one. The loss is a result of that the average stimulated emission is proportional to the repetition rate due to the finite lifetime of upper level of gain medium. Besides, amplified spontaneous emission is observed owing to the high gain property in fiber lasers, which could be stronger than the laser and often misunderstands the measured laser power at low repetition rate. The pulse width, $\tau_p$, increases in proportion to the repetition rate while the pulse energy, $E_p$, decreases at higher repetition rate. As the repetition rate decreases, the time between pulses is sufficient for the inversion to reach its maximum value $R_p\tau_f$, meaning $E_p$ and $\tau_p$ approach nearly constant in accordance with the finite gain.

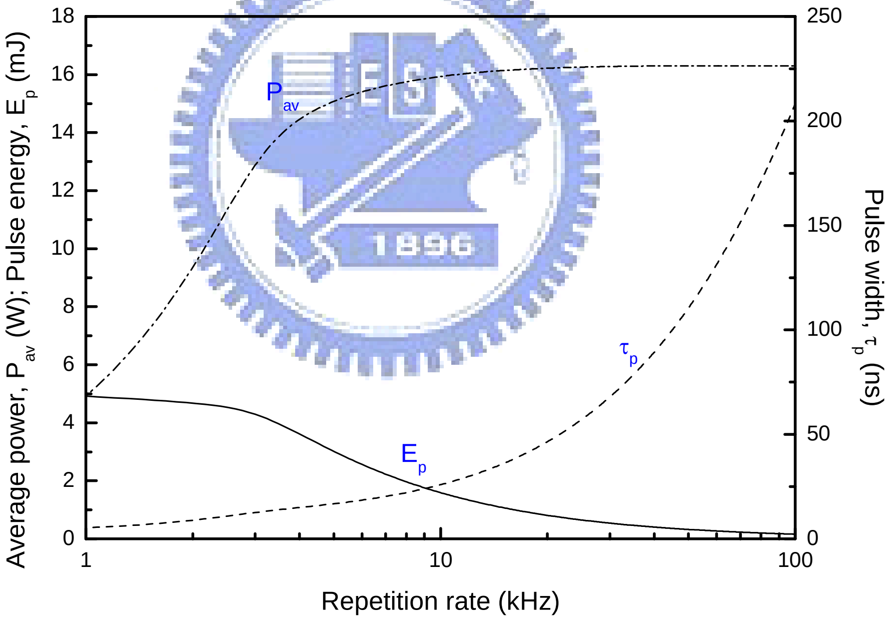

Fig. 5.1. Performance of an actively Q-switched laser. The pulse energy, pulse width, and average power are presented as a function of repetition rate.

## 5.2 Fiber Lasers Q-switched by an acousticoptic modulator

### 5.2.1 Experimental setup

The schematic of the experimental setup for the passively Q-switched Yb-doped fiber laser is shown in Fig. 5.2. The setup comprises a 3-m Yb doped fiber and an external feedback cavity. The external cavity comprises a re-imaging lens, a Fabry-Pérot etalon for controlling the lasing wavelength, an acousto-optic Q-switch mounted on a copper heat sink and was chilled actively by water, and a highly reflective mirror at 1060 nm~1100 nm for feedback. Note that a beam is incident into an AO Q-switch and then be diffracted by the phase grating resulted from the RF wave-introduced refractive-index change of the AO crystal. Therefore I will call the un-modulated condition as RF-off while the modulated one as RF-on in this chapter. The end facets of the fiber were cut to be normal incident, so the laser resonator is a simple Fabry-Perot (F-P) structure. One side of the cavity was a dichroic mirror and was coated high reflection at 1030 nm~1100 nm; the other side was the fiber end which is cut normally as the lasing output with ~4% reflection. The fiber has a peak cladding absorption coefficient of 10.8 dB/m at 976 nm and a double-clad structure with a diameter of 350 μm octagonal outer cladding, diameter of 250 μm octagonal inner cladding with a numerical aperture (NA) of 0.46, and 30-μm circular core with a NA of 0.07.

The pump source was a 35-W 976-nm fiber-coupled laser diode with a core diameter of 400 μm and a NA of 0.22. A focusing lens with 25 mm focal length and 90% coupling efficiency was used to re-image the pump beam into the fiber through a dichroic mirror with high transmission (>90%) at 976 nm and high reflectivity (>99.8%) at 1066 nm. The pump spot radius was approximately 200 μm. With launching into an undoped fiber, the pump coupling efficiency was measured to be approximately 80%. The pulse temporal behavior was recorded with a digital oscilloscope (LeCroy Wavepro 7100; 10G samples/sec; 4 GHz bandwidth) and a fast InGaAs photodiode. The spectral information was measured by an optical spectrum analyzer (Advantest Q8381A) that utilizes a grating monochromator for the high speed measurement of pulse light with the resolution of 0.1 nm.

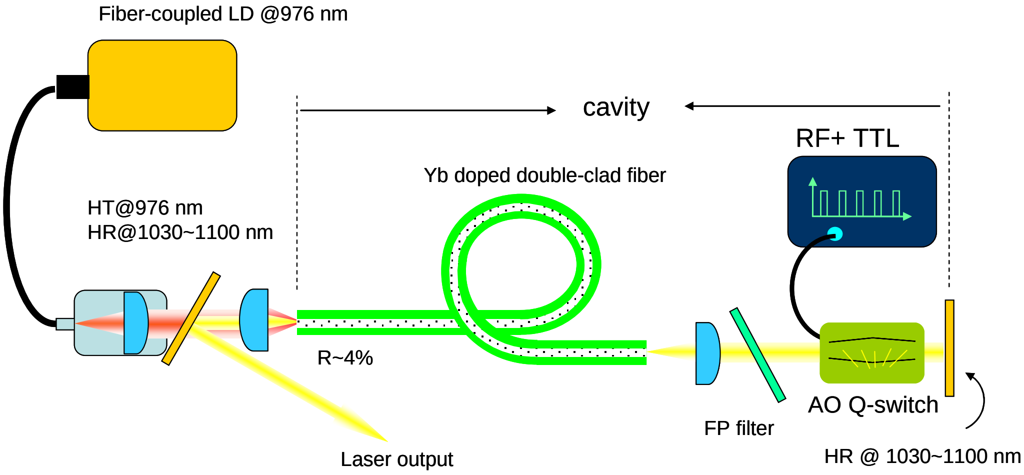

Fig. 5.2. Schematic of diode-pumped actively Q-switched double-clad fiber laser. HT: high reflection; HR: high reflection

### 5.2.2 Experimental results and discussions

Firstly the cw operation was examined where the AO Q-switch was off (RF off). In this section we control the resonating wavelength at 1075 nm for the largest output power as seen in chapter 2. The AO Q-switch was coated anti-reflection at 1050~1100 nm to reduce reflective loss. However we still observed that as in Fig. 5.3, the output power was 95% of the laser without AO Q-switch inside the cavity. The modulation loss was measured to be 20 % in single-pass by measuring the power of undeflected beam at the RF-on and RF-off operation. The RF-signal is turned on at first to diffract the incident beam, which leads a build-up of population inversion of the gain medium. Then the Q-factor is switching at the onset of turn-off of the RF-wave to output a short pulse after some delay. Figure 5.4 shows that the gating time (i.e. the RF-off time) is set shorter than the pulse build-up time leads a “missing pulse” and the gain is stored until the next RF-off, at which a stronger pulse (consuming more population inversion) is generated. Because the amplified pulse in this situation is stochastic, the pulse train is less stable than a normal Q-switched laser. Accordingly the gating time have to be set longer than the build-up time for stable operation.

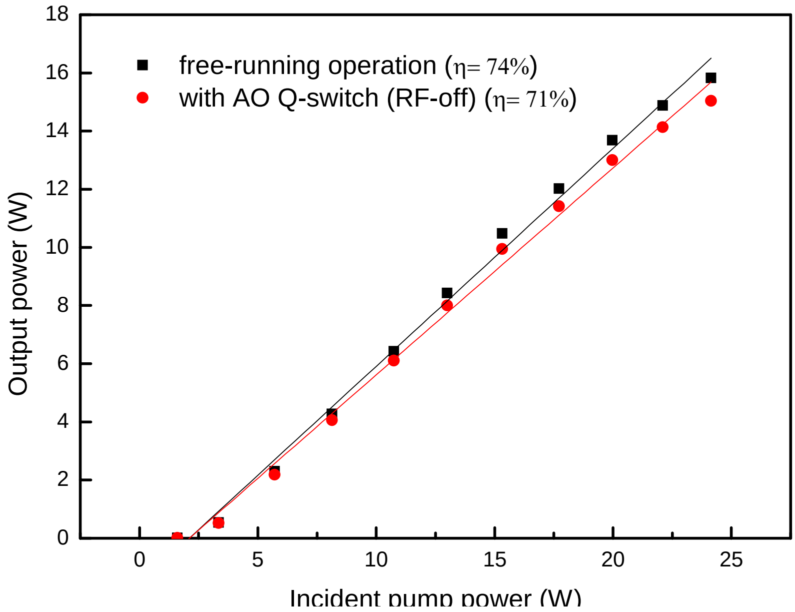

Fig. 5.3. Output power of cw operation and Q-switching operation versus pump power in cw operation.

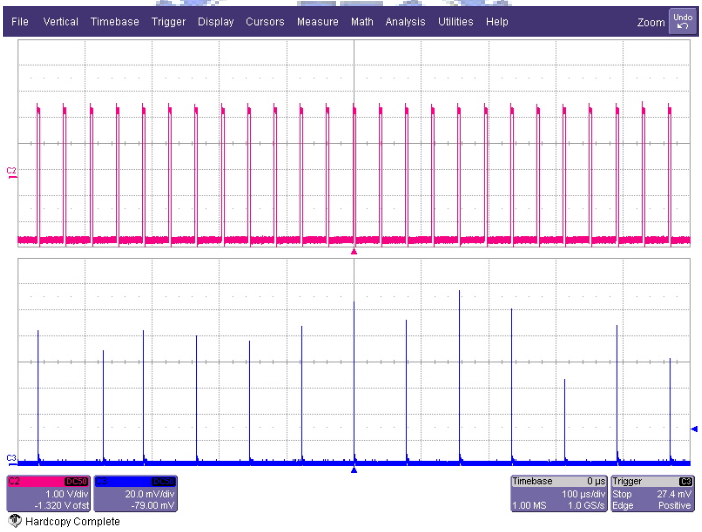

C2 DC50 1.00 V/div -1.320 V ofst
C3 DC50 20.0 mV/div -79.00 mV
Timebase 0 µs 100 µs/div 1.00 MS 1.0 GS/s
Trigger C3 Stop 27.4 mV Edge Positive
Hardcopy Complete

Fig 5.4. Plot of the condition that a gating time is shorter than the pulse builds up time.

Figure 5.5 shows the average power as a function of the frequency of the AO modulation at three different incident pump powers. The Q-switching efficiency is about 87 % corresponding to a high efficient Q-switching fiber laser. Moreover the operation frequencies could be operated from 53 kHz to 200 kHz stably at incident pump power of 24 W and 35 kHz~140 kHz at pump power of 16 W. The upper operating frequency is constrained by the fixed pumping rate, an even higher operating frequency requires higher pumping rate to furnish the population inversion of the gain medium. The lower limit is due to the pre-lasing resulted from the feedback of the undeflected beam [1]. As shown in Fig. 5.6 (a), several spiking signal occur a delay after the Q-switched pulse, which means the RF-on time is too long to prevent the lasing by feedback of the undeflected beam. An interesting phenomenon as shown in Fig 5.6 (b) reveals that a mode-locked resembling pulse occurs beyond the lowest repetition rate. Several groups have attempted to explain it such as self-phase-modulation induced self-mode-locking [2], the beating of undeflected beam with 1st order beam [3], harmonics of the modulation frequency corresponding to round-trip frequency stimulate the laser [4] etc. In our case we observed that the pulse was modulated by two frequencies corresponding to the frequency of the external cavity and the total cavity. At the rise of the Q-switched pulse it was modulated at the frequency of the external frequency and was modulated at the frequency of the total cavity.

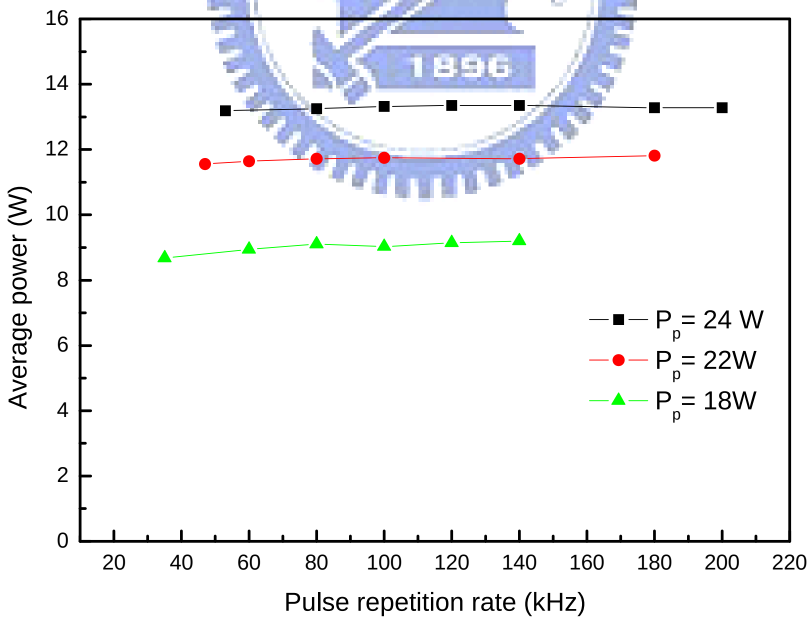

Fig 5.5. Average power as a function of the pulse repetition rate for three incident pump power.

The SPM induced spectral broadening was about 30 MHz [3], which matched the frequency of total cavity but shorter than that of the external cavity of 300 MHz.

Hence it is difficult to judge whether the mode-locked resembling pulse was induced by SPM. Besides, the pre-lasing is unfavorable for application. However, due to the high gain of fiber lasers, they are easily to lase even for a weak feed back. Consequently how to efficiently enhance the modulation loss of Q-switch is an important issue in actively Q-switched fiber lasers.

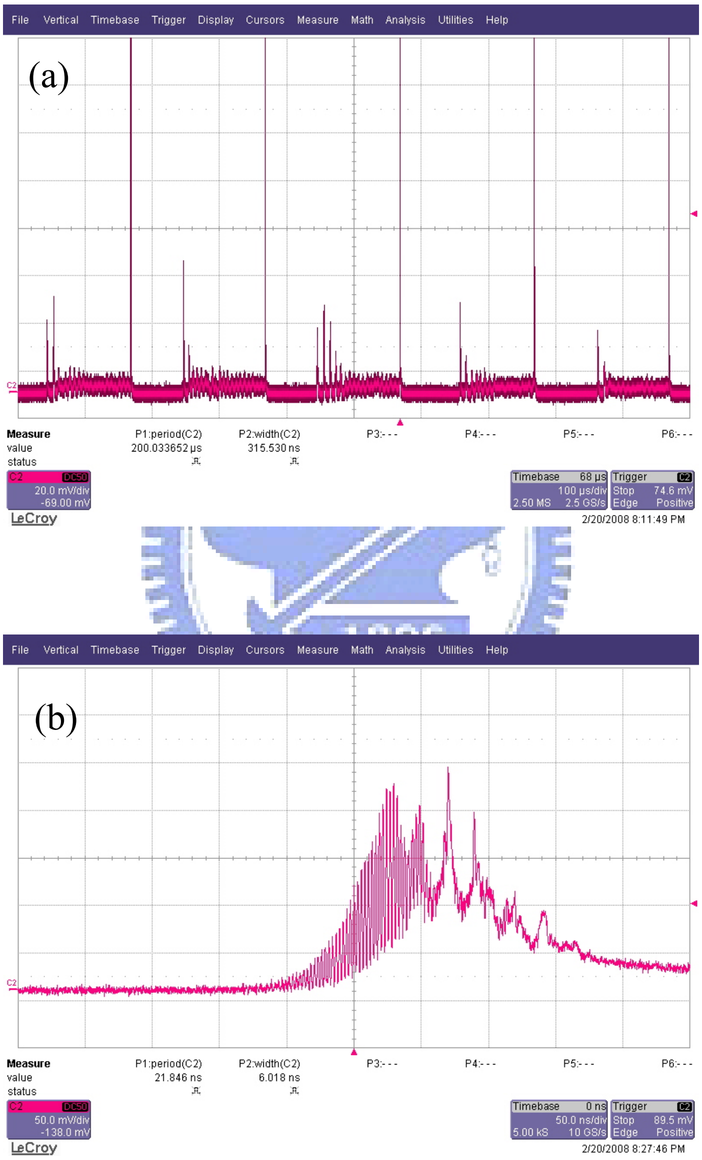

Fig. 5.6. Pre-lasing of an actively Q-switched fiber laser. (a) The pre-lased signal occurred a time delay after the Q-switched pulse. (b) The mode-locked resembling pulse.

Figure 5.7 shows the corresponding pulse energy of the average power and the operating frequency. In this figure there is a clear view of the limited condition that there is an upper limit and a lower one of pulse energy. The upper pulse energy is 250 μJ and the lower one is 55 μJ.

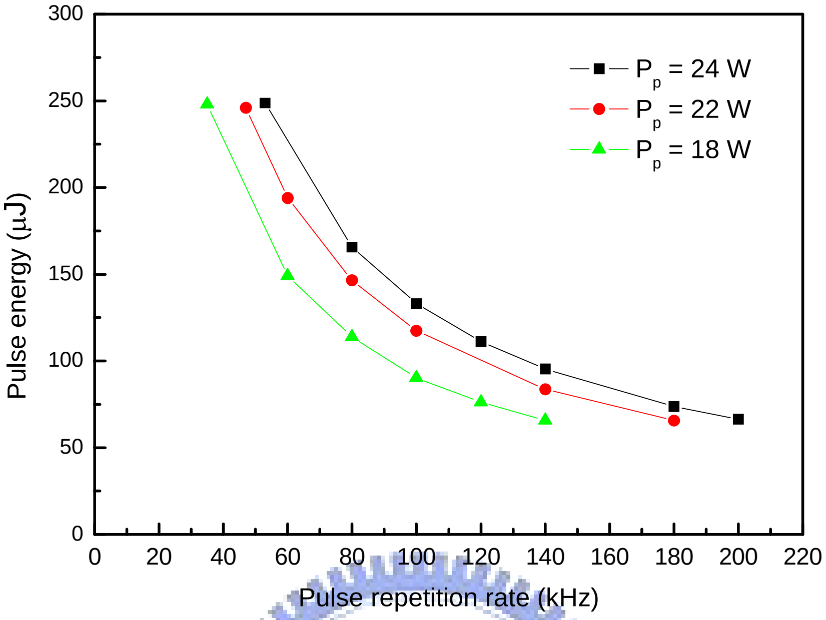

Fig. 5.7. Pulse energy at three different pump powers as a function of the pulse repetition rate.

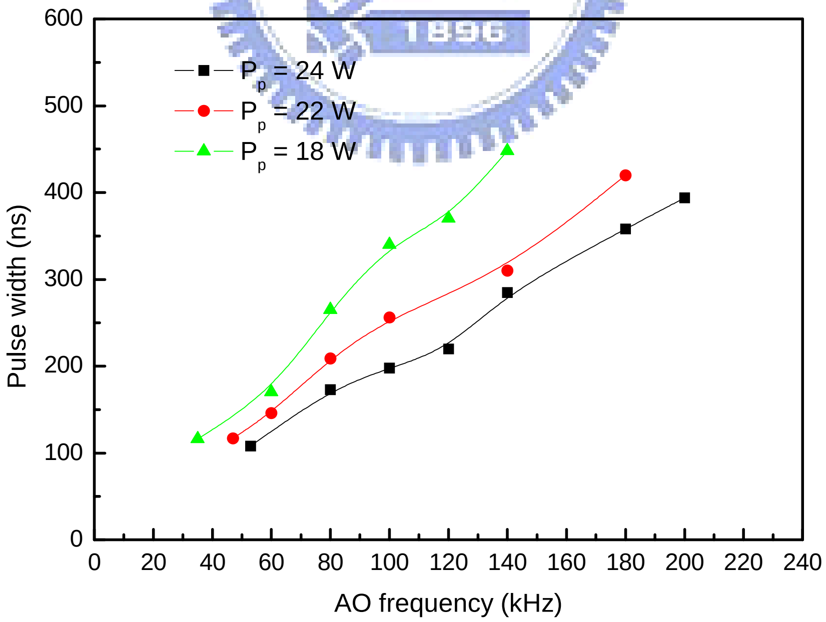

Fig 5.8 Pulse width at three different pump powers as a function of the pulse repetition rate.

Figure 5.8 shows the corresponding pulse width as a function of pulse repetition rate. The pulse width is shortened from 400 ns at the highest repetition rate to 100 ns at the lowest one. From Fig.5.7 and Fig. 5.8 the maximum pulse peak power is calculated to be around 2 kW. Fig. 5.9 shows the pulse train and a single pulse at repetition rate at 53 kHz and 200 kHz under pump power of 24 W. Under careful alignment, the pulse-to-pulse stability was found to be < 5% at 53 kHz and < 15% at 200 kHz. The pulses are smooth without any breaking and self-mode-locking phenomena [2-4].

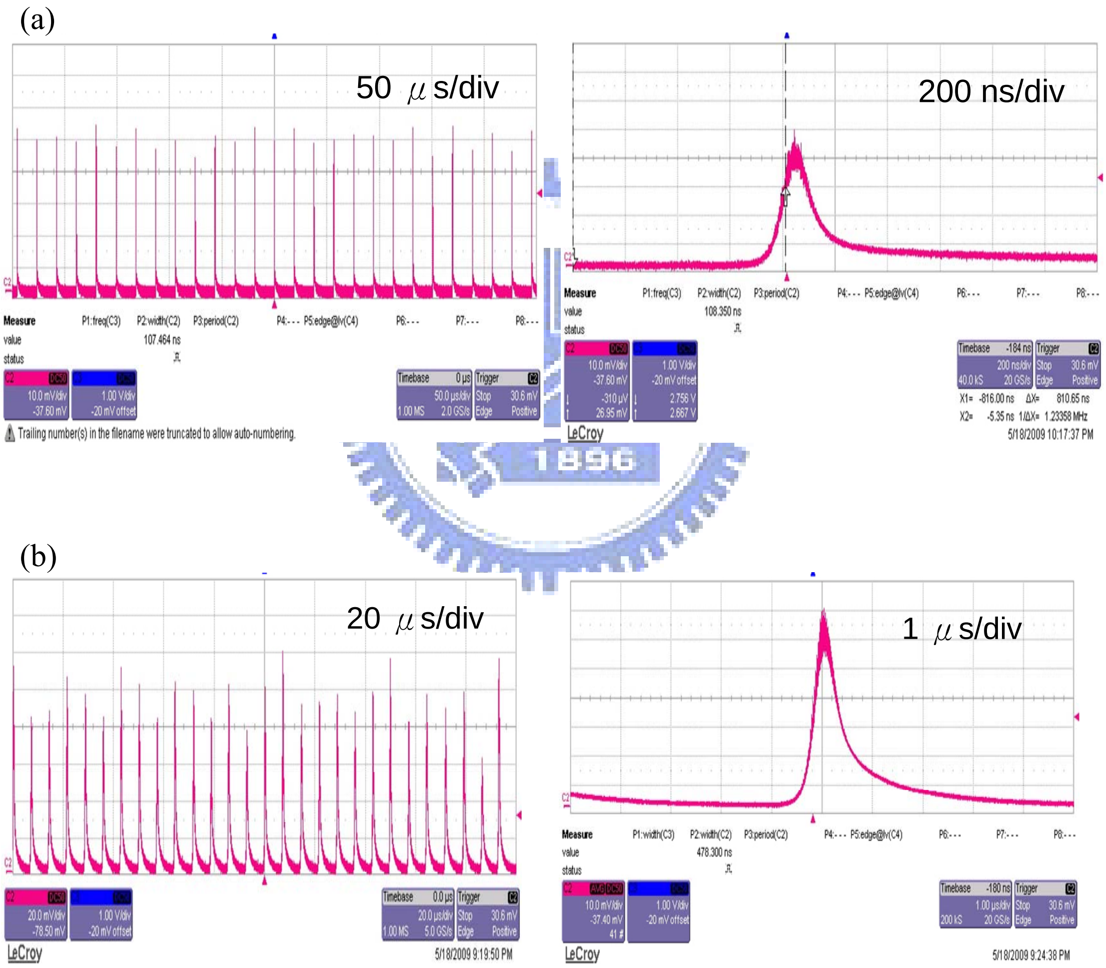

Fig. 5.9. Oscilloscope traces of a train and a typical Q-switched envelope of Q-switched pulses at pulse repetition rate of (a) 53kHz; (b) 200 kHz.

Fig. 5.10 shows the output spectrum of the Q-switched fiber laser at 53 kHz under pump power of 24 W. The FWHM of the linewidth is about 1.2 nm and the ratio of signal to ASE is estimated 50 dB. It is noted that the narrow linewidth of a laser is preferred in most applications.

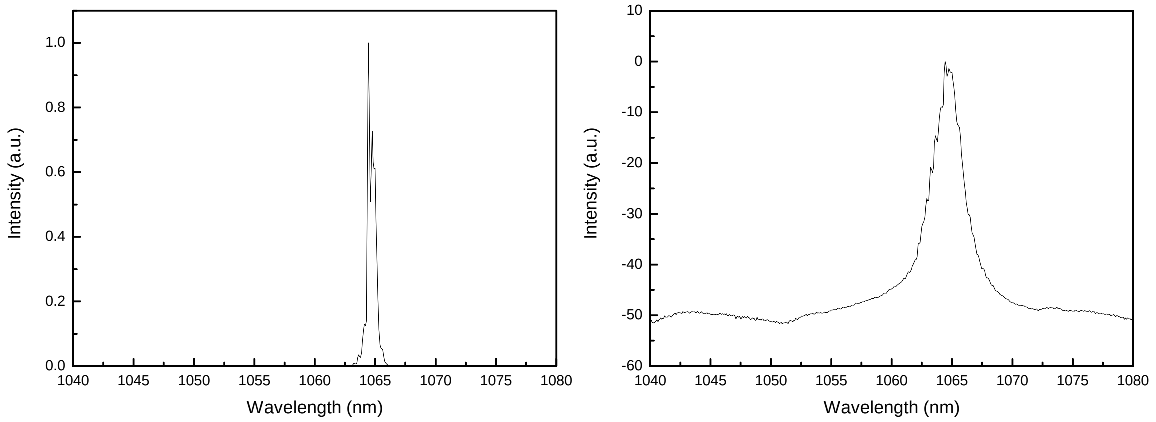

Fig 5.10 Spectral spectrum of the Q-switched laser at 53 kHz under the pump power of 24 W. The left one shows the intensity in linear scale while the right is in log scale.

## 5.3 Fiber Lasers Q-switched by acousticoptic modulator and AlGaInAs semiconductor saturable absorber

As mentioned in last section the AO Q-switch can only produce a loss modulation of 20 % in a single pass. The characteristic is exactly true for each AO-Q-switch for any pumping level and any repetition rate. This limits the flexibility of the AO Q-switch toward high pulse energy operation. In this section we utilize a hybrid Q-switching method to enhance the loss modulation of the Q-switch to improve the limited pulse energy and can improve the timing jitter of the passively Q-switched fiber lasers.

### 5.3.1 Experimental setup

The schematic of the experimental setup for the passively Q-switched Yb-doped fiber laser is shown in Fig. 5.11. The setup comprises a 3-m Yb doped fiber and an external feedback cavity. The external cavity comprises a re-imaging lens, a Fabry-Pérot etalon for controlling the lasing wavelength, an acousto-optic Q-switch mounted on a copper heat sink and was chilled actively by water, a AlGaInAs SESA as employed in section 4.2 for Q-switching, and a highly reflective mirror at 1060 nm~1100 nm for feedback. The end facets of the fiber were cut to be normal incident. One side of the cavity was a dichroic mirror and was coated high reflection at 1030 nm~1100 nm; the other side was the fiber end which is cut normally as the lasing output with ~4% reflection. The fiber has a peak cladding absorption coefficient of 10.8 dB/m at 976 nm and a double-clad structure with a diameter of 350 μm octagonal outer cladding, diameter of 250 μm octagonal inner cladding with a numerical aperture (NA) of 0.46, and 30-μm circular core with a NA of 0.07.

The pump source was a 35-W 976-nm fiber-coupled laser diode with a core diameter of 400 μm and a NA of 0.22. A focusing lens with 25 mm focal length and 90% coupling efficiency was used to re-image the pump beam into the fiber through a dichroic mirror with high transmission (>90%) at 976 nm and high reflectivity (>99.8%) at 1066 nm. The pump spot radius was approximately 200 μm. With launching into an undoped fiber, the pump coupling efficiency was measured to be approximately 80%. The pulse temporal behavior was recorded with a digital oscilloscope (LeCroy Wavepro 7100; 10G samples/sec; 4 GHz bandwidth) and a fast InGaAs photodiode. The spectral information was measured by an optical spectrum analyzer (Advantest Q8381A) with a resolution of 0.1 nm.

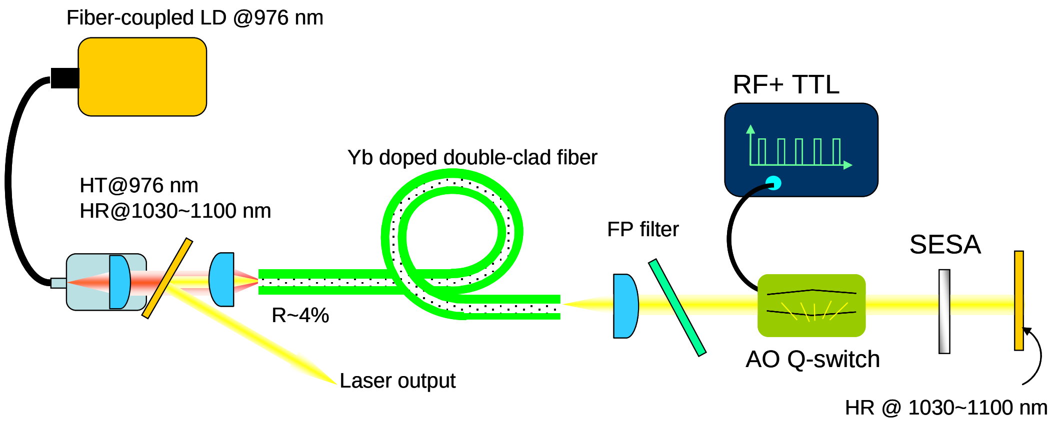

Fig 5.11. Schematic of hybrid Q-switched double-clad fiber laser.

### 5.3.2 Experimental results and discussion

#### 5.3.2.1 Sub-harmonic frequency locking

The performances of the passively Q-switched fiber laser by employing the AlGaInAs SESA is that 450-μJ energy per pulse with duration of 60 ns at the repetition rate of 30 kHz under the pump power of 24 W. Therefore the pulse repetition rate in this hybrid Q-switching must has a maximal repetition rate corresponding to where close to the frequency of PQS fiber laser for each pump power. Fig. 5.12 shows the corresponding output pulse repetition rate as a function of the AO Q-switch (AO Q). The function is a zigzag shape as a result of a limit repetition rate exists by the saturable absorber. It can be seen that with an increase in the operating frequency, the pulse repetition rate first increases accordingly until the operating frequency exceeds the value of $0.85\times f_{PQS}$. For higher operating frequencies, the output pulse train switch to a chaotic pulse train as shown in Fig. 5.12. This is attributed to nonsynchronization of the two Q-switches. For even higher operating frequency of $1.47\times f_{PQS}$ the pulse repetition rate switches back to stable pulse train with subharmonic M of the operating frequency, i.e. pulse repetition rate = operating frequency/M, for example the pulse repetition rate is $0.73\times f_{PQS}$ kHz at the operating frequency of $1.47\times f_{PQS}$, corresponding subharmonic M=2.

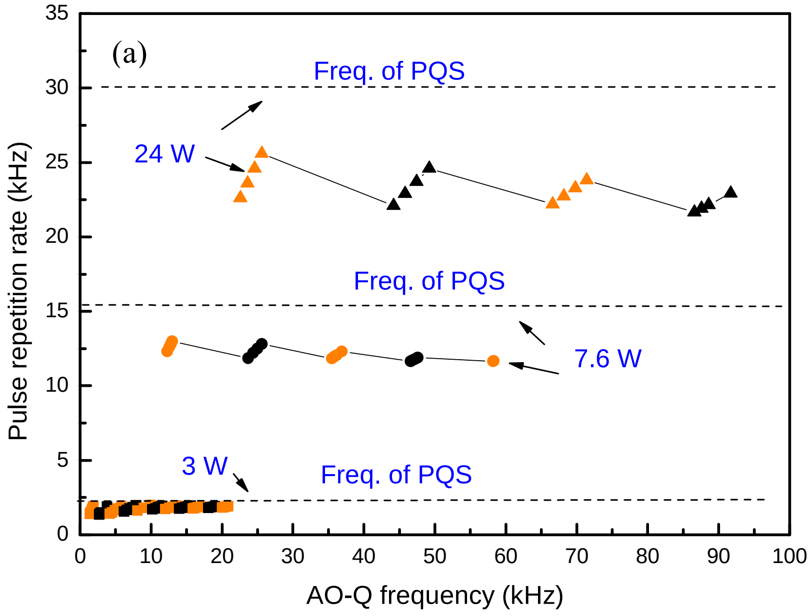

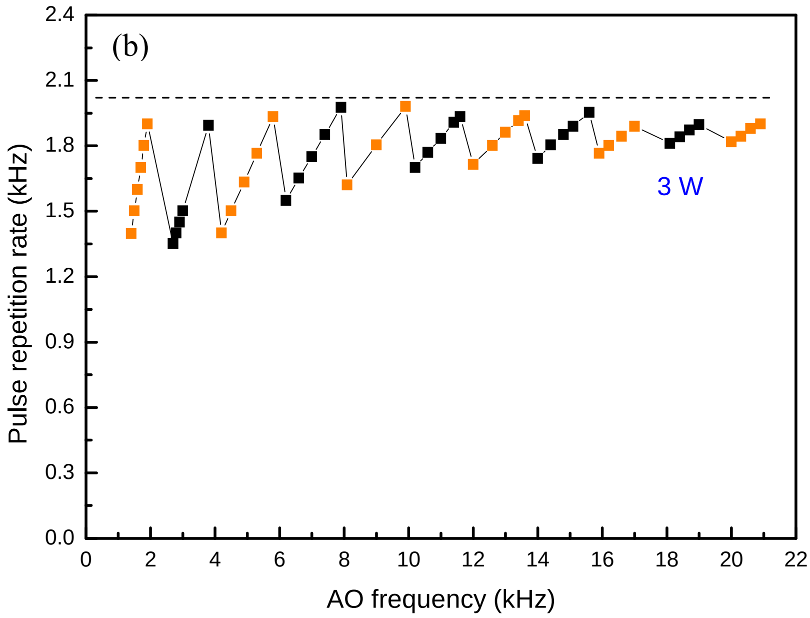

Fig. 5.12. (a) The pulse repetition rate as a function of the frequency of the AO Q-switch; (b) Detail of (a) for pump power of 3 W.

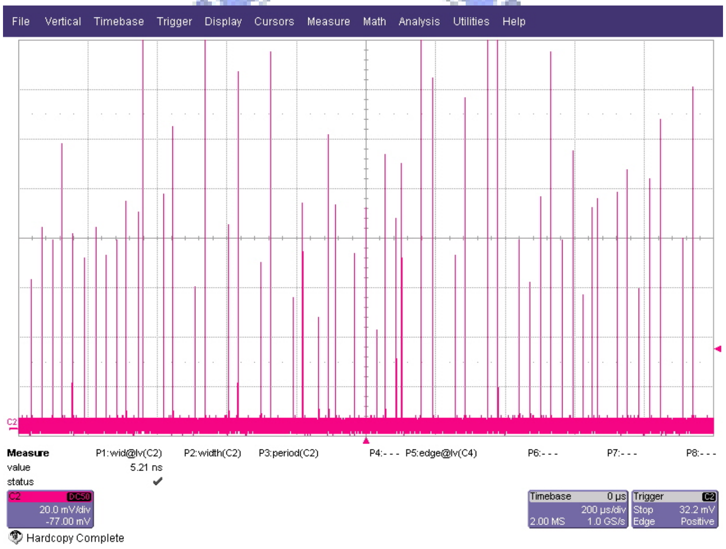

Measure P1:wid@lv(C2) P2:width(C2) P3:period(C2) P4:- - - P5:edge@lv(C4) P6:- - - P7:- - - P8:- - -
value 5.21 ns
status ✓

C2 DC50
20.0 mV/div
-77.00 mV

Timebase 0 μs
200 μs/div
2.00 MS 1.0 GS/s

Trigger C2
Stop 32.2 mV
Edge Positive

Hardcopy Complete

Fig. 5.13 The chaotic pulse train at the non-synchronized frequency.

### 5.3.2.2 Improvement of timing jitter at low pump power

The PQS fiber laser with an AlGaInAs SESA as a saturable absorber is stable at high pump power of >15 W while is less stable at low pump power around 3 W. With the aid of the AO Q-switch it is effectively to improve the stability and timing jitter. Figure 5.14 shows the timing jitter versus the duty cycle at the three pump power. The timing jitter at pump power of 3 W could be improved from 8 % to almost < 0.5

% with a duty cycle lower than 70 %. Figure 5.15 shows the time domain of the pulse train of passively Q-switched fiber laser and hybrid Q-switched fiber lasers. From this plot it is obviously the stability of the pulse train is increased.

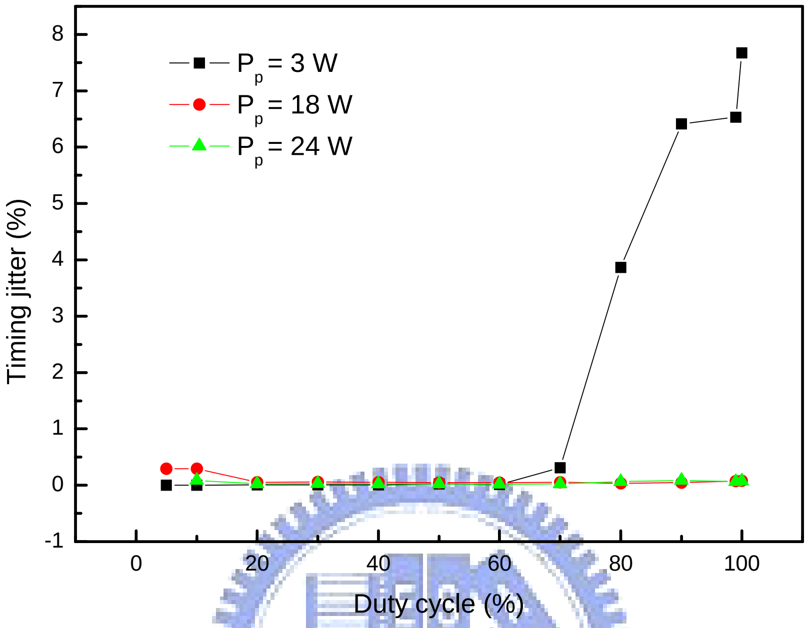

Fig. 5.14. Timing jitter versus the duty cycle for the three pump power.

Fig.5.15. The improvement of the stability of the pulse train. Left: the PQS pulse train; right: the hybrid Q-switched pulse train.

### 5.3.3.3 Increase of pulse energy

The hybrid Q-switch can effectively and easily enhance the modulation loss of the Q-switch to generate higher energy per pulse. It is noted that a hybrid Q-switch would also increase the non-saturable loss which is harmful to the performance of a Q-switched laser. Figure 5.16 shows the pulse energy versus the operating frequency at the three pump power. The dash line in this plot means the pulse energy of the passively Q-switched fiber laser by use of the AlGaInAs SESA. The maximum pulse energy is 450 μJ in PQS fiber laser by use of the AlGaInAs SESA while in the former section the maximal pulse energy is 250 μJ. The combination of the these two passive and active Q-switch can enhance the to 560 μJ, where the passive Q-switch can absorb efficiently the undeflected photons when the RF-wave is on. The average power at the highest pump power of 24 W can be calculated and the result is about 12.4 W corresponding 78 % of the Q-switching efficiency. Fig 5.17 shows the oscilloscopic traces of a train and a typical Q-switch pulse at the maximum pulse energy. The pulse-to-pulse stability is estimated to be < 5 % and the pulse width was about 50 ns.

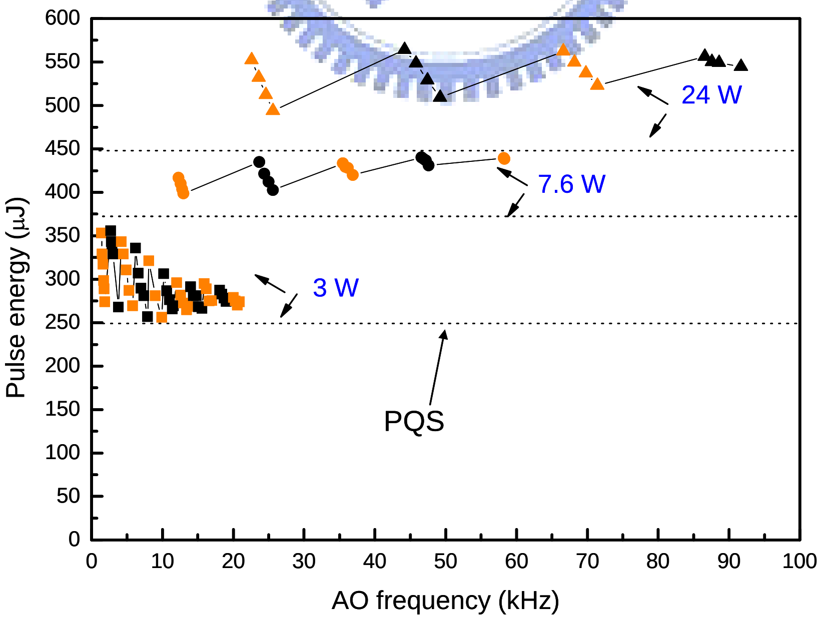

Fig. 5.16. Pulse energy versus the operating frequency for the three pump power. The dash line indicates the pulse energy of passively Q-switched fiber laser.

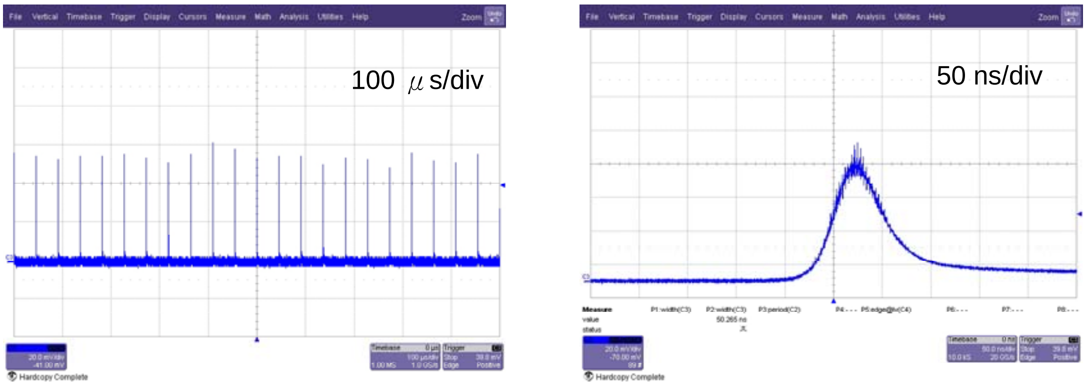

Fig. 5.17. Oscilloscope traces of a train and a typical Q-switched envelope of the hybrid Q-switched laser at maximum pulse energy.

## 5.4 Fiber Lasers Q-switched by acousticoptic modulator with polarization control

In this section we attempt to enhance the loss modulation by controlling the polarization of the incident beam into the AO Q-switch. As a result of the effective phase-grating formed in the AO crystal is transverse to the incident beam, the diffraction efficiency or modulation loss is accordingly polarization-dependent. Hence it should be beneficial to produce a higher extinction rate at lower repetition rate by polarization controlling.

### 5.4.1 Experimental setup

The schematic of the experimental setup for the passively Q-switched Yb-doped fiber laser is shown in Fig. 5.18. The setup comprises a 3-m Yb doped fiber and an external feedback cavity. The external cavity comprises a re-imaging lens, a Fabry-Pérot etalon for controlling the lasing wavelength, an acousto-optic Q-switch mounted on a copper heat sink and was chilled actively by water, a polarization beam splitter for polarization control, and a highly reflective mirror at 1060 nm~1100 nm for feedback. The end facets of the fiber were cut to be normal incident. One side of the cavity was a dichroic mirror and was coated high reflection at 1030 nm~1100 nm; the other side was the fiber end which is cut normally as the lasing output with ~4% reflection.

The fiber has a peak cladding absorption coefficient of 10.8 dB/m at 976 nm and a double-clad structure with a diameter of 350 μm octagonal outer cladding, diameter of 250 μm octagonal inner cladding with a numerical aperture (NA) of 0.46, and 30-μm circular core with a NA of 0.07.

The pump source was a 35-W 976-nm fiber-coupled laser diode with a core diameter of 400 μm and a NA of 0.22. A focusing lens with 25 mm focal length and 90% coupling efficiency was used to re-image the pump beam into the fiber through a dichroic mirror with high transmission (>90%) at 976 nm and high reflectivity (>99.8%) at 1066 nm. The pump spot radius was approximately 200 μm. With launching into an undoped fiber, the pump coupling efficiency was measured to be approximately 80%. The pulse temporal behavior was recorded with a digital oscilloscope (LeCroy Wavepro 7100; 10G samples/sec; 4 GHz bandwidth) and a fast InGaAs photodiode. The spectral information was measured by an optical spectrum analyzer (Advantest Q8381A) with a resolution of 0.1 nm.

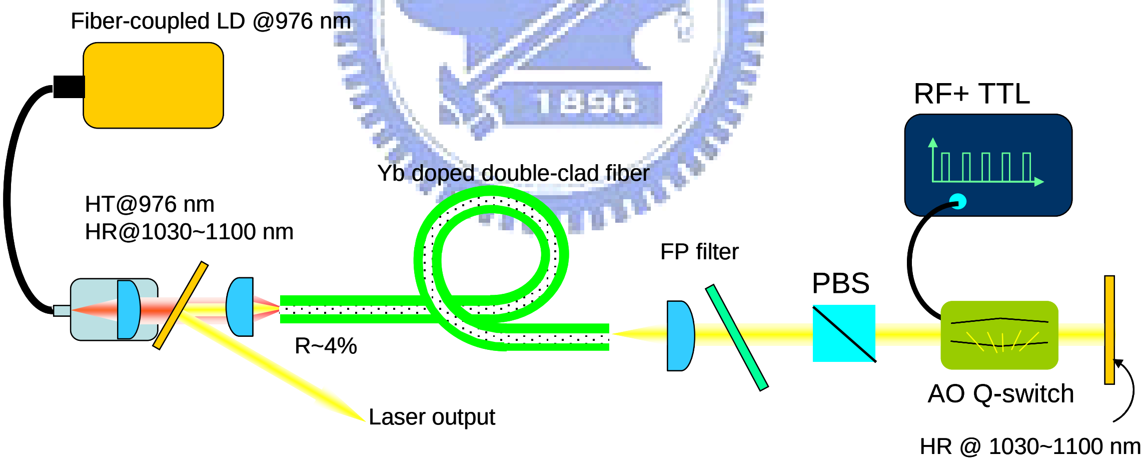

Fig. 5.18. Schematic configuration of the actively Q-switched fiber laser with polarization control.

### 5.4.2 Experimental results and discussion

Figure 5.19 shows the average power as a function of the frequency of the AO modulation at three different incident pump powers. The average power is almost constant over the operating frequency for the four pump power. From this figure we can calculate the ratio of average power in this experiment to that obtained in section

5.1. The ratio was obtained to be 96 %, which reveals the loss introduced by the PBS is low. However, the loss still limits the range of the operating frequency, which is shorter than that obtained in section 5.1. The lower operating frequency is reduced from 53 kHz in section 5.1 to 20 kHz through the help of the polarization control with a power efficiency of 96 %. Consequently the method of polarization control by a polarization beam splitter is efficient and uncomplicated. The average power also reveals that no significant ASE loss occur at the lowest operating frequency. Fig. 5.20 shows the corresponding pulse energy of the average powers multiplying the operating frequency. Lower pulse energy is approximately observed to be 100 μJ to 120 μJ; however, we did not see there was any upper limit of pulse energy for each pump power as seen in section 5.1.

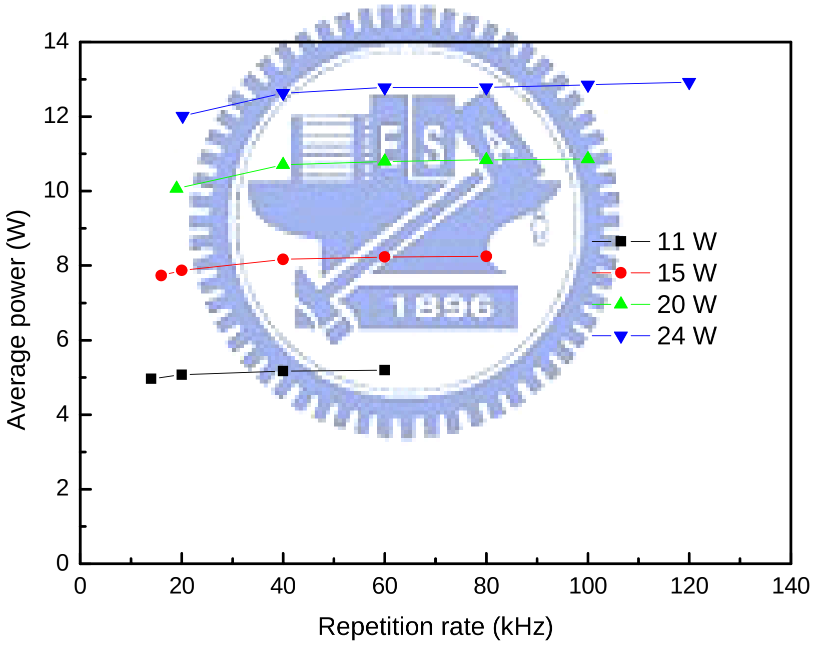

Fig. 5.19. Average power as a function of the operating frequency for four incident pump power.

It is reasonable that at high repetition rate the gain of fiber is modulated at high repetition rate that the undeflected beam can not lase the fiber. Oppositely the polarization beam splitter weakened the undeflected beam such that we can operate at lower repetition rate frequency. The maximum pulse energy was obtained at the pump power of 24 W and the repetition rate of 20 kHz.

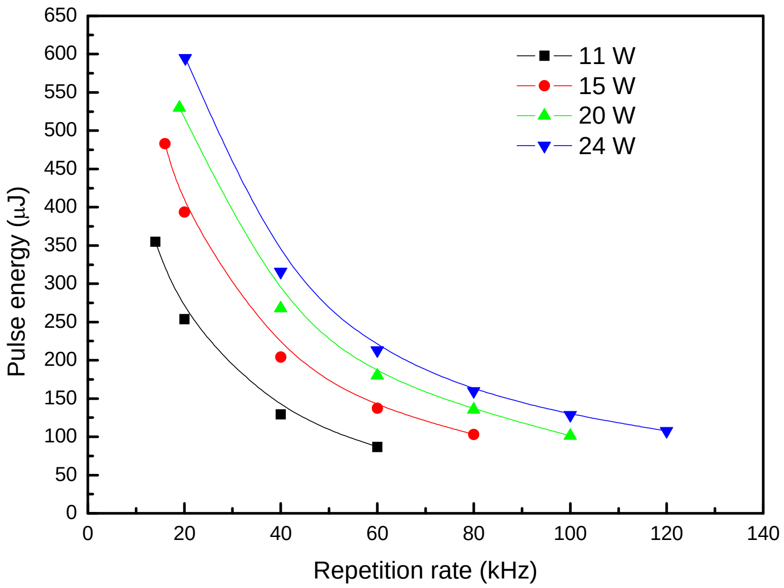

Fig 5.20. Pulse energy as a function of the pulse repetition

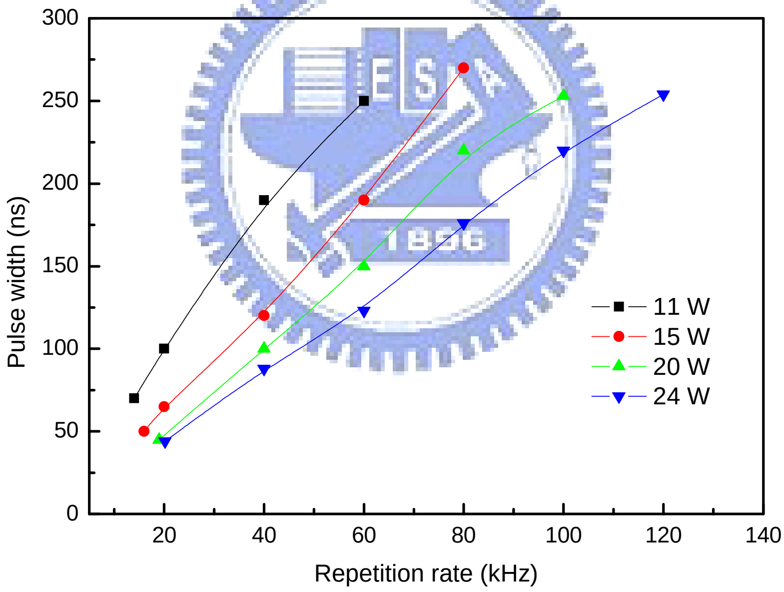

Fig 5.21. Pulse width as a function of the pulse repetition rate.

Figure 5.21 shows the pulse width as a function of pulse repetition rate. The pulse width is shortened from 250~270 μJ ns at high repetition rate to 45~60 ns at the lowest repetition rate. The results are similar to that in section 5.2 where we used saturable absorber to enhance the loss modulation. From Fig.5.20 and Fig. 5.21 the maximum pulse peak power is calculated to be around 14 kW. Fig. 5.22 shows the pulse train and a single pulse at repetition rate at 20 kHz and 120 kHz under pump power of 24 W. Under careful alignment, the pulse-to-pulse stability was found to be < 5% at 20 kHz and < 15% at 120 kHz. Fig. 5.23 shows the output spectrum of the Q-switched fiber laser at 20 kHz under pump power of 24 W. The FWHM of the linewidth is about 1.68 nm and the ratio of signal to ASE is estimated 50 dB.

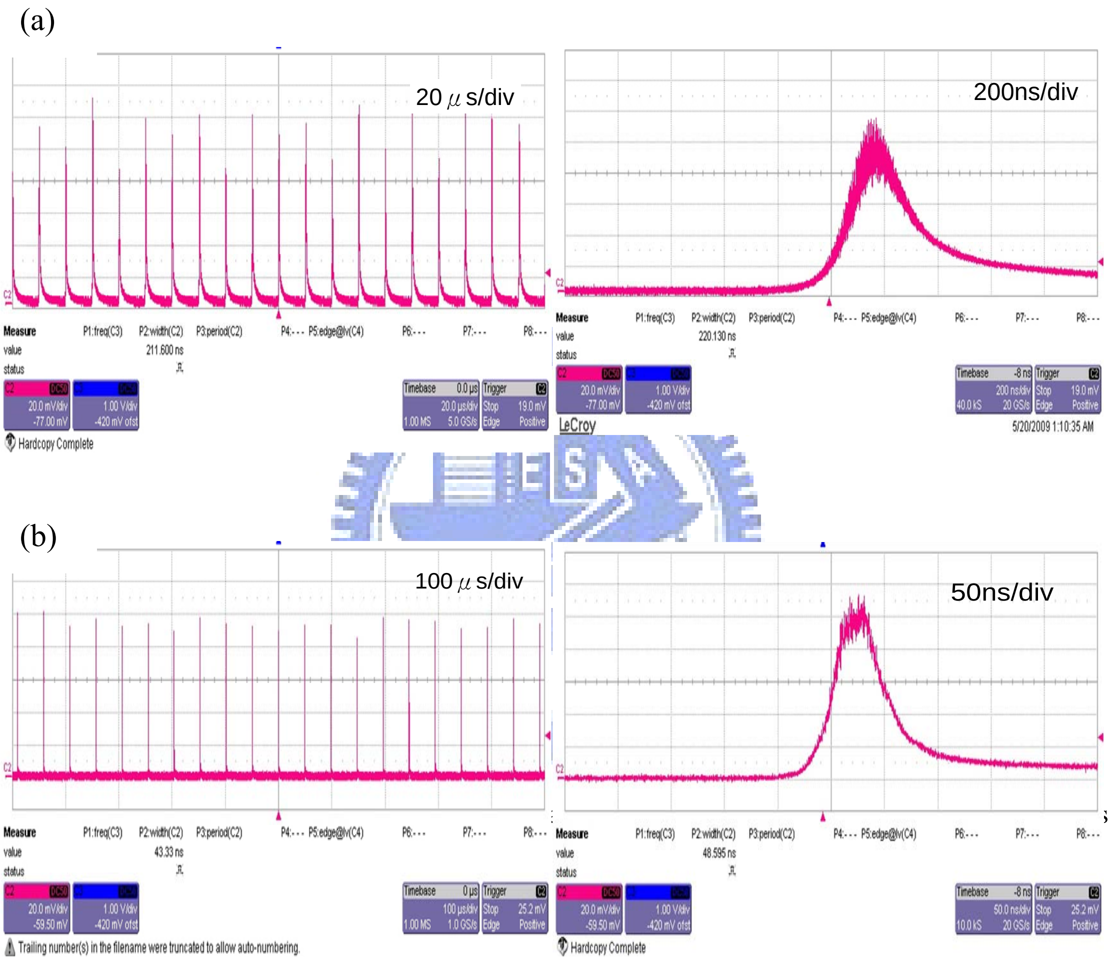

Fig. 5.22. Oscilloscope traces of a train and a typical Q-switched envelope of Q-switched pulses at pulse repetition rate of (a) 120 kHz; (b) 20 kHz.

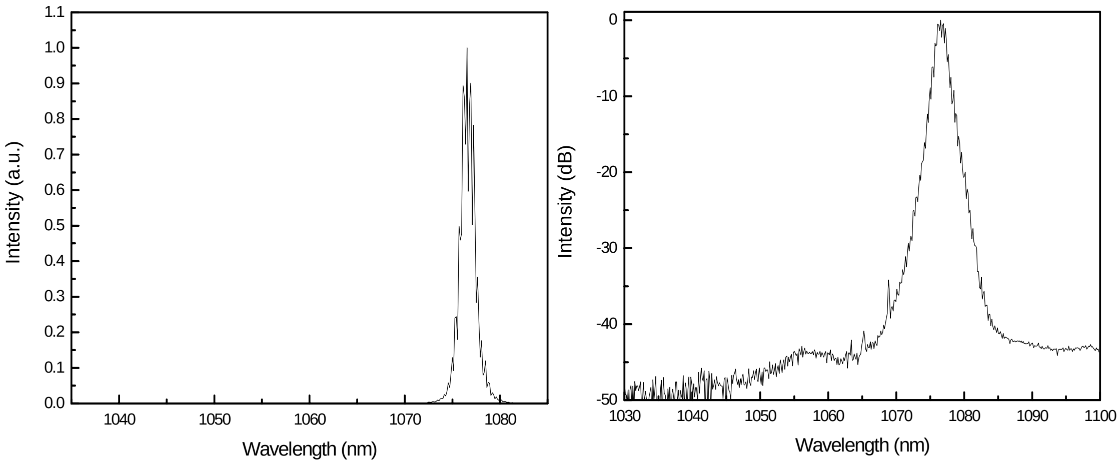

Fig 5.23. Spectral spectrum of the Q-switched laser at 20 kHz under the pump power of 24 W. The left one shows the intensity in linear scale while the right is in log scale.

## 5.5 Conclusion

We have demonstrated Q-switched Yb fiber lasers by use of acousticoptic Q-switch and combination of SESA and polarization control respectively. . Firstly by use of an acousticoptic Q-switch to Q-switch a fiber laser we have obtained a pulse with energy of 250 μJ and duration of 100 ns. The laser can operate at repetition rate from 53 kHz to 200 kHz with an average power of 13 W. Secondly we combined the active Q-switch and the passive Q-switch to generate a pulsed fiber laser. The laser possesses the merits of larger loss modulation than the former experiment and smaller timing jitter at low pump power than the passively Q-switched laser depicted in section 4.2. The hybrid Q-switched fiber laser can provide a larger pulse energy up to 560 μJ with a pulse duration of 50 ns. Finally we added a polarization control into the first experiment by inserting a PBS inside the external cavity. This method is efficient and simple to enhance the modulation loss. Pulse energy of 600 μJ with pulse duration of 45 ns was obtained at repetition rate of 20 kHz. Besides, all the three experiments are narrowband with a FWHM of < 1.5 nm.

# Reference

1. R. J. Collins and P. Kisliuk, “Control of Population Inversion in Pulsed Optical Masers by Feedback Modulation,” J. Appl. Phys. **33**, 2009 (1962).

2. B. A. Davydov, V. R. Muratov, L N. Soms, A. I. Stepanov, and V. K. Stupnikov, “Q-switched neodymium-glass laser generating short pulses ,” Sov. J. Quant. Electron. **4**, 1406-1407 (1975).

3. Valery N. Filippov, Andrei N. Starodumov, and Alexander V. Kir'yanov, "All-fiber passively Q-switched low-threshold erbium laser," Opt. Lett. **26**, 343-345 (2001).

4. H. Cai, X. Jiangzhen, H. Zhao, C. Gaoting, F. Zujie, I. S. Kim, and Y. Kim, "All-fiber q-switched erbium laser using a fiber bragg grating placed in loop mirror as a wavelength-selective intensity modulator," in *Optical Fiber Communications Conference*, A. Sawchuk, ed., Vol. 70 of OSA Trends in Optics and Photonics (Optical Society of America, 2002), paper ThGG31.

5. M. Fabert, A. Desfarges-Berthelemot, V. Kermène, A. Crunteanu, D. Bouyge and P. Blondy, “Ytterbium-doped fibre laser Q-switched by a cantilever-type micro-mirror,” Opt. Express **16**, 22064-22071 (2008).

6. H. L. Offerhaus, N. G. Broderick, D. J. Richardson, R. Sammut, J. Caplen, and L. Dong, "High-energy single-transverse-mode *Q*-switched fiber laser based on a multimode large-mode-area erbium-doped fiber," Opt. Lett. **23**, 1683-1685 (1998).

7. Z. J. Chen, A. B. Grudinin, J. Porta, and J. D. Minelly, "Enhanced *Q* switching in double-clad fiber lasers," Opt. Lett. **23**, 454-456 (1998).

8. J. Limpert, N. Deguil-Robin, I. Manek-Hönninger, F. Salin, F. Röser, A. Liem, T. Schreiber, S. Nolte, H. Zellmer, A. Tünnermann, J. Broeng, A. Petersson, and C. Jakobsen, "High-power rod-type photonic crystal fiber laser," Opt. Express **13**, 1055-1058 (2005).

9. J. A. Alvarez-Chavez, H. L. Offerhaus, J. Nilsson, P. W. Turner, W. A. Clarkson, and D. J. Richardson, "High-energy, high-power ytterbium-doped Q-switched fiber laser," Opt. Lett. **25**, 37-39 (2000).W. Koechner, Solid State Laser Engineering, Chap 8, Springer (2006).

10. P. Myslinski, J. Chrostowski, J. A. K. Koningstein and J. R. Simpson, “Self-mode locking in a Q-switched erbium-doped fiber laser,” Appl. Opt. **32**, 286-290 (1993).

11. B. N. Upadhyaya, Usha Chakravarty, A. Kuruvilla, K. Thyagarajan, M. R. Shenoy, and S. M. Oak, "Mechanisms of generation of multi-peak and mode-locked resembling pulses in Q-switched Yb-doped fiber lasers," Opt. Express **15**, 11576-11588 (2007).
12. Y. Wang, A. Martinez-Rios and Hong Po, “Analysis of a Q-switched ytterbium-doped double-clad fiber laser with simultaneous mode locking,” Opt. Commun. **224**, 113-123 (2003).
13. G. P. Lees and T. P. Newson, “Diode pumped high power simultaneously Q-switched and self modelocked erbium doped fiber laser,” Electron. Lett. **32**, 332-333 (1996).
14. S. Adachi and Y. Koyamada, “Analysis and design of Q-switched erbium-doped fiber lasers and their application to OTDR,” J. Lightwave Technol. **20**, 1506-1511 (2002).

# *Chapter 6 Summary and Future works*

## 6.1 Summary

### 1. Tunable Yb and Er/Yb codoped fiber lasers

In this section I demonstrated efficient narrowband and tunable Yb-doped and Er/Yb-codoped fiber lasers by use of all-dielectric Fabry-Perot thin film filters. The filters have low insertion loss and high transmission at the central wavelength. Therefore FP thin film filters are suitable for efficiently narrowing and tuning broadband lasers. The performances of the Yb and the Er/Yb fiber lasers are shown as table 6.1.

Table 6.1. Performances of the tunable fiber lasers.

| | Tunable range | $\Delta\lambda_{narrowband}/\ \Delta\lambda_{TFF}$ (nm) | $\Delta\lambda_{na}/\ \Delta\lambda_{br}$ (nm) | $P_{na}/\ P_{br}$ | Power (W) |
|---|---|---|---|---|---|
| Yb fiber laser | 60 nm | 0.36/5 | 0.36/14 | >0.9 | 14 |
| Er/Yb fiber laser | 28 nm | 0.15/0.4 | 0.15/5 | >0.9 | 3.2 |

### 2. Passively Q-switched fiber lasers

In this section I have developed a model and optimized an external Q-switch of fiber lasers Q-switched by $Cr^{4+}$:YAG crystals. Besides, I also demonstrated that passively Q-switched Yb fiber lasers by a $Cr^{4+}$:YAG crystal and an AlGaInAs semiconductor saturable absorbers respectively; and Er/Yb fiber lasers by an AlGaInAs semiconductor saturable absorber. The performance of Yb fiber lasers are shown in table 7.2. As seen in the table both the saturable absorbers possess low insertion loss with > 85% Q-switching efficiency. On the other hand the pulse energies obtained in these two experiments are superior to those of others are thanks to the use of a

LMA fiber with core diameter of 30 μm and saturable absorbers with large modulation depth and low nonsaturable loss.

Table 6.2. Performances of the passively Q-switched Yb fiber lasers

| | by AlGaInAs QWs | by Cr4+:YAG crystal |
|---|---|---|
| Q-switching efficiency | 87% | 90% |
| PRR (kHz) | 30 | 38 |
| pulse energy (μJ) | 450 | 350 |
| pulse width (ns) | 65 | 75 |
| pulse stability | ±10% | ±15% |

As for the Er/Yb fiber laser, we have also obtained an efficient Q-switched fiber laser with Q-switching efficiency >85 %. Beside, the generated single pulse owns energy of 100 μJ at pulse repetition rate of 12 kHz, corresponding average power of 1.2 W. The result manifested the AlGaInAs material are also suitable for Q-switching Er/Yb fiber lasers in the spectral domain of 1.5 μm.

## 3. Actively Q-switched fiber lasers

In this section we actively Q-switch an Yb fiber laser by use of an acoustic-optic Q-switch. The results reveal that Q-switching by an acoustic-optic Q-switch is efficient and flexible. The pulse repetition rate ranges 53 kHz to 200 kHz at pump power of 24 W and the maximum pulse energy obtained is 250 μJ at repetition rate of 53 kHz. However due to the high gain of the gain fiber it is difficult to prevent the pre-lasing resulted from the feedback of undeflected beam at low pulse repetition rate. Hence by means of the aid of the saturable absorber or polarization controlling, we have successfully enhanced the loss modulation of the Q-switch. In the hybrid Q-switching experiment, the pulse energy was increased to 550 μJ and pulse width was shortened from 100ns to 50 ns at repetition rate of 22 kHz under pump power of

24 W. Besides the hybrid Q-switch reduced the timing jitter at low pump power occurred in the passively Q-switched fiber lasers. In the actively Q-switching with polarization controlling experiment, a polarization beam splitter was inserted in front of the acoustic-optic Q-switch to control the polarization of incident beam. An output pulse of energy of 600 μJ and width of 45 ns was obtained at repetition rate of 20 kHz under pump power of 24 W. The results manifested that it is efficient and simple to directly control the polarization of the resonant beam in the external cavity to enhance the performance of a Q-switched fiber laser by use of an acoustic-optic Q-switch.

## 6.2 Future works

Applications of nonlinear optical effects can be another interesting research direction. For example a narrowband and high-peak-power pulsed fiber lasers are suitable for frequency-doubling and OPO experiments. On the other hand, besides the Q-switched fiber lasers we are attempted to generate a mater-oscillation-power- amplifier system by injecting a short pulse with duration of 1 ns into a fiber to generate a high-pulse-energy and short-duration pulse. This object is interesting because it improve the drawback of long-pulse-duration of typical Q-switched fiber lasers. Another improvement to the drawback is to use a rod-type fiber as the gain medium because their large core size and shorter length can be used to generate a short Q-switched pulse.

# Appendix: List of publications

## Journals publications

- J. Y. Huang, H. C. Liang, K. W. Su, and Y. F. Chen, “High power passively Q-switched ytterbium fiber laser with Cr4+:YAG as a saturable absorber,” Opt. Express **15**, 2, 473-479 Jan 22 (2007).
- J. Y. Huang, H. C. Liang, K. W. Su, and Y. F. Chen” Analytical model for optimizing the parameters of the external cavity in passively Q-switched fiber lasers ,” Appl. Opt. **47**, 2297-2302 (2008).
- J. Y. Huang, S. C. Huang, H. L. Chang, K. W. Su, Y. F. Chen*, and K. F. Huang, “Passive Q switching of Er-Yb fiber laser with semiconductor saturable absorber,” Opt. Express **16**, 3002-3006 (2008).
- J. Y. Huang, W. C. Huang, W. Z. Zhuang, K. W. Su, Y. F. Chen, and K. F. Huang, “High-pulse-energy passively Q-switched Yb-doped fiber laser with AlGaInAs quantum-wells as a saturable absorber,” accepted by Op. Lett.
- J. Y. Huang, H. C. Liang, K. W. Su, H. C. Lai, Y.-F. Chen, and K. F. Huang, “InGaAs quantum-well saturable absorbers for a diode-pumped passively *Q*-switched Nd:YAG laser at 1123 nm,” Appl. Opt. 46, 239-242 Jan 10 (2007).
- Huang YP, Liang HC, Huang JY, Su KW, Li A, Chen YF, Huang KF, “Semiconductor quantum-well saturable absorbers for efficient passive Q switching of a diode-pumped 946 nm Nd:YAG laser,” Appl. Opt. 46, 25, 6273-6276 Aug 23 (2007).
- H.C. Liang, J.Y. Huang, K.W. Su, H.C. Lai, Y.F. Chen, K.F. Huang, Zhang HJ, J.Y. Wang, M.H. Jiang. “Passively *Q*-switched Yb3+:YCa4O(BO3)3 laser with InGaAs quantum wells as saturable absorbers,” Appl. Opt. 46, 2292-2296 (2007).

# Conferences

- 黃哲彥，梁興弛，蘇冠暐，陳永富，林志平，陳思武，“光纖雷射研製計畫,” 96 年度國防科技學術合作計畫成果發表會 55CS, 論文集 B-33, 龍潭 (2007).
- J.Y. Huang, H.C. Liang, K.W. Su, and Y.F. Chen, “Analytical model for the design of external-cavity passively Q-switched fiber lasers,” Fiber Lasers V, PW2008, Proceedings of SPIE 6873, San Jose, USA (Jan 2008).
- H.C. Liang, J.Y. Huang, S.C. Huang, K.W. Su, Y.F. Chen, and K.F. Hunag, “High-peak-power flashlamp-pumped passively Q-switched Nd:YAG laser with AlGaInAs quantum wells as a saturable absorber,” Solid State Lasers XVII, PW2008, Proceedings of SPIE 6871, San Jose, USA (Jan 2008).
- J.Y. Huang, H.C. Liang, K.W. Su, and Y.F. Chen, “Analytical model for optimizing the parameters of the external cavity in passively Q-switched fiber lasers,” Annual Meeting of the Physical Society of Republic of China, Hsinchu (Jan 2008).